Chapter 8
Chemical and Structural Modifications of Nanoporous Alumina and Its Optical Properties

Agnieszka Brzózka, Anna Brudzisz, Katarzyna Hnida and Grzegorz D. Sulka

Abstract A growing scientific interest in the fabrication of porous anodic aluminum oxide (AAO) films and their further applications for the fabrication of various devices, has given rise to many studies of porous alumina properties. Highly ordered porous alumina exhibits some unique physical and optical characteristics, especially in the visible spectrum. These properties are of technological importance for applications in the fields of micro and nanotechnology.

8.1 Introduction

In recent decades, anodic aluminum oxide (AAO) has attracted scientific and technological interest due to its numerous applications. The protective AAO layer on aluminum increases its oxidation resistance [1], and after incorporation of organic or metallic pigments can act as a decorative layer [2]. As the insulator with a large surface area, porous alumina is used in electrolytic capacitors [3]. The most common application of AAO is its use as a template for fabrication of nanowires [4], nanodots [5], nanotubes [6], porous membranes [7], etc. [8]. The porous AAO membranes are also used as molecular sieves [9] and masks for selective etching [10]. In recent years, more and more attention has been devoted to optical properties of nanoporous AAO films. Due to the specific interaction of light with a porous medium, an incident light beam can be (i) reflected from the AAO surface or from the Al_2O_3/Al interface, (ii) absorbed by the oxide structure, (iii) transmitted across the pore walls, and also (iv) reflected inside the nanopores [11] as shown in Fig. 8.1.

A. Brzózka · A. Brudzisz · G.D. Sulka (✉)
Department of Physical Chemistry and Electrochemistry, Faculty of Chemistry, Jagiellonian University in Krakow, Ingardena 3, 30060 Krakow, Poland
e-mail: sulka@chemia.uj.edu.pl

K. Hnida
AGH University of Science and Technology, Academic Centre for Materials and Nanotechnology, al. A. Mickiewicza 30, 30-059 Krakow, Poland

D. Losic and A. Santos (eds.), *Electrochemically Engineered Nanoporous Materials*, Springer Series in Materials Science 220,
DOI 10.1007/978-3-319-20346-1_8

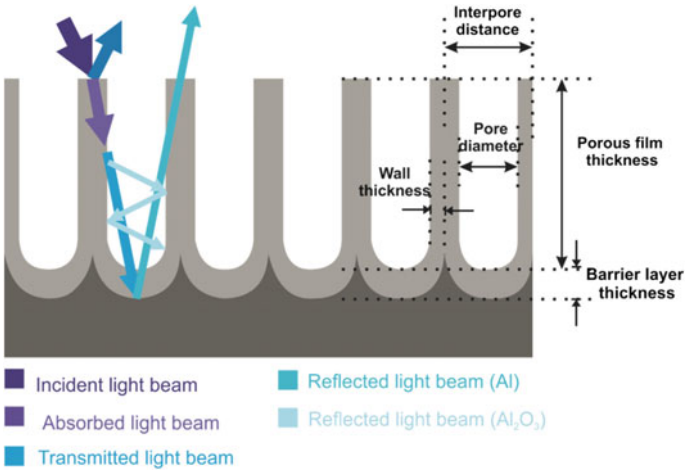

Fig. 8.1 Schematic representation of different phenomena occurring when a light beam incident on the AAO surface and selected characteristic parameters of the AAO film which affect its optical properties

All interactions of the incident light beam with porous AAO depends considerably on the characteristic geometrical parameters of AAO (e.g., pore diameter, interpore distance, wall thickness, oxide layer thickness) and its chemical composition.

It is widely recognized that freestanding AAO films are transparent in the UV-visible range [12]. Porous alumina exhibits a blue photoluminescence band, with the emission bands being attributed to optical transition in the singly ionized oxygen vacancies or to electrolyte impurities embedded in the porous alumina membranes. The previous studies have shown that the photoluminescence of porous alumina relies upon such fabrication parameters as the electrolyte type, anodization voltage, pore diameter, thermal treatment, and anodization regime. It is possible to tune the photoluminescent behavior of AAO by simple modification of the characteristic geometrical parameters of porous alumina. A relatively new approach is to use a pulse anodization, which has been developed for the formation of well-ordered porous alumina with periodically modulated pore diameter. Due to the fact that porous alumina films with modulated diameters have typically a structure based on a stack of thin transparent dielectric layers with alternating high and low refractive indices, they have found applications as distributed Bragg reflectors which offer a high reflectance similar to metallic mirrors. Modification of the optical properties of the porous alumina films can be realized by changing the anodization conditions (e.g., voltage, electrolyte composition, temperature) and by chemical treatment of AAO after anodization (e.g., etching, coloring with dyes, sandblasting, modification by metal nanoparticles, pore filling with polymers).

Highly ordered porous anodic aluminum oxide can be synthesized via two-step anodization of aluminum in acidic electrolytes. The process of AAO membrane formation is relatively simple and inexpensive. AAO formed by the self-organized

anodization of aluminum consists of regularly arranged hexagonal cells with parallel nanopores at their centers [8]. Depending on the anodizing conditions (concentration and type of the electrolyte, applied potential, temperature, and anodizing time), this electrochemical process results in typical nanoporous oxide structures with the pore diameter ranging from about 10 to over 300 nm and the corresponding interpore distance varies in a range of about 35–500 nm.

8.2 Structural Engineering of AAO

During the electrochemical anodization of aluminum carried out in acidic electrolytes including sulfuric acid [13–16], oxalic acid [4, 17] and phosphoric acid [18], anodic aluminum oxide (AAO) with a periodic hexagonal structure can be produced by a self-organized process. Through strict control of anodization conditions it is possible to obtain porous alumina with well-defined characteristic geometrical parameters such as pore diameter, interpore distance (cell diameter), wall thickness, and barrier layer thickness. All geometrical parameters of AAO are easily controllable by anodization conditions (type of electrolyte, anodizing potential or current, time, temperature, and agitation speed) and by post-anodization treatment (etching and annealing) [8].

For self-ordered porous AAO it was found that the interpore distance, pore diameter and barrier layer thickness increase linearly with anodizing potential. The proportionality constants for AAOs formed by conventional mild anodization (MA) processes are 2.5 nm V^{-1} for the interpore distance, 1.29 nm V^{-1} for the pore diameter and 1.2 nm V^{-1} for the barrier layer thickness [8, 19]. In case when hard anodizing (HA) conditions are applied, the interpore distance and barrier layer thickness depend also linearly on the anodizing potential with proportionality constants of about 1.8–2.1 and 0.6–1.0 nm V^{-1}, respectively [19]. On the other hand, the pore diameter of AAOs formed by hard anodization at potentiostatic conditions depends on the anodizing current density [19, 20].

The chemical composition of the AAO membranes is strongly dependent on the type and concentration of electrolyte used for anodization, anodizing potential, current density and temperature [8]. For typical acids used as the anodizing electrolyte (H_2SO_4, H_3PO_4 and $H_2C_2O_4$), incorporation of the acid anions occurs due to their migration in an electric field during the anodizing process. The mechanical properties of AAO such as hardness, elasticity, wear resistance and durability, are determined by the presence of water and embedded anions [19]. The alumina obtained by anodization has a different chemical composition across the pore depth. In other words, the concentration of incorporated ions is much higher at the external oxide layer formed at the beginning of anodization (high acid concentration) than that at the electrolyte/oxide interface where the oxide layer is formed at the end of anodization (low acid concentration) [21]. It is generally accepted that pore walls of AAO have a duplex structure with regard to chemical composition [22]. The outer layer close to the pore channel is rich in the incorporated ions due to the contact

with the electrolyte. The inner layer of pore walls is substantially made of pure Al_2O_3. As-prepared AAO is amorphous and contains water. The water content in porous alumina depends on the anodizing conditions. Annealing of AAO, depending on the applied temperature, may lead to the removal of embedded water from the pore walls, thermal decomposition of build-in anions or a phase transition from amorphous to crystalline. The internal pore structure of nanoporous AAO can be engineered by controlling anodization conditions or by applying an appropriate post-anodization treatment. For instance, by control of the applied anodizing potential it is possible to obtain Y-branched [23–27], multi-branched [27–29] and hierarchically branched pore structures [30–35] as well as periodically modulated nanopore diameters along the pore axes [20, 36–48].

It is widely recognized that for the mild anodization of aluminum performed in sulfuric, oxalic, and phosphoric acid the interpore distance depends on the applied potential with a proportionality constant of about 2.5 nm V^{-1} [8]. Therefore, the reduction of the applied potential by a factor of $1/\sqrt{2}$ during anodization results in branching of stem pores and, consequently, porous AAO with Y-branched nanopores is formed [25]. The AAO structures with a few generations of branched pores can be obtained by further sequential reductions of anodizing potentials by the same factor (Fig. 8.2). The reduction of the anodizing potential by a factor of $1/\sqrt{n}$, where n is a number of branches, results in a n-branched nanopores.

The ordered nanoporous AAO with a complex internal pore structure can be formed by combining the mild and hard anodizations in a process of so called pulse anodization [43]. This approach allows for a continuous modulation of internal pore diameter along the pore axis. The principle of the pulse anodization is based on applying a relatively long low potential/current pulses (MA regime) followed by short high potential/current pulses (HA regime). The length of MA and HA segments in AAO structure are fully controlled by varying anodizing time and MA, HA conditions (applied potential/current). The schematic representation of the applied potential–time waveforms used for the pulse anodization of aluminum is shown in Fig. 8.3a. The effect of applying of HA and MA pulses on the structure of porous anodic alumina is shown in Fig. 8.3b. Figure 8.3c shows the cross-sectional

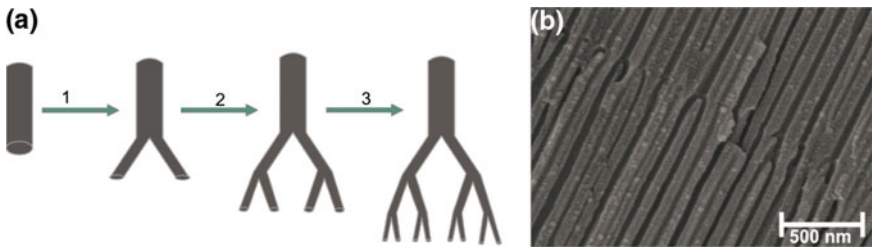

Fig. 8.2 Schematic representation of the anodization procedure used for the fabrication of AAO with hierarchical Y-branched nanopores (*1*, *2*, *3* subsequent reduction of the potential by a factor of $1/\sqrt{2}$) (**a**) together with a SEM microphotograph of the cross-section of porous AAO with Y-branched nanopores (**b**)

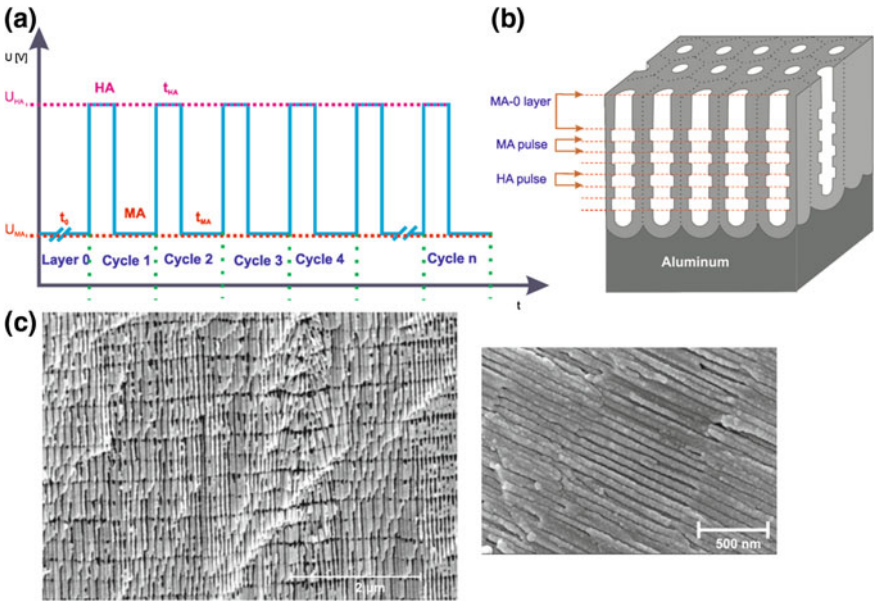

Fig. 8.3 Pulse anodization of aluminum for pore diameter modulations. Typical voltage signal applied during the pulse anodization of aluminum, where U_{MA} and U_{HA} are the anodizing potentials used to achieve mild anodizing (MA) and hard anodizing (HA) conditions, respectively (**a**). Schematic representation of AAO structure grown after a few HA and MA pulses (**b**). SEM microphotograph showing the cross-sectional views of prepared AAO layers produced by pulse anodization in 0.3 M H_2SO_4 at U_{MA} = 25 V and U_{HA} = 32 V (**c**)

views of AAO layers formed by pulse anodization in 0.3 M H_2SO_4 with a potential waveform varied between U_{MA} = 25 V and U_{HA} = 32 V.

Porous alumina with shaped pore geometries and complex pore architectures can be fabricated by periodic anodization. The concept of periodic anodization is based on the application of a periodically oscillating signal in either potentiostatic or galvanostatic mode during the anodization process. The periodic anodization of aluminum with controlled anodizing potential followed by subsequent chemical etching can lead to a periodically branched nanopores [30–32]. In this method, the anodization potential decreases linearly to a certain value of the anodizing potential, and then increases sinusoidally to the initial value of the potential. By repeating this process, a periodic structure with a main (stem) channel and branched channels is formed. The straight stem channel is formed during the high-voltage duration and each stem channel branches into several small channels during the low-voltage duration [30, 35]. The process of periodic anodization is shown in Fig. 8.4. Some modifications of the applied potential signal wave were also proposed to slightly engineer the internal pore geometry [35, 49–52]. For instance, the linear decrease in the applied potential occurring in time t_1 (as denoted in Fig. 8.5) was split into two periods with different linear slopes [35]. For the fabrication of anodic alumina with

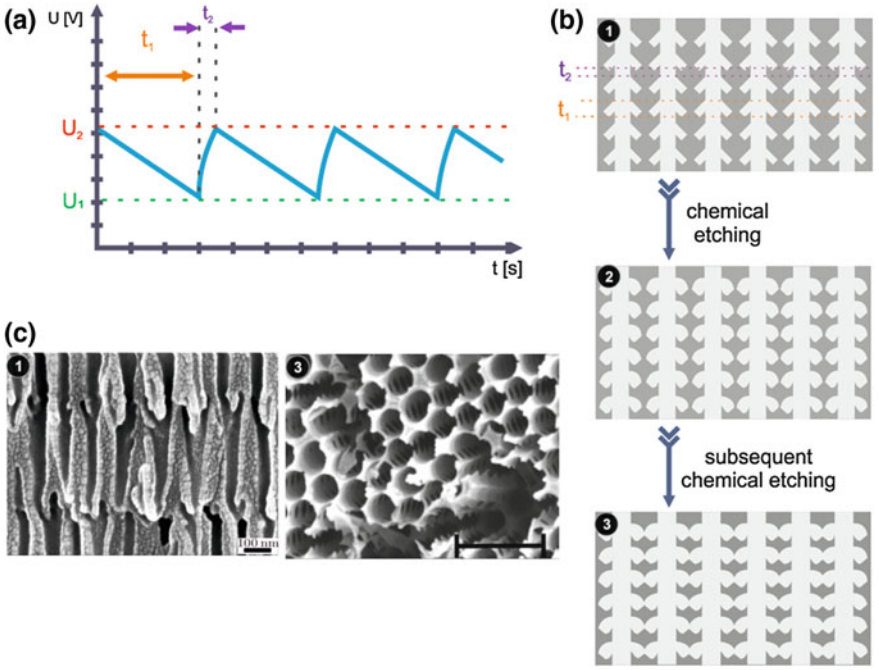

Fig. 8.4 Schematic illustration of the synthesis process for a porous anodic alumina oxide with periodically branched nanopores. Typical voltage signal applied during the periodic anodization of aluminum (**a**). Schematic representation of AAO structure grown after (*1*) a few cycles of periodic anodization and (*2*, *3*) subsequent chemical etching (**b**). SEM microphotograph showing the cross-sectional views of prepared AAO layers by (*1*) periodic anodization and (*3*) after subsequent chemical etching (**c**). **c** reprinted with permission from [32]

2-branched channels, the oxidation potential was periodically reduced by a factor of $1/\sqrt{2}$ (~ 0.71). Figure 8.5 shows schematic representation of the applied potential wave and scheme of the internal geometry of pores with a bilayered structure consisting of the layer with one large channel (layer I) and layer with two small channels (layer II). The layer I is formed during high-voltage anodization (≥ 0.71 U_H, t_1 and t_2). When the applied potential is reduced to $\sim 0.71 U_H$, the channels in the layer I begin to branch into small channels. The small channels grow during the time t_3.

Losic et al. [45, 46] for the first time demonstrated that by applying during anodization periodically oscillating current signals with different profiles, amplitudes and periods, it is possible to perform structural modulation of AAO and to control the internal geometry of nanopores. Figure 8.6 shows the concept of cyclic anodization.

They showed that this approach allows to control the internal geometry of pores by a slow change of anodization conditions (voltage or current) between the MA and HA modes using periodically oscillating signals. This is in contrast with the

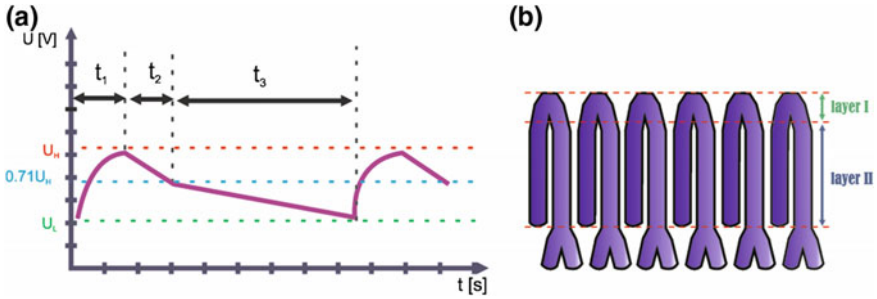

Fig. 8.5 Schematic representation of the synthesis of AAO membranes with a bilayered structure. Typical voltage signal applied during the periodic anodization of aluminum (**a**) and the scheme of the high-quality AAO prepared under the newly-designed periodic oxidation voltage (**b**). Adapted with permission from [35]

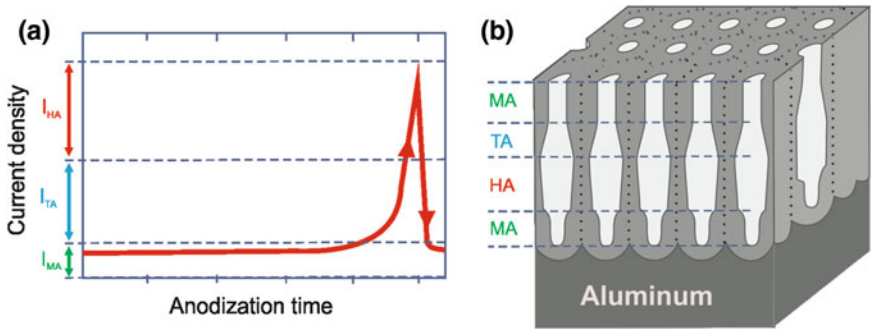

Fig. 8.6 Schematic representation of cyclic anodization of aluminum. Typical current signal applied in a single anodization cycle showing different anodization conditions (I_{MA} mild anodization current, I_{TA} transitional anodization current, and I_{HA} hard anodization current) during the process (**a**). Schematic representation of the AAO structure grown after the MA, TA and HA pulses (**b**)

concept of the pulse anodization [37, 43], where the changes between the MA and HA modes are very fast.

The modulation of the pore diameter can be also obtained by spontaneous current oscillations during hard anodization performed in an unstirred electrolyte [20, 47, 53]. The current oscillations usually appear when stirring is stopped. The observed oscillatory behavior is directly related to the diffusion of the electrolyte from the bulk solution to the bottom of the nanopores. During oxidation of aluminum under the HA regime, oxygen-containing anionic species at the bottom of pores are rapidly consumed, what is indicated by an increase in ionic current and, consequently, a large concentration gradient of anions along the pore channels is established. Depletion of anions at the pore bottoms results in retardation of the

oxidation process and thus to a decrease in current density. A new cycle starts when ions from the bulk solution will influx to the reaction interface at the bottom of pores.

The another approach to alter the internal pore structure is based on alternating repetition of anodization and pore-widening process. This method allows the synthesis inverted-cone-shaped [54–57] and step-shaped pores [26, 54, 58–60]. Figure 8.7 shows schematic illustration of the fabrication of AAO with cone-shaped and step-shaped pores. To fabricate the AAO with inverted cone-shape nanopores, repeated alternating anodization and pore widening treatments should be performed [54–57]. The shape and size of the pores in this process depends on both the anodization and etching conditions. Typically 5–7 full cycles are required to obtain desired pore shape. The main disadvantage of the method is that it leads to AAOs with very low aspect ratios (not exceeding 5). In addition, the combination of anodization and pore widening processes is used to form the AAO with step-shaped pores [26, 54, 58–60]. The procedures includes anodization followed by chemical etching of formed pore walls and finally, the sample is anodized once again for a short of time. Moreover, the AAO with reversed step-shaped pores can be

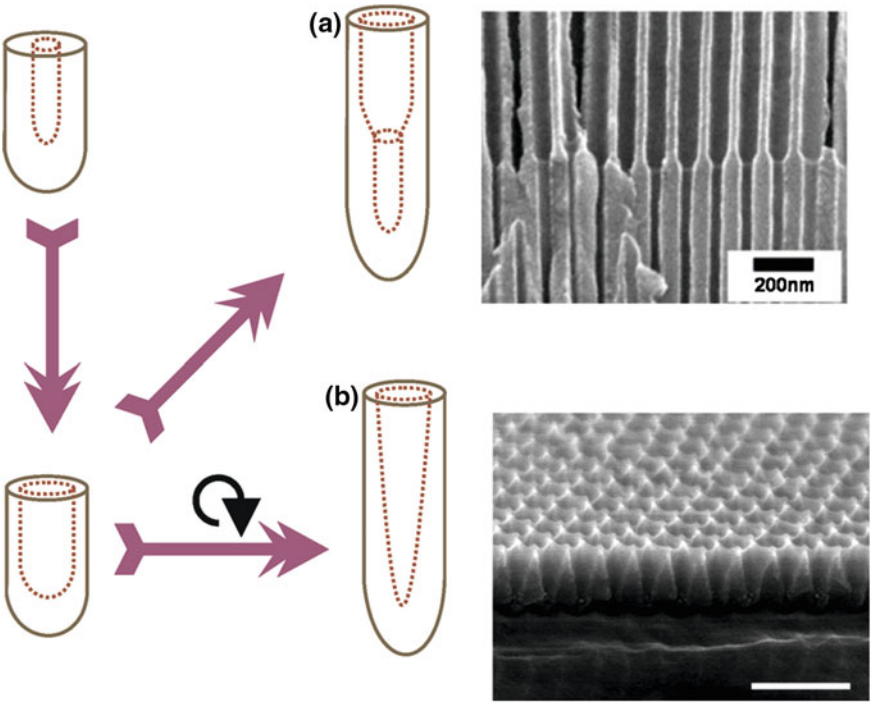

Fig. 8.7 Schematic diagram of fabrication process for the multi-step structure in single pore. Fabrication of step-shaped (**a**) and conical (**b**) pore structure. **a** and **b** reprinted with permission from [56, 58], respectively

fabricated by changing the electrolyte and applied potential during anodization [37, 59]. In turn, serrated nanopores with periodic intervals are formed in AAO when oxygen bubbles are periodically generated during anodization [61–63].

8.3 Optical Response of AAO to Light

When a beam of light is incident on the surface of porous alumina the following physical phenomena can be observed: reflection of light from the air/Al_2O_3 interface and Al_2O_3/Al interface [11, 64–75], partial absorption [11, 68, 76–87] or transmission [11, 12, 71, 77, 88–104] the remaining beam along the pores walls. Those effects were schematically shown in Fig. 8.1.

8.3.1 Reflection and Transmission in AAO

A very significant application of porous anodic aluminum oxide is its use as a decorative and protective coating. Porous alumina films can produce bright colors on reflections in the visible light range but their saturation is relatively low [73]. The low color saturation of AAO on the Al substrate is due to the fact that aluminum highly reflects visible light. A good way to change the AAO color or increase its saturation is (i) sputtering a thin metallic layer (e.g. Ag [33, 68, 105], Cr [105] and Pt [106]), (ii) deposition of metallic nanowires in the pores (Ni [107–109], Co [110], and Ag [33]), (iii) removal of the aluminum substrate after anodization [73, 74], and (iv) modification of internal pore structure [105–110]. The reflection of light from the porous alumina layers is affected by many factors including residues of the Al substrate [73, 74], pore diameter [64, 67], thickness of AAO [66, 69, 71, 73–75], and the existence of other molecules and compounds in the pores or on the AAO surface [101, 105–108, 110].

Xu et al. [73, 74] studied the effect of remaining aluminum substrate on the optical properties of porous anodic alumina oxide. Figure 8.8 shows schematically the interaction of the incident light beam with the porous AAO film before (Fig. 8.8a) and after (Fig. 8.8b) removal of the aluminum substrate. The color of AAO film with the supporting Al substrate mainly comes from the interference of two beams reflected from the air/Al_2O_3 interface and Al_2O_3/Al interface. The phase difference is related only with the optical path difference. After removal of the supporting Al layer, except the phase difference caused by the path difference there is additional a phase change difference between the two reflections. Therefore, the removal of the Al substrate affects the observed color of AAO. Figure 8.8c illustrates this effect. The observed pink color corresponds to the AAO film on the Al substrate while the deep green area in the center of the sample shows the AAO film after the removal of the Al substrate. This indicates that the reflected light from the

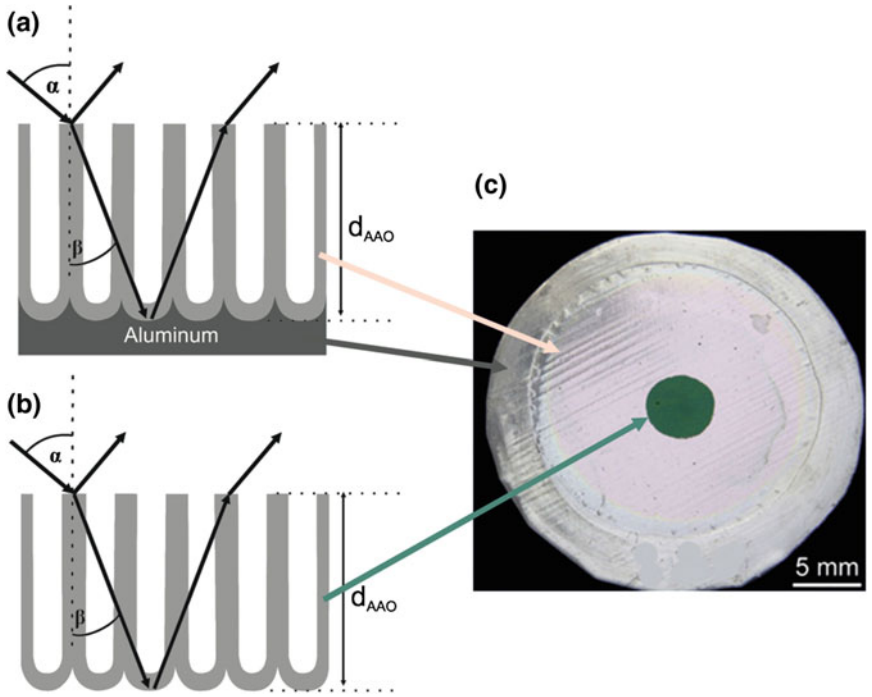

Fig. 8.8 Schematic interaction of the light beam with a porous AAO film before (**a**) and after **b** removal of the Al substrate. Optical photograph of the AAO film after a partial removal of Al substrate in the center of the sample (**c**). Reprinted with permission from [74]

alumina/Al interface has an important effect on the color of AAO. The color can be altered by changing of incident angle as is expected by Bragg's equation [73].

Reflectance of AAO films depends also on the thickness of the anodic alumina oxide layer [66, 69, 71, 73, 74]. The thickness of the aluminum oxide layer can be controlled by anodization time [69, 73, 74], and temperature [66]. By varying the anodizing time, it is possible to modulate reflectance of AAO. Figure 8.9 shows the influence of oxide thickness on the reflectance spectra for the AAO with or without the remaining Al layer. By increasing the anodization time, the thickness of the oxide layer increases and a red shift in the peak position is observed for both types of AAO samples. On the other hand, as was previously mentioned, the removal of the Al layer results in a blue shift of the peak position.

The reflectance spectrum of the porous AAO film depends on the pore diameter of the AAO membrane [64, 67]. Kant et al. [67] studied the influence of pore diameter of AAO on its reflectance. The pores of different sizes were generated on the same sample along a longitudinal direction by a non-uniform anodization of unpolished aluminum alloy. The SEM microphotographs taken at different parts of the sample show that the nanopores are aligned in parallel lines in the same manner as rows are distributed on the rolled and unpolished Al foil (Fig. 8.10a–e).

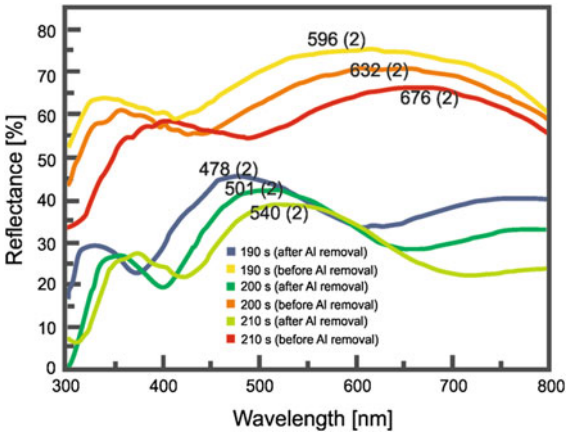

Fig. 8.9 Reflectance spectra of the AAO films before (*top*) and after (*bottom*) removal of the Al layer for different anodizing durations: 210, 200, and 190 s. Reprinted with permission from [74]

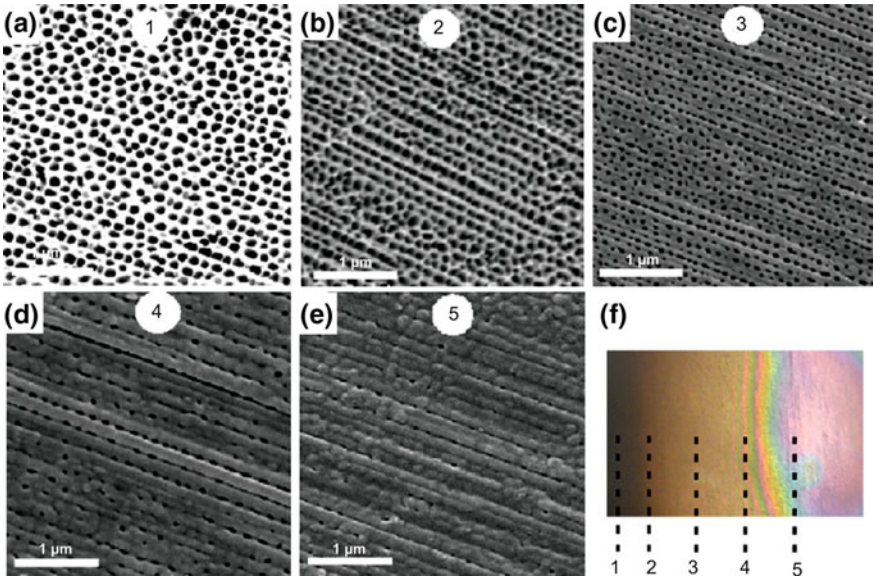

Fig. 8.10 SEM microphotographs of the AAO surface with different pore diameters at different locations on the tilted electrode formed by anodization of low purity Al foil (**a**–**e**). The anodization was performed in 0.3 M phosphoric acid at the current density of 100 mA cm^{-2} and 0 °C. The angle between electrodes was 45°. Photo of the prepared AAO surface with marked locations (*1*–*5*) where SEM images were acquired (**f**). Reprinted with permission from [67]

Figure 8.10f shows the photo of the prepared AAO sample. A gradual change of color from golden to pink corresponding to the gradual change of pore diameter is visible.

Ghrib et al. [64] studied the effect of annealing temperature on the reflectance spectra of AAO. It was found that the reflectance of AAO increases from about 80 to 96 %, respectively before and after annealing at 650 °C. The increase in reflectance of the annealed AAO is caused by decreasing porosity of alumina and modification of the structure leading to higher packing density.

The observed reflectance spectra depend also on which side of the AAO membrane was tested (Fig. 8.11) [111]. As can be seen, the reflected light shows complementary colors, while the transmitted light presents similar colors. The corresponding reflectance and transmittance spectra of the AAO sample are presented in Fig. 8.11e. In the reflectance spectra some oscillations are clearly visible and their presence can be ascribed to a complex interference occurring in the AAO film.

As was shown in Fig. 8.1 the incident beam light can be also partially reflected inside the nanopores of the anodic film, and therefore the AAO can be treated as a Fabry-Pérot interferometer [112]. Consequently, well resolved fringe patterns (oscillations) result from Fabry-Pérot interference of the light reflected from multiple interfaces can be observed in the reflectance spectrum as shown in Fig. 8.11 [111, 113, 114]. The signal oscillations are commonly observed also in transmission [12] and photoluminescence spectra [67, 115–117] of AAO films.

The transmittance spectra tested from the top and the back sides of the AAO membrane are nearly the same. These result correlates perfectly with the observed similar color of the sample (see Fig. 8.11). A strong absorption below 350 nm visible in the transmittance spectra (Fig. 8.11e) is induced by a supporting glass substrate. In general, porous anodic aluminum oxide is transparent to visible light, however, its permeability depends on many factors such as type and amount of

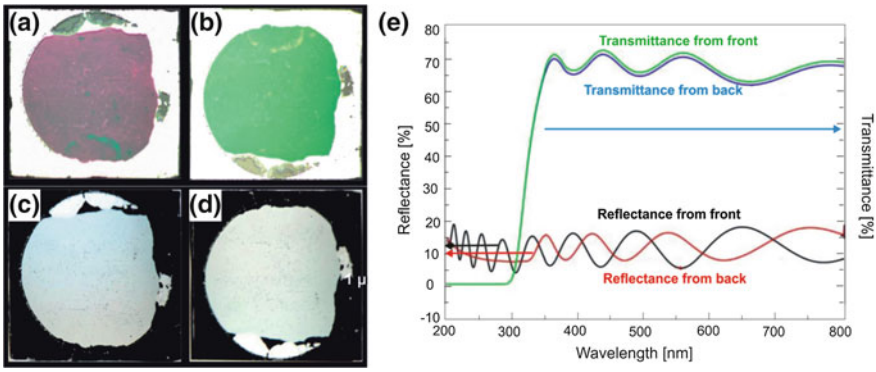

Fig. 8.11 Reflectance (**a**, **b**) and transmittance (**c**, **d**) photographs taken from the top side (**a**, **c**) and back side (**b**, **d**) of the AAO membrane together with the corresponding reflectance and transmittance spectra (**f**). Reprinted with permission from [111]

incorporated impurities [77, 87, 93, 95–98, 103, 104, 118], thickness of the oxide layer [12, 71, 89, 95, 102, 103], and pore diameter [12, 88, 89, 91, 93, 94, 103, 119]. Not surprisingly, it was shown that the increased transmittance of AAO film with increased pore diameter is attributed to the decreased refractive index of AAO layer. It was also reported that during the heat treatment impurities incorporated in the AAO structure are removed and phase transitions occurred [95]. As a result of that, a decrease in the number of absorption centers and increase in transmission are observed [103, 119]. The transparency of porous anodic alumina films in the visible light range is very important for LCD panel applications [90].

8.3.1.1 Absorption in AAO

The beam of light incident on the surface of porous anodic alumina can be absorbed. The absorption of the incident beam depends on the film thickness [11], pore diameter [11], impurities in the oxide structure [19, 76–78, 80, 83, 85, 87, 91, 120, 121], impurities in the pores [81, 94], and post annealing process [83]. Absorption of incident light beam on the porous AAO film depends also on the structural characteristic of anodic aluminum oxide [11, 91] and beam incident angle [11]. The AAO films synthesized at different anodization conditions have different dimensional features (pore diameter, wall thickness, etc.). Therefore, the incident light beam interacts with the AAO surfaces with different geometrical parameters and light is absorbed in different degree. Figure 8.12a shows the influence of porous film thickness on the optical path length of incident beam and the number of

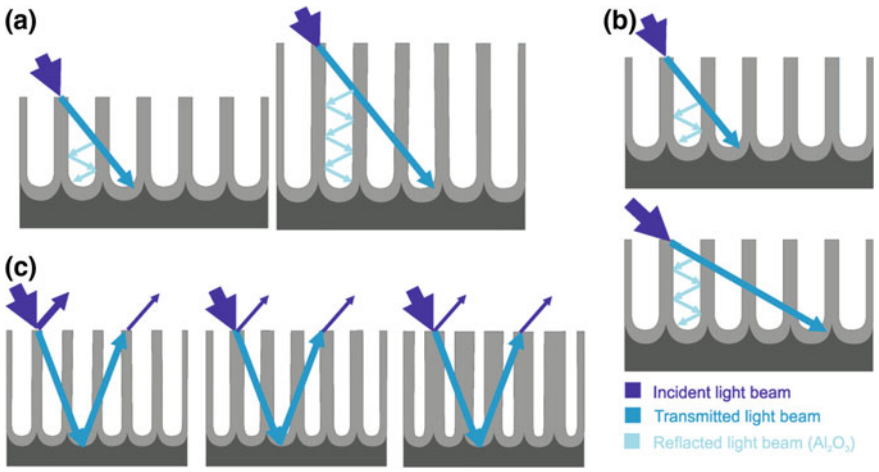

Fig. 8.12 Diagram showing the influence of the AAO thickness (**a**) and incident angle (**b**) on the passage length of penetrated beam and the number of reflections inside the pores. Influence of pores area percentage (porosity) on the reflected beams intensity (**c**). Reprinted with permission from [11]

reflections inside the pores. For the light beam incident on the porous AAO surfaces with different film thicknesses it can be seen that absorption increases with increasing AAO thickness [11, 91]. It comes from the fact that the incident beam becomes weaker when passing across the increasing number of pore walls. In addition, as the pore length increases more reflections occur inside the nanopores. Figure 8.12b shows the effect of incident angle on the optical path length of light beam and the number of reflections inside the nanopores. It can be seen also that optical absorption increases with increasing incident angle. With increasing incident angle the light beam passes across the higher number of pore walls. Figure 8.12c shows the effect of porosity of the AAO layer on its optical properties. According to Moghadam et al. [11] light absorption in AAO increases with decreasing porosity, and then after reaching the maximum for about 15 % decreases with a further porosity decrease. The poor absorption of light observed for the sample with the highest porosity was attributed to a high pore fraction which make it easier for the incident beam to access the high reflective Al surface. According to this hypothesis, the reduction of AAO porosity diminishes the intensity of reflected beams to the point when the thickness of pore walls is large enough to provide a significant planar surface area on AAO top for enhanced light reflection.

It is widely recognized that during anodization of aluminum in acidic electrolytes, acid anions are incorporated into the AAO structure [8, 19]. Due to the larger size and lower mobility of acid anions compared with O^{2-} and OH^{-}, the acid anions migrate in the electric field during anodization from the solution to anode and their content decreases from the outer to the inner layer of the pore walls [8, 77]. The anions incorporated into the AAO film play a role of absorption centers to the incident light beam. Recently Fan et al. reported that with decreasing concentration of $C_2O_4^{2-}$ ions an increase in the refractive index and absorption coefficient was observed [77].

Li et al. [83] recorded the absorption spectra for the AAO membranes formed in oxalic acid and sulfuric acid. The absorption spectrum for the oxalic AAO membrane showed an additional absorption band at 294 nm when compared to that for the sulfuric AAO membrane. It was considered that this absorption band is derived from $C_2O_4^{2-}$ ions which are incorporated in the AAO structure. The samples annealed above 550 °C do not absorb at 294 nm and it is associated with a heat-dissolution of $C_2O_4^{2-}$ in the AAO membrane [81]. With increasing annealing temperature, the intensity of both absorption bands at 370 and 254 nm, increases, reaches a maximum (at 480 and 550 °C, respectively), and then decreases. The observed changes in intensity of the absorption bands were attributed to effective number of oxygen vacancies in the oxide structure. In addition, as the annealing temperature increases the shift of absorption bands to shorter wavelengths was reported. In turn, this phenomenon was ascribed to the release of internal stress of the AAO film.

Fan et al. [77] examined the role of $C_2O_4^{2-}$ anion impurities on absorption coefficient. The absorption spectra of the AAO films with different thicknesses were recorded. It was found that the absorption band gradually broadens as the thickness of AAO film increases. Such behavior is caused by increasing amount of $C_2O_4^{2-}$

anion impurities incorporated in AAO films. Gao et al. [78–80] obtained similar results. They conducted anodization of aluminum in oxalic acid, sulfuric acid, and in a mixture of oxalic and sulfuric acids. The results indicated that the absorption spectra for the oxalic AAO film showed the absorption bands, in contrast to the sulfuric AAO film. Yang et al. [87] studied the influence of sulfosalicylic acid (SSA) presence in the electrolyte on the optical properties of porous anodic alumina membranes. For this purpose, they conducted anodization of aluminum in the different mixtures of sulfosalicylic acid and sulfuric acid. The recorded absorption spectra in the UV-Vis range showed that for the sample prepared in sulfuric acid only, an absorption band edge of alumina was observed as previously reported [78–80, 83]. For the AAO films obtained through anodization in the mixed electrolytes (H_2SO_4 + SSA) absorption bands at about 343 and 248 nm were observed. It was revealed that the intensity of the absorption bands in the absorption spectra of the AAO films, increases with increasing of concentration of SSA. These results indicate that the AAO samples obtained by anodization in various acidic electrolytes have a different intrinsic structural characteristics.

The absorption of the incident light beam on the porous AAO film can be enhanced by other ions [84, 122] incorporated during anodization in the oxide structure. The absorption of light in the UV-Vis region can be enhanced by incorporated Cr^{3+} ions [84, 121]. The absorption bands are associated with three electron transitions of Cr^{3+} in α-Al_2O_3 [84]. Similar results were obtained by Stępniowski et al. [121].

The absorption centers of AAO films can be changed by thermal annealing. Efeoglu et al. [76] studied the anodization of aluminum sputtered on Si substrate in oxalic acid. To deactivate the absorption centers, the AAO films were thermally annealed at 250–950 °C. It was found that the optical activity of the AAO film is attributed to oxygen-related defects and partly to impurities that may be originated from oxalic acid. As can be seen in Fig. 8.13 the absorption is sensitive to a high density of defect levels within the band gap. The theoretical band gap of Al_2O_3 is around 200 nm, however the effective absorption within the band gap is evident and becomes stronger after annealing at 550 °C. Such a strong absorption is related with an increase in oxygen defect density to the highest level. With a further temperature increase the tails decrease at 950 °C and, finally disappear at 1050 °C. It indicates that the annealing above 1000 °C results in a less defected material and Al_2O_3 becomes optically transparent from deep UV to NIR region.

8.4 Photoluminescence Properties of AAO

8.4.1 The Origin of Optical Centers in AAO

The optical properties of aluminum oxide have attracted the attention of scientists since the 70s of the last century, however, the first report on the photoluminescence (PL) properties of nanoporous AAO appeared in 1999 [123]. Since then, many

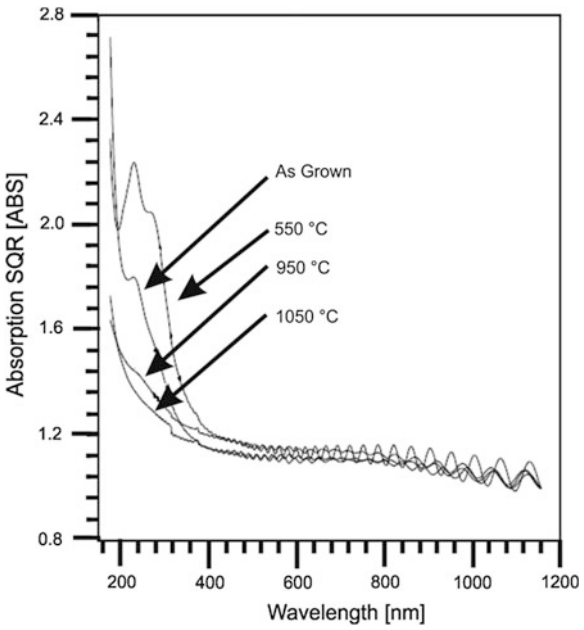

Fig. 8.13 Optical absorption of Al_2O_3 for different annealing temperatures. Reprinted with permission from [76]

studies have been done to clarify the mechanism of PL spectra and to determine the parameters which affect the optical properties of AAO [79, 124, 125]. The initial studies have primarily focused on the determination of types of optical centers present in the structure of porous alumina oxide obtained through anodization. For this purpose, the obtained PL spectra were compared with the corresponding results for sapphire [85, 126, 127]. In 2003, Gao et al. [79] found that the photoluminescence properties of AAO are induced by electrolyte ions incorporated into the oxide structure during anodization. Recently, it has been postulated that the PL mechanism of the anodic aluminum oxide is complex and depends on both the optical center distribution and embedded anions.

Optical centers dispersed in the porous structure of anodic aluminum oxide are associated with the presence of oxygen vacancies. Depending on the type of electrolyte used for anodization, it is possible to produce oxide coating containing two or more layers [8, 19]. The outer layer (which is in contact with the electrolyte or air) contains a higher amount of impurities (e.g. embedded ions or structural defects) than the inner layer close to the cell boundaries (Fig. 8.14) [128]. During anodization OH^- ions are transferred to the vicinity of the oxide/metal interface, where are converted to O^{2-} ions which react with Al to form Al_2O_3 and oxygen vacancies. Generally, the concentration of oxygen vacancies in the formed AAO film is inversely proportional to the concentration of hydroxide ions in the electrolyte. Huang et al. found that the photoluminescence properties of porous alumina correspond to more than one type of optical centers [129]. Besides F^+ defects, being oxygen vacancies with one electron and giving an intensive peak in PL spectra, it is

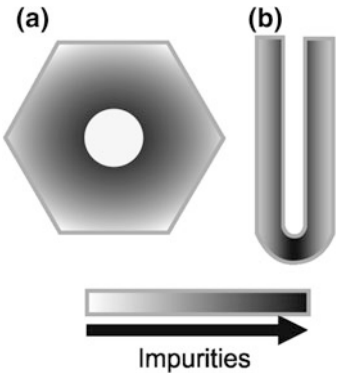

Fig. 8.14 The layered structure of AAO nanopore: top (**a**) and cross-sectional (**b**) view. Reprinted with permission from [128]

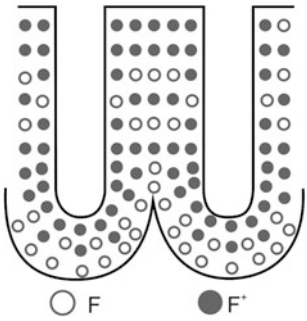

Fig. 8.15 Arrangement of optical centers in the porous structure of the AAO. After [94, 129]

also possible to observe F centers (doubly ionized oxygen vacancies) and less likely unstable F^{++} centers (vacancies without electrons) [94, 129–131]. Figure 8.15 presents a distribution model of different type of optical centers in AAO. According to previous research [94, 129], F^{+} centers are located mainly in the outer layer of AAO, while the F type centers are distributed in the inner oxide layer.

The second factor influencing the PL spectrum is the previously mentioned effect of incorporated acid-anions that contaminate the outer oxide layer next to the pores [99, 101, 122, 132–134]. The incorporation of acid anions during the anodization is possible due to their inward migration under an electric field toward the oxide/metal interface. Acid anions, formed by the dissociation of the anodizing electrolyte can be incorporated into the structure of oxide during its growth, and may replace O^{2-} in the oxide [12]. Due to the influence of a high electric field or by Joule heating inside the pores, incorporated oxalate ions can be transformed into optical centers

[104, 135]. For example, during anodization in oxalic acid the following reactions take place (8.1, 8.2):

$$^{3}/_{2}H_2O \rightarrow 3H^+ + {}^{3}/_{2}O^{2-} \tag{8.1}$$

$$HC_2O_4^- \rightarrow C_2O_4^{2-} + H^+ \tag{8.2}$$

As a result, the O^{2-} ion in the oxide layer could be easily substituted by the oxalate anion. The similar situation is in the case when other acids are used for anodization. The concentration of incorporated ions depends on the conditions of anodization i.e. the type and concentration of the electrolyte, temperature and applied anodizing potential. In the following subsections, the factors affecting the shape of the peaks, their spectral shift and PL intensity of AAO will be throughly discussed.

8.4.2 Factors Affecting PL of AAO

Among the factors having a significant impact on photoluminescence spectra of anodized alumina, special attention should be given to the following:

a. purity and polishing of the starting material
b. anodizations regimes: mild and hard anodizations
c. pore diameter and porosity of AAO, which depend on the anodization conditions (type of electrolyte, applied potential, temperature, etc.)
d. thickness of the oxide layer
e. etching and widening of pores
f. post-annealing of AAO
g. different internal pore structure of AAO
h. modification of the AAO surface and pore walls with nanoparticles
i. filling the pores of AAO with metals/oxides/polymers/dyes organic compounds, etc.

8.4.2.1 Purity and Polishing of the Starting Material

The purity of the aluminum foil and the preparation of the starting material for anodization significantly affect the quality of obtained AAO nanostructures. Pershukevich et al. [136] carried out a study on the anodization of aluminum alloy and high-purity Al foil. It was shown that the recorded photoluminescence spectra are comparable and the type of active centers does not depend on the purity of the starting material. On the other hand, Kokonou et al. [137] reported that the intensity of the PL spectrum of the AAO film obtained in citric acid by anodization of the

aluminum alloy containing 1 % of Si was lower compared to the PL intensity of the AAO from pure aluminum.

The pre-treatment of the starting material has a huge impact on the quality of nanopore order and presence of defects, and consequently, on the PL spectrum [138]. It was found that the PL spectra are affected by the electropolishing pre-treatment mainly by the type of the used electropolishing mixture. A red shift in the PL spectra was observed for the Brytale solution compared to the perchloric acid-alcohol solution used for electropolishing samples anodized at 40 V. The opposite shift in PL spectra was noticed for the higher anodizing potentials. When the defect density (pore disorder) of AAO increases a red shift in the PL spectrum is observed due to probable enhanced accommodation of F centers at defects [138]. This is attributed to increased number of pentagons and hexagons with missing pores and, consequently, to a large number of metallic protrusions (hills) which change the relative curvatures of the electrolyte/oxide interface with respect to the oxide/metal interface. In the aftermath of that the field distribution at the barrier layer is different from the rest of the oxide, electrostriction, volume expansion stresses and flow of the oxide are different at the defects.

8.4.2.2 Anodizing Regimes: Mild and Hard Anodizations

It is worth mentioning that the anodizing protocol influences the photoluminescence spectra of AAO films. It was found that the PL intensity of the AAO formed in the mixture of oxalic acid and ethanol is higher under mild anodization regime than under hard anodization conditions (Fig. 8.16) [139]. It has been shown that the presence of ethanol as a coolant does not affect significantly the PL spectra (curves 1 and 2 in Fig. 8.16). The AAO sample obtained in the same electrolyte but at 130 V has much lower PL intensity (curve 3). There is also observable a shift of the peak position from 440 to 490 nm. Both decline of intensity and red shift can be attributed to the reduction of single ionized oxygen vacancies [139]. The optical properties of the AAO films formed by hard anodizations performed at different anodizing conditions will be discussed in detail below.

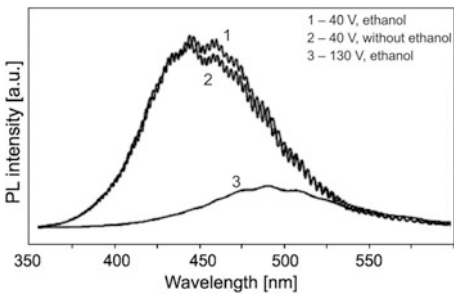

Fig. 8.16 PL spectra obtained for the nanoporous AAO films received by hard anodization of Al foil in 0.1–0.5 M oxalic acid with and without ethanol. Reprinted with permission from [139]

8.4.2.3 Anodization Conditions

Depending on the electrolyte used for anodization it is possible to obtain AAO structures with different geometrical parameters, i.e. pore diameter, interpore distance, porous oxide layer thickness, porosity etc. [4, 87, 97–99, 118, 121, 122, 134, 136, 140–143]. The photoluminescence properties of AAO formed in commonly used acid electrolytes such as sulfuric, oxalic and phosphoric acid, were studied in detail [137, 144–148]. It has been proven that the AAO films obtained in oxalic acid have a different photoluminescence excitation mechanism than those formed in phosphoric or sulfuric acid [137, 145]. The comparison of photoluminescent spectra for AAO samples formed in oxalic, sulfuric and phosphoric acid is shown in Fig. 8.17. Clearly, the intensity of the PL spectrum for the AAO anodized in oxalic acid is much higher compared to other electrolytes. Deconvolution of this spectrum obtained for AAO anodized in oxalic acid showed the presence of three peaks associated with the presence of the different optical centers namely F (435 nm), F^+ (398 nm) and oxalate impurities (473 nm) [145]. The observed high intensity of the spectrum is caused by the high concentration of oxygen vacancies. Oxalic acid belongs to the dihydric acids group. The presence of σ bonds and especially delocalized π bonds are responsible for easy excitation of incorporated oxalate ions in the ultraviolet region [100]. Therefore, high intensity of the PL spectra of AAO formed in oxalic acid can be explain by combining the effect of high concentration of oxygen vacancies and the luminescence properties of oxalate ions due to the presence of delocalized electrons of π bonds. On the other hand, low PL intensity of AAOs obtained in sulfuric and phosphoric acid is caused by the presence of two optical centers F and F^+, and much smaller contribution of embedded acid anions in the spectrum. Shi et al. showed that photoluminescence intensity of AAO prepared in phosphoric acid is higher compared to those obtained in sulfuric acid. This is due to the increased incorporation of PO_4^{3-} ions compared to SO_4^{2-} [132].

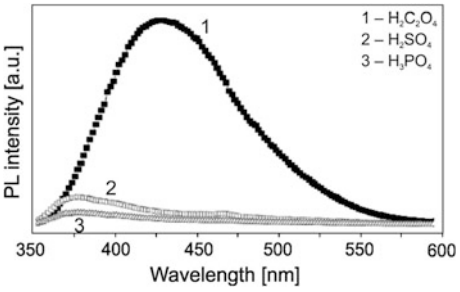

Fig. 8.17 PL spectra obtained for porous AAO by anodization in optimal conditions in: (*1*) 0.3 M oxalic acid, 40 V, 11 °C, (*2*) 0.3 M sulfuric acid, 25 V, 6 °C, (*3*) 10 % phosphoric acid, 60 V, 6 °C. Reprinted with permission from [145]

In 2003, Li et al. [144] postulated that the origin of photoluminescence from AAO obtained in sulfuric and oxalic acid is the same. It is widely recognized that $C_2O_4^{2-}$ and SO_4^{2-} ions incorporate during anodization into the oxide layers. Recently, it has been revealed that not only the oxalic impurities but also the sulfuric and sulfosalicylic impurities incorporated in AAOs can be converted into luminescent centers and both affect the PL properties of AAOs [87, 149]. In order to demonstrate the influence of oxalate and sulfate anions on the PL spectra of AAOs, a number of experiments on Al anodization in various mixtures of these acids was performed [78, 80, 133, 146, 149]. The obtained PL spectra are shown in Fig. 8.18. Besides the typical emissions centered at 370, 385 and 470 nm, Li et al. observed the new emission peak at 290 and 325 nm for AAOs anodized in sulfuric acid and oxalic acid, respectively. The same PL peaks appeared when the AAO sample was formed in the mixed solution of both acids [149]. Furthermore, as the volume ratio of acids changes the intensity of both peaks changes as well. With the increase of SO_4^{2-} concentration in the electrolyte, the intensity of peak centered at 325 nm initially increases ($V_{sulf}/V_{ox} < 6$), and then decreases ($V_{sulf}/V_{ox} > 6$). The opposite tendency was observed for the 290 nm emission. In order to understand the PL behavior it is necessary to analyze the mechanism of energy transfer in AAO formed during anodization in a mixture of acids (Fig. 8.19). According to Li et al., the process of energy transfer can be divided into three stages: (1) absorption of photon energy by electrons, (2) thermal relaxation of electrons to a lower energy level, e.g. impurity levels of sulfate and/or oxalate ions, (3a) the spontaneous radiation of energy by decay from the impurity energy levels (S or C) to the ground state and (3b) nonradiative energy transfer between the impurity levels of SO_4^{2-} and $C_2O_4^{2-}$ accompanied by the weakened emission 3a and enhanced emission 3b [149]. Due to the incorporation of both types of ions in the oxide structure, step 3b is the most favored. According to the data published by Wang et al., the intensity of

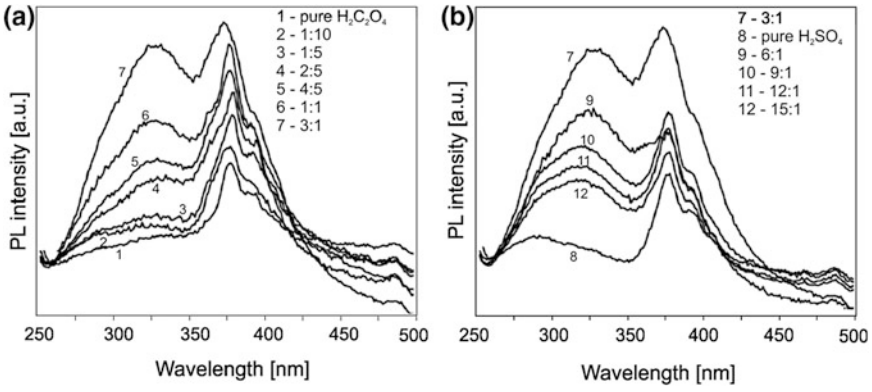

Fig. 8.18 Comparison of PL spectra for AAO obtained in the mixture of 0.3 M sulfuric acid and 0.3 M oxalic acid: **a** *(1)* pure oxalic acid, *(2)* 1:10, *(3)* 1:5, *(4)* 2:5, *(5)* 4:5, *(6)* 1:1, *(7)* 3:1, **b** *(8)* pure sulfuric acid, *(9)* 6:1, *(10)* 9:1, *(11)* 12:1, *(12)* 15:1 the volume ratio of sulfuric to oxalic acid. Reprinted with permission from [149]

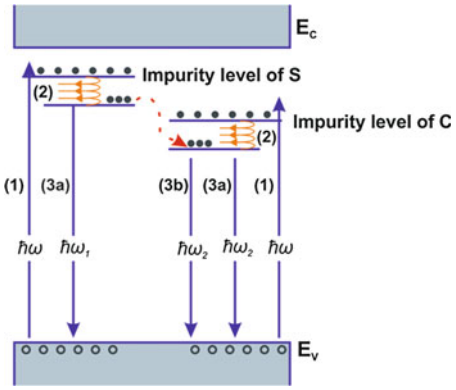

Fig. 8.19 Energy transfer mechanism in porous alumina with embedded SO_4^{2-} and $C_2O_4^{2-}$ ions. Reprinted with permission from [149]

Table 8.1 The effect of electrolyte used for anodization on the position of the maxima of the peaks in the PL spectrum

Electrolyte	Anodization conditions	PL peaks position	Type of optical centers	References
0.3 M chromic acid	20–50 V, 50 °C	255 nm, 350 nm	Embedded chromate ions	[121]
0.01 M citric acid	15 mA cm^{-2}, 17 °C	425 nm	F^+	[99]
		460 nm	F	
1 wt% citric acid	Room temperature	550–580 nm	F^+	[137]
0.8 M malonic acid	80 V, 18 °C	440–450 nm	Embedded malonate ions	[118]
0.8 M malonic acid	6 mA cm^{-2}, 18 °C	438 nm	Embedded malonate ions	[134]
		501 nm	F^{2+}	
0.3 M sulfamic acid	30 V, 24 °C	460 nm	F	[98]
0.4 M tartaric acid	6 mA cm^{-2}, 18 °C	440–450 nm	Embedded tartarate ions	[143]
2 wt% sulfuric acid + 0.02 M Cu^{2+} + 0.02 M EDTA	15–21 V, 15 °C	280 nm	Embedded Cu-EDTA anionic species	[122]
		320 nm		
		>360 nm	F	

peak in the PL spectrum for the AAO obtained in the mixture of sulfuric and oxalic acids depends mainly on the concentration of oxalate ions [133]. Changes in the content of SO_4^{2-} anions can, however, cause a shift of the peak towards lower wavelengths (410 nm → 345 nm). When the concentration of the sulfate anions remains constant, a decrease of peak intensity with increasing concentration of $C_2O_4^{2-}$ ions is observed [133].

Although the most commonly used acids for the anodization are sulfuric, oxalic and phosphoric acid, scientists have tested other electrolytes as well, for example: chromic acid [121], citric acid [99, 137], malonic acid [118, 134], sulfamic acid

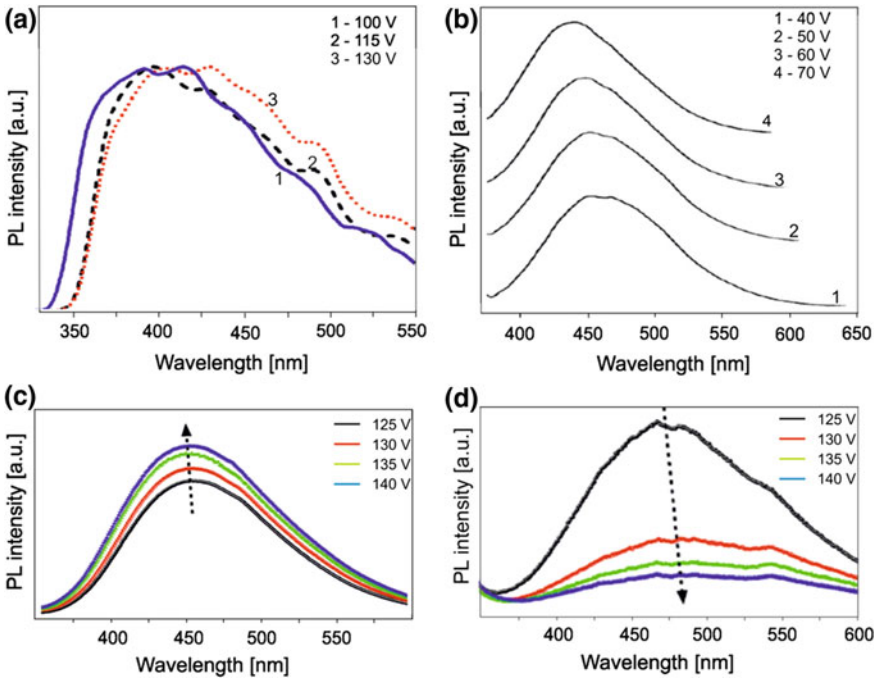

Fig. 8.20 The influence of anodizing potential on the peak position in the PL spectrum for AAO obtained by mild anodization in: 85 wt % H_3PO_4, 1 °C (**a**), 0.3 M $H_2C_2O_4$, 1 °C (**b**), and by hard anodization in: 0.3 M oxalic acid (**c**), 1.7 M malonic acid (**d**). Reprinted with permission from [150] (**a**), [138] (**b**), and [142] (**c** and **d**)

[98], tartaric acid [143], electrolyte containing the Cu-EDTA complex [122], etc. Clearly, the AAOs obtained in all these electrolytes exhibit differences in the PL spectra especially in peak positions (see Table 8.1). This is mainly related with differences in the electronic structure of embedded ions.

It has been proven that the anodization potential greatly affects the position of the peaks in the PL spectrum and, thereby, the type and arrangement of optically active centers in the porous oxide structure. Nourmohammadi et al. [150] showed that during anodization performed in phosphoric acid, an increase in anodization potential up to 115 V causes a slight red shift of the PL peak (Fig. 8.20a). The increase in applied anodizing potential results in the formation of optically active defects which subband gaps are in the range of visible light. Deconvolution of the PL spectra showed the presence of the five components [150]. Similar studies were performed for the AAOs obtained in oxalic acid [138]. Figure 8.20b shows the effect of potential used for anodization in oxalic acid on the peak position in the PL spectra. A significant shift towards the longer wavelengths (similarly to that observed for AAO membranes formed in phosphoric acid) was observed with increasing anodization potential (40 → 70 V). Despite the large number of published papers on photoluminescence properties of AAO obtained in sulfuric acid,

there is no conclusive research on the effect of anodizing potential on the PL peak position. It should be noted, that the potential of anodization influences not only the geometric parameters of AAO, but also the thickness of resulting oxide and, thus, the amount of incorporated acid ions from the electrolyte. Santos et al. conducted a study on the effect of anodizing potential on optical properties of the AAO films formed by hard anodization of aluminum in oxalic acid and malonic acid [142]. They showed that for oxalic acid with increasing potential of hard anodization from 125 to 140 V (Fig. 8.20c) a slight increase in the intensity of the PL peak can be observed [142]. For the AAOs formed in malonic acid at the same potential range, the decrease in the peak intensity and the red shift of peak were observed with increasing anodization potential (Fig. 8.20d).

Another parameter that significantly affects the growth of oxide during anodization and, consequently, PL properties of AAO is temperature. Green et al. have demonstrated that during anodization in oxalic acid the increase in temperature from 2 to 20 °C results in a 10 nm red shift [66]. As mentioned previously, the photoluminescence properties of AAO are affected by the presence of oxygen vacancies and acid ions impurities. As shown by Stępniowski et al., the lower the anodization temperature the less ions from the electrolyte are incorporated into the oxide structure [121]. It can therefore be concluded that for the AAO films obtained at low temperatures the predominant optical centers are single ionized vacancies (F^+). Increasing anodizing temperature leads to an increase in current density during anodization process, and thus enhances the ability of oxygen vacancies to capture electrons (conversion of optical centers from F^+ on F). Therefore, a higher density of F centers should be expected for higher anodizing temperature (lower energy PL peak) [66].

8.4.2.4 Thickness of the Oxide Layer

The thickness of oxide layer obtained by anodization depends directly on the total amount of charge involved in the electrochemical process. Consequently, for a steady-state conditions of anodization, the thickness of the porous oxide layer increases with increasing anodization time [141]. The thickness of the oxide layer has an obvious impact on the shape and intensity of the PL spectrum. For the AAOs obtained in phosphoric acid (t = 11–40 h), Novrmohammadi et al. found that the thicker the alumina layer the widen the whole emission PL spectrum is (Fig. 8.21a) [150]. Moreover, a peak shift toward shorter wavelengths was observed. According to the model shown in Fig. 8.15, the distribution of the F and F^+ optical centers is not uniform in the oxide structure. Thus, the longer the anodization process and, consequently, the thicker the resulting oxide layer, the greater the possibility of creation new point defects. It is worth mentioning that applying a potential to the electrode for a long period of time may cause conversion of the F^+ centers into the neutral F centers by trapping electrons from negatively charged electrolyte anions.

The effect of anodization time and hence thickness of the oxide layer on PL of AAOs formed in oxalic acid was studied by Chen et al. [124]. It was found that for anodizations shorter than 15 min (oxide thickness of about 850 nm) a small red shift

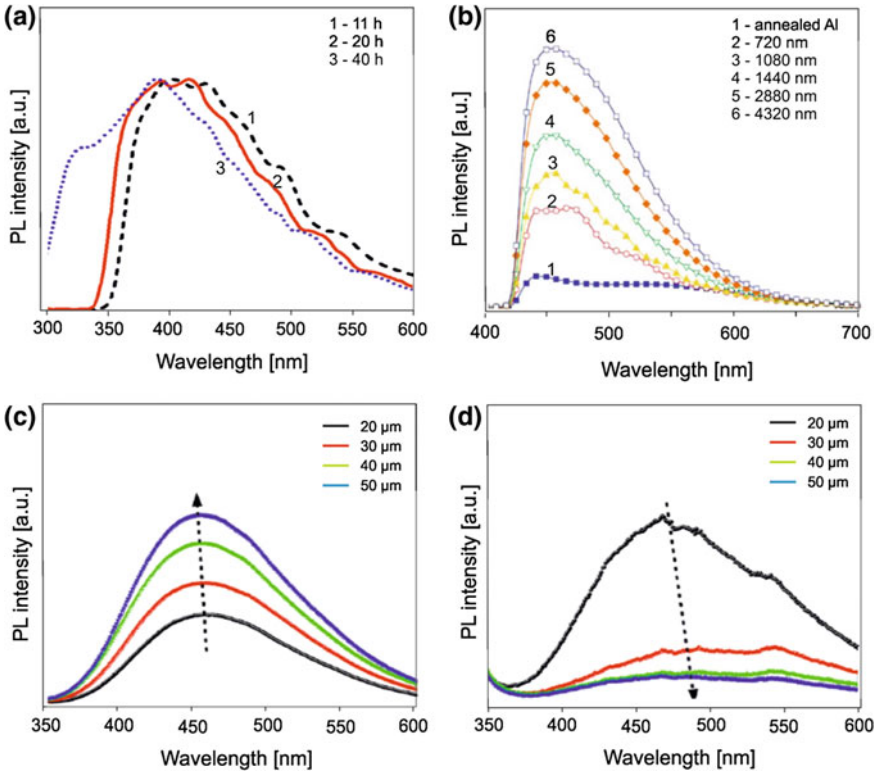

Fig. 8.21 The influence of anodizing time on PL spectra of AAO obtained by mild anodization in: phosphoric acid (85 wt%, 1 °C, 100 V) (**a**), oxalic acid (0.3 M, 20 °C, 40 V) (**b**), or by hard anodization in: oxalic acid (0.3 M, 0 °C, 120–140 V) (**c**), and malonic acid (1.7 M, 0 °C, 120–140 V) (**d**). Reprinted with permission from [150] (**a**), [124] (**b**), and [142] (**c** and **d**)

of the PL peak occurs (Fig. 8.21b). On the other hand, for anodizations longer than 15 min the peak shift is not observed, but the intensity of PL peak gradually increases with increasing oxide thickness [124]. The most plausible explanation for these results is increasing number of optical centers within the increased depth of the pores. More than this, for the prolonged anodization AAO is longer exposed for oxalate anions, and higher concentration of oxalate impurities can be incorporated in the oxide structure. The results presented by Chen et al. are consistent with the findings of other researchers who studied the effect of the membrane thickness on the PL of AAO fabricated in oxalic acid under the mild anodization [151] and hard anodization (Fig. 8.21c) [142] conditions.

Surprisingly, for the AAOs formed by hard anodization in malonic acid the opposite correlation between the oxide thickness and the PL peak intensity was observed. The thicker the AAO layer, the lower PL peak intensity (Fig. 8.21d). In addition, upon increase of the oxide layer a red shift (longer wavelengths) in the PL peak position was reported.

8.4.2.5 Etching and Widening of Pores

The characteristic parameters of porous AAO are affected not only by the conditions of anodization, but also by post-anodizing treatment such as etching and widening of pores [4, 140]. The pore etching process changes significantly the geometric parameters of the AAO and consequently the PL spectra [94]. Liu et al. studied the effect of pore etching in 5 % H_3PO_4 on the PL properties of AAO formed in oxalic acid [94]. It was found that the applied etching procedure increases the pore diameter of AAO from about 40 to nearly 100 nm. With increasing pore diameter of AAO (increasing porosity) an increase in the intensity of the PL peak was noticed (Fig. 8.22a). The observed increase in the peak intensity, by a factor of 1/3, was attributed to better access to the F^+ centers in the walls of enlarged pores. A slight blue shift in the peak position was also observed. Stojadinovic et al. studied

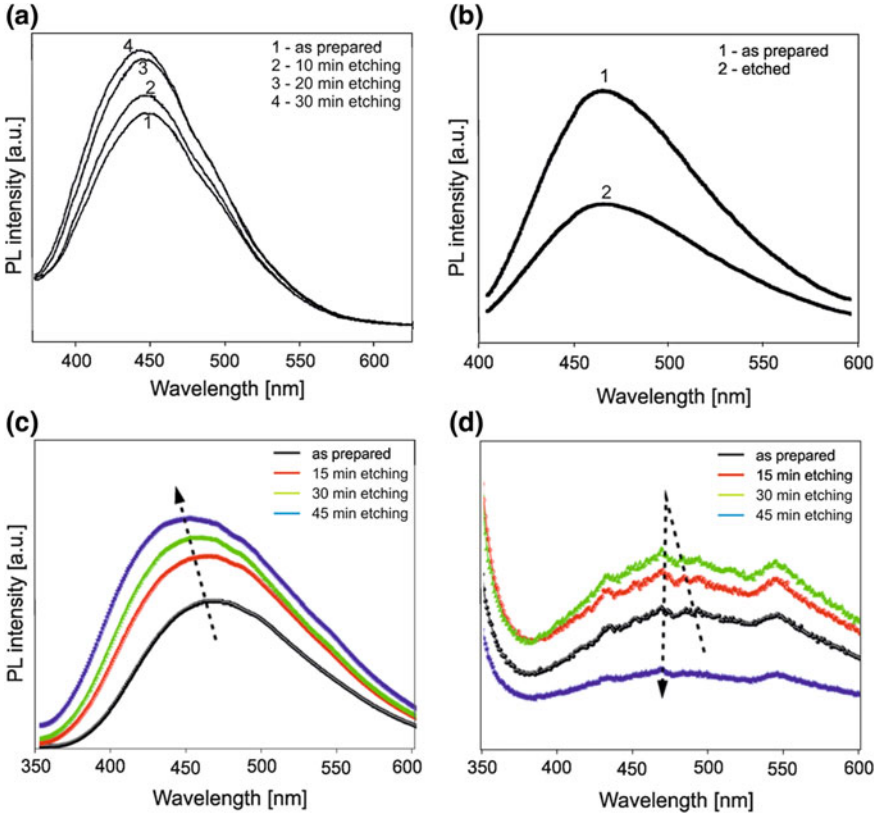

Fig. 8.22 The influence of etching time on PL spectra of AAO obtained by mild anodization in oxalic acid (0.3 M, 40 V) (**a**), sulfamic acid (0.3 M, 30 V) (**b**) and by hard anodization in oxalic acid (0.3 M, 120–140 V) (**c**) and malonic acid (1.7 M, 120–140 V) (**d**) . Reprinted with permission from [94] (**a**), [98] (**b**), and [142] (**c** and **d**)

the effect of short-time etching on the intensity and peak position of photoluminescence spectra for AAOs obtained through anodization in sulfamic acid [98]. It was shown that the chemical etching results in the removal of the thin oxide layer of the pore walls (outer layer), and consequently reduction of the peak intensity in the PL spectrum was observed (Fig. 8.22b). Stojadinovic et al. postulated that the intensity of PL band decreases due to the removal of adsorbed water on pore walls. The similar effect of pore etching on PL was reported for AAOs formed in sulfuric acid [115].

For the AAOs obtained by hard anodization in oxalic acid, a slight blue shift in the peak position and noticeable linear increase of the PL peak intensity with the pore diameter were reported (Fig. 8.22c) [142]. These results are in agreement with the PL data obtained for AAOs formed by mild anodization performed in oxalic acid. When porous anodic oxide was formed by hard anodization in malonic acid, a complex effect of pore etching on PL spectra was observed (Fig. 8.22d) [142]. It was shown that the intensity of PL peak linearly increases until 10 min of pore widening (pore diameter of 111 nm), and then abruptly decreases between 10 and 15 min (pore diameter of 116 nm).

8.4.2.6 Postannealing

Numerous research on annealing the AAO films in the context of their photoluminescence properties have been made in order to determine the origin and type of optical centers existing in the porous oxide structure. In 1999, Du et al. observed that the PL intensity of AAO formed in sulfuric and oxalic acid can be enhanced by a heat treatment [123]. For the AAO membranes obtained in sulfuric and oxalic acid, the intensity of the PL band increases with the annealing temperature up to 400 and 500 °C, respectively [64, 83, 104, 123, 144, 152, 153]. The intensity of the PL peak for the AAOs formed in sulfamic acid increases with annealing temperature, and at about 300 °C reaches its maximum value, followed by the PL intensity decrease with a further temperature increase [98]. The increase in the PL intensity was assigned to the formation of new oxygen vacancies in the newly formed (during annealing) aluminum oxide by the reaction of remaining aluminum with oxygen diffusing from air and/or located in the AAO layer. Above the annealing temperature of 500 °C for the AAO formed in oxalic acid and 400 °C for sulfuric acid, the intensity of the peaks in the PL spectrum decrease. Du et al. attributed this effect to the enhanced rate of oxygen vacancy annihilation compared to the rate of their formation [123]. As it was shown by Sun et al. and then proven by other investigators, dehydration, decomposition of embedded anion impurities, and amorphous-crystalline phase transition occur during annealing of AAO formed in oxalic acid [77, 85, 95, 98, 100, 153, 154]. Figure 8.23 shows typical thermogravimetric analysis (TG) and differential thermal analysis (DTA) curves for the AAOs obtained through anodization in 0.3 M oxalic acid [154]. The weight loss observed in the Sect. 8.1 (up to 100 °C) is caused by the desorption of weakly bound water from the AAO surface and pore walls [153, 154]. At temperatures

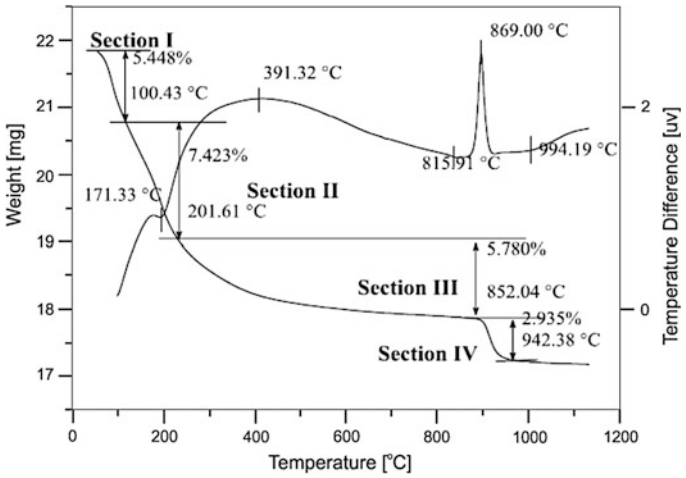

Fig. 8.23 TG and DTA curves for the AAO layer obtained by anodization in 0.3 M oxalic acid at 40 V. Reprinted with permission from [154]

higher than 171 °C (Sect. 8.2), the removal of structural water from hydroxide and oxy-hydroxide of aluminum is observed. In the Sect. 8.3, from 200 to 852 °C, the decomposition of oxalic impurities takes place. It is believed that the decomposition of metal oxalates, according to the reaction (8.3) [155], occurs at temperatures above 350 °C [153].

$$(COOH)_2 \xrightarrow{T} CO_2 + CO + H_2O \tag{8.3}$$

According to Mukhurov et al., CO_2 is not chemically bound to oxide but only trapped in the crystal structure [146]. This assumption was confirmed by the IR spectra analysis for the annealed AAO film. The progressive decomposition of embedded oxalate ions (above 500 °C), and continuous ordering of Al and O atoms in the crystal structure result in immobilization of CO_2 in the oxide lattice (aluminum–carboxylate complex) [109, 147] and lead to decrease in the intensity of PL spectra. In the Sect. 8.4, the phase transitions to γ–Al_2O_3 (above 800 °C) and then to α-Al_2O_3 (at 1100 °C) are observed [104]. During the former transformation, the –OH groups in crystalline structure of γ–Al_2O_3 are lost [104, 146, 153]. At the temperature of about 930 °C, the decompositions of aluminum carbonate ($Al_2(CO_3)_3$) and $Al_2(C_2O_4)_3$ took place [153, 154]. Typical PL spectra of the AAOs annealed at different temperatures are shown in Fig. 8.24 [154].

A significant influence of incorporated ions on photoluminescence properties of the AAOs formed by anodization in malonic acid and tartaric acid was reported by Vrublevsky et al. (Fig. 8.25) [134, 143]. Similarly to the AAOs obtained in oxalic acid, the AAOs formed in malonic acid and tartaric acid exhibit a substantial change in the intensity of PL peaks with annealing temperature. For temperatures higher

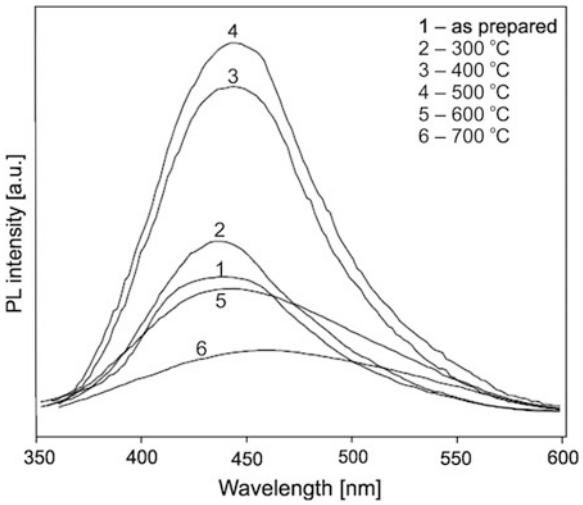

Fig. 8.24 PL spectra for AAOs obtained by anodization in 0.3 M $H_2C_2O_4$ at 40 V and annealed at different temperatures. Reprinted with permission from [154]

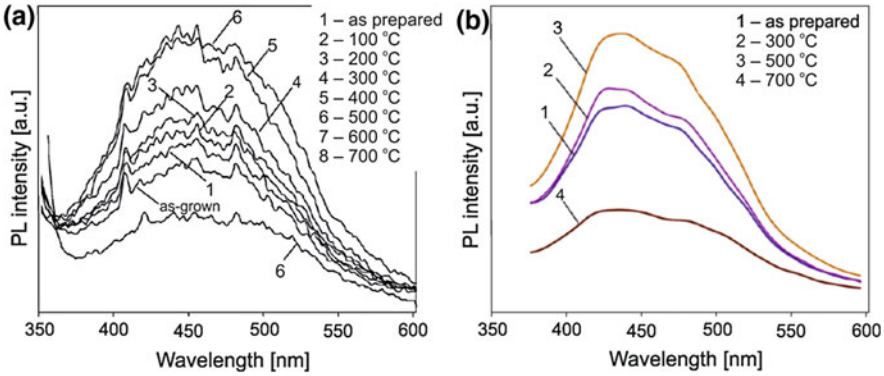

Fig. 8.25 PL spectra for AAOs obtained through anodization in malonic acid (0.8 M, 6 mA cm^{-2}, 18 °C) (**a**), tartaric acid (0.4 M, 6 mA cm^{-2}, 18 °C) (**b**) and then annealed at different temperatures. **a** and **b** reprinted with permission from [134, 143], respectively

than 600 °C, a drastic decrease in the intensity of the PL peak, due to the decomposition of organic ions to CO_2, is observed [118, 143]. Deconvolution of the PL spectra obtained for the AAOs formed in malonic acid and annealed at temperatures not exceeding 600 °C indicated two peaks centered at 437 and 502 nm. Vrublevsky et al. proposed that the peak at 437 nm originates from the optical centers with incorporated malonate ions, which decompose at higher temperatures, while the peak observed at 502 nm comes from the defects in the oxide structure caused by a lattice mismatch and difference in the coefficients of thermal expansion between alumina and incorporated acid impurities [134].

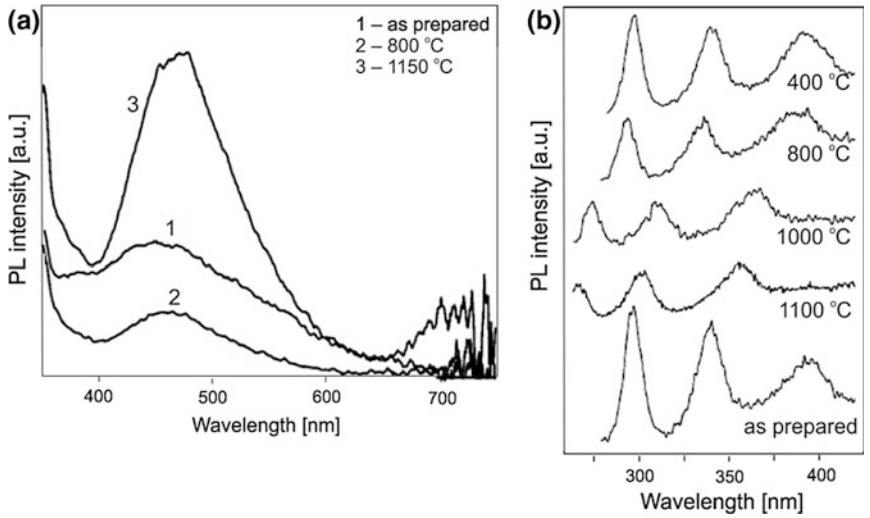

Fig. 8.26 The influence of annealing temperature on the PL spectra of porous alumina obtained through anodization in sulfuric acid of the aluminum foil (**a**) and 400 nm Al film on Si (**b**). **a** and **b** reprinted with permission from [85, 156], respectively

For the AAO films obtained in sulfuric acid, a different effect of the annealing temperature (in the range 800–1150 °C) on the PL intensity was observed (Fig. 8.26a) [85]. After annealing at 800 °C, the less intense PL peak of the AAO compared to the spectrum of the as-prepared AAO was observed. When the annealing temperature was raised to 1150 °C a sharp increase in PL intensity was detected. This kind of variation in the photoluminescence intensity with thermal processing was attributed to (i) partial oxidation of the AAO surface by atmospheric oxygen at 800 °C resulting in a reduction in the density of divacancies and, consequently, decreasing PL intensity, and (ii) thermal decomposition of incorporated sulfate ions, occurring at temperatures between 950–1230 °C, and resulting in the removal of decomposition products from the oxide structure what increases the concentration of oxygen vacancies in the oxide [85]. The presence of decomposition products, mainly SO_2 and O_2, was confirmed by IR analyses. It is worth noting that the position of the PL peak does not change with annealing temperature. In analogy to the PL spectra observed for sapphire, Mukhurov et al.[85] proposed that the photoluminescence properties of the AAO obtained through anodization in sulfuric acid are affected mostly by concentration and distribution of oxygen vacancies F_2^+, F_2, F_2^{2+}, while the effect of embedded SO_4^{2-} ions is negligible.

The different results on the annealing temperature influence on the PL of AAOs formed in sulfuric acid was reported by Wu et al. [156]. It was found that the porous thin AAO layers on p-Si substrate show three strong PL bands at 295, 340, and 395 nm. A blue shift of these peaks and decrease in their intensity were observed with increasing annealing temperature (Fig. 8.26b) [156]. It was also shown that the

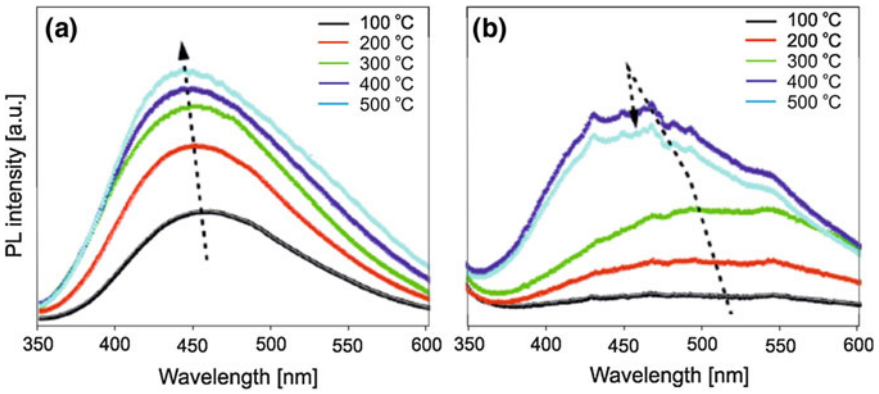

Fig. 8.27 The influence of annealing temperature on the PL spectra of porous alumina obtained through hard anodization in oxalic acid (0.3 M, 120–140 V) (**a**) and malonic acid (1.7 M, 120–140 V) (**b**). Reprinted with permission from [142]

heat-treatment time and the type of gas used for this process affect the intensity of the PL peaks. According to Wu et al., the photoluminescence activity of the AAO on Si substrate depends mainly on the presence of oxygen vacancies F^+.

Figure 8.27 shows the PL spectra of AAO samples formed in oxalic acid and malonic acid by hard anodization and annealed at different temperatures. Similarly to the PL spectra for the AAOs anodized under the mild anodization conditions in oxalic acid, an increase in the PL peak intensity and a slight blue shift of the peak position with annealing temperature were observed [142]. For the AAO obtained in malonic acid by hard anodization, the intensity of the PL peak gradually increases up to 400 °C, and then decreases at 500 °C. The changes in the PL peak intensity are related to the thermal decomposition of malonic and oxalic acid impurities located at the pore walls (i.e. outer layer). In both types of AAOs, the PL peak is shifted towards shorter wavelengths as a result of the decomposition of superficial impurities at low temperatures, which allows increase the light emission from the outer layer [142].

8.4.3 Applications of AAO Photoluminescence

Photoluminescence spectra of the porous alumina is stable in time and therefore it is not necessary to cover AAO films with protecting layers. PL spectra of AAO may change due to alteration of geometric parameters, modification of the oxide surface or filling the pores with some substances. Last type of modification has been used in optical biosensors. Due to the Fabry-Pérot effect in the PL spectrum of AAO modified with organic particles, oscillations appear. These oscillations can be converted into a barcode (Fig. 8.28a). The more oscillations in the PL spectrum the

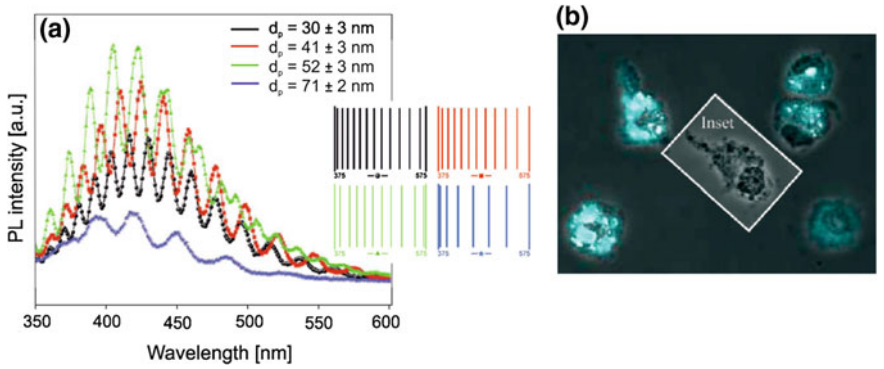

Fig. 8.28 Examples of practical application of photoluminescent properties of AAO in biological barcodes (**a**) and fluorescent biological labeling (**b**). **a** and **b** reprinted with permission from [157, 161], respectively

more strokes in the code, so it is possible to increase the sensitivity of the sensor to the determined molecule [157]. With a large stability, sensitivity and biocompatibility, porous AAO was applied in the determination of DNA [158], glucose [157, 159], organic dyes [157, 160], enzymes [157] or amino acid [159]. The photoluminescence properties of AAO also allow use it as a fluorescent biological label for i.e. dendritic cells (Fig. 8.28b) [161]. This is possible by controlling the distribution of the oxygen vacancies and alumina nanoparticles in a porous film. The optical properties of AAO enable the use of it as color display decorations or in anti-counterfeiting technology [86].

8.5 Photonic Crystals and Bragg Reflectors

Photonic crystals are structures in which refractive index varies periodically in space. This variation of refractive index is obtained by combining at least two different materials/dielectrics with different refractive indices. There are three groups of photonic crystals-1D, 2D, and 3D, depending on how many spatial directions are involved in refractive index changes. The incident light beam on the photonic crystal will be scattered because of the refractive index variation in the structure. As long as the wavelength of the electromagnetic radiation is much larger than the lattice constant of the photonic crystal, the structure behaves as an effective medium. However, if the wavelength is comparable with the periodicity of the photonic crystal, Bragg scattering occurs and light beam with a particular frequency (or wavelength) that radiates the crystal could be totally reflected. Similar to the X-ray diffraction, the Bragg scattering can be interpreted as constructive interference of scattered waves, which are emitted by parallel lattice planes of the photonic crystal. The energy range corresponding to frequencies at which the light is reflected (not allowed to be transmitted) is called the photonic band gap.

In one-dimensional photonic crystals, periodic modulation of the permeability occurs in two directions [162]. Such structures can be used as the Bragg grating, antireflection coatings, and Bragg stacks [44]. It was shown that porous one-dimensional photonic crystals or Bragg stacks can be fabricated by periodic altering the potential during the anodization process [163]. Two-dimensional photonic crystals have the periodic permeability in two directions while the third direction is uniform. Therefore, 2D photonic crystals can have a large variety of configurations. An interesting example of 2D photonic crystals is porous silicon [164], and porous alumina [165, 166]. Three-dimensional photonic crystals have periodic permeability in three directions, hence the number of possible configurations is very high [167]. 3D photonic crystals are found in nature, for example opal and diamond [168].

The ordered nanoporous AAO films are intrinsically 2D photonic crystals with photonic band gaps centered at wavelengths in the range of near infrared (IR) and visible light [169]. A great advantage of this type of photonic crystals is almost a non-limited depth of pores and, consequently, large aspect ratio. For photonic crystal applications, porous alumina with a perfect nanopore order, is usually fabricated by one-step anodizing of the pre-patterned Al foil. There are a number of reports on 2D photonic band gap crystals made of AAO with a typical internal pore structure i.e. parallel pores with uniform diameter along their depth [170–178]. It was shown that AAO photonic crystals exhibit a photonic band gap between 600 and 1350 nm. The influence of the pore diameter of AAO with 500 or 100 nm intervals on the band gap position was investigated in detail [174]. On the other hand, it was reported that with decreasing interpore distance of the AAO photonic crystal a red shift in the transmission dip is observed [170, 172].

A number of interesting observations have been recently made on birefringence occurring in 2D photonic crystals based on AAO layers. The birefringence is often defined as a difference in the normal and tangential refraction indices or in other words as the maximum difference between refractive indices exhibited by the material. It was found that quasi-ordered porous anodic aluminum oxide has anisotropy on the scale of the wavelength of light, and therefore shows birefringence in the visible region [179–182]. The effect of pore diameter of the AAO film on refractive index and birefringence was detailed examined by Lutich et al. [183]. It was demonstrated that AAO films could offer a wide range of refractive index and birefringence values for optical device applications. It was shown for the low porosity range that the birefringence increases (29–39 %), with the porosity increase from 0.033 to 0.062 [183]. These results were confirmed by Gong et al. who observed that for the increasing pore diameter in the range of about 13–37 nm, the birefringence of the AAOs increases from 0.02 to 0.06 [65].

Photonic crystals made of anodic alumina with periodically branched nanopores were prepared by adjusting the anodizing cell voltage periodically during electrochemical oxidation and followed by chemical etching [30]. To enlarge the main and branched channels the samples were etched in a phosphoric acid solution for an appropriate time. Figure 8.29 shows the optical photograph of porous alumina membranes before and after chemical etching for different times. Figure 8.29a shows that the AAO sample after anodization and before chemical etching (sample 1) is

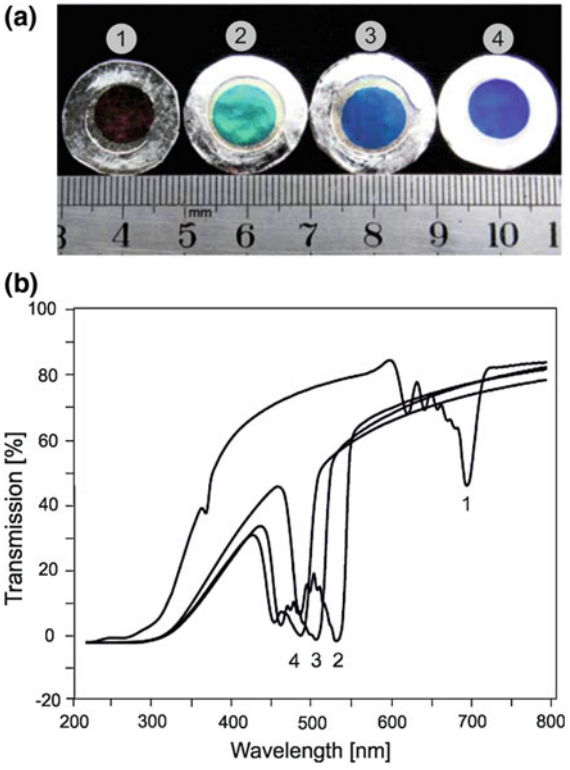

Fig. 8.29 Optical photograph of porous anodic alumina membranes (*1*) before, and after chemical etching for: (*2*) 15 min, (*3*) 18 min and (*4*) 20 min (**a**), and the corresponding optical transmission spectra (**b**). Reprinted with permission from [30]

almost transparent, while the samples after chemical etching are green (sample 2) and blue (samples 3 and 4). The bright colors come from optical reflections from the AAO membranes which occur at wavelengths corresponding to the forbidden photonic band gap region. The observed effect of the chemical etching duration on the color of AAO samples may originate from the different sizes pores (different effective dielectric constants). The existence of photonic band gap in those porous membranes is also confirmed by the transmission spectra recorded before and after chemical etching for 15, 18, and 20 min (Fig. 8.29b). For wavelengths lower than 400 nm, a low transmission was observed for all samples. This behavior was caused by a strong reflection and absorption of alumina. The transmission spectrum of the sample without chemical etching (sample 1) shows only a weak peak at 700 nm. As the etching time was prolonged (samples 2–4), a gradual blue shift in position of the peak was observed. The intensity of transmission light decreases with increasing etching time because of the increasing porosity of AAO. The similar results for photonic crystals made of AAO with branched pores were reported by Hu et al. [184].

In a similar manner using cyclic anodization with a slightly modified voltage signal (see Fig. 8.5), the photonic crystals based on AAOs were synthesized by Su et al. [35]. In order to study if the photonic band gaps of the fabricated photonic crystals based on the AAOs are tunable and controllable, the transmission spectra

were recorded for the samples with different thicknesses (different times, t_3) of the branched channel layer (layer II). It was found that the photonic band gaps of the AAO photonic crystals are tunable and controllable in the wavelength range from 350 to 1330 nm. In addition, it was shown that the peak shifts to longer wavelengths when the thickness of layer II increases.

One of the most remarkable accomplishments of the fabrication of photonic crystals with very narrow photonic band gaps located in the near infrared region was reported by Shang et al. [185]. Using the cyclic anodization with a compensation potential mode, they prepared the photonic crystals based on AAOs with narrow photonic band gaps which the full width at half maximum was only 30 nm. The transmission spectra showed that the AAO-based photonic crystal is transparent (about 90 %) in the region out of the band gap and reflects the transmitted light only in the center of the band gap at 1150 nm. This photonic crystal was used also as a sensor for detection of ethanol vapor [185]. Recently, the same research group reported fabrication of the AAO-based photonic crystals with extremely narrow (full width at half maximum less than 10 nm) photonic band gaps which centers were located at 440 and 652 nm [186]. It is worth mentioning that the observed asymmetric line-shape profiles of the photonic band gaps were attributed to Fano resonance between the photonic band gap state of photonic crystal and continuum scattering state of the porous structure [186].

Distributed Bragg reflectors are one-dimensional photonic structures which can be considered as a stack of thin layers of transparent dielectric with alternating high and low refractive indices. Such layered structures exhibit a high reflectance similar to metallic mirrors [187]. As number of alternating layers increases in the Bragg reflector, the stop band enlarges and sharpens [188]. The spectral width of the reflected wavelength ($d\lambda_{Bragg}$) (at full width at half maximum) is proportional to the reflected wavelength (λ_{Bragg}) [189] and decreases when the number stacks (N) increases according to

$$d\lambda_{Bragg} = \frac{2\lambda_{Bragg}}{N} \tag{8.4}$$

Furthermore, the intensity of the reflected light depends on the number of stacks (N), and the low (n_L) and high (n_H) refractive indices of the alternating layers [190].

The cyclic anodization technique was also used to synthesize distributed Bragg reflectors based on nanoporous anodic alumina [34]. The cyclic anodization approach results in an in-depth modulation of the pore geometry and, consequently, the refractive index. Four different potential profiles (potential wave structures) in which the amount of charge passing in stage b (horizontal upper line in the voltage profile) was different and varied from 0 to 4 °C (Fig. 8.30a). Rahman et al. studied the effect of the applied potential profile and pore-widening treatment on photonic band gaps. The transmittance spectra for the potential profiles with the passing charge of 1 C is presented in Fig. 8.30b.

As can be seen, the transmittance decreases and is blue shifted when the pore-widening time increases. It can be ascribed to increasing porosity of AAO and to scattering losses produced by the irregular interfaces between cycles [34].

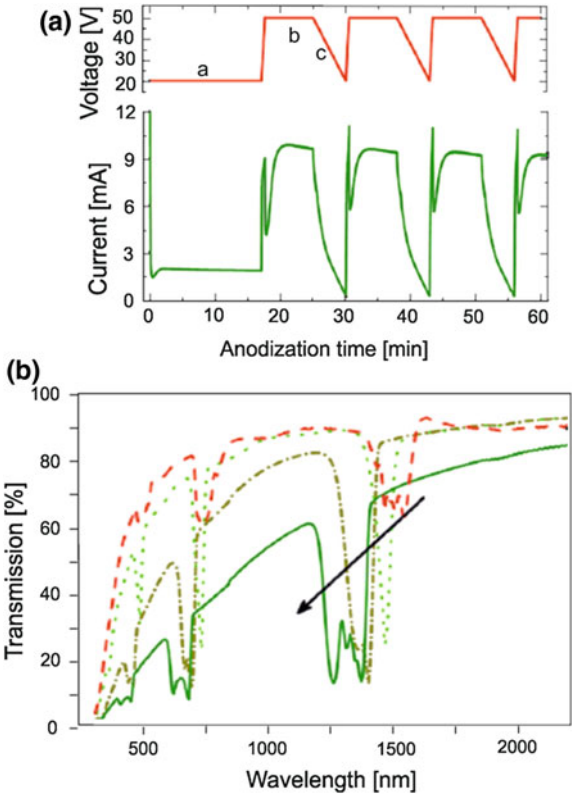

Fig. 8.30 Applied voltage profiles (*red*) and measured current transients (*green*) (**a**) and transmittance spectra (**b**) of the sample with passing charge of 1 C for different pore widening times. Reprinted with permission from [34]

Using cyclic anodizations performed at different temperatures ranging from 6 to 18 °C, Zheng et al. synthesized the AAO-based Bragg reflectors with the transmission peak covering almost any wavelength range of the visible light region [50]. It was found that as anodizing temperature increases, a red shift in the transmission peak is observed. On the other hand, the same researchers demonstrated that by adjusting the anodizing potential waveform applied during cyclic anodization, the first Bragg condition peak of the AAO-based Bragg reflectors could be modulated from 727 to 1200 nm [49].

A remarkable distributed Bragg reflector based on nanoporous anodic aluminum oxide and fabricated by pulse anodization in a sulfuric acid solution was recently presented by Sulka and Hnida [44]. Taking into account the fact that pore diameter of AAO, can be tuned by the applied potential under a constant potential regime (or current density under a constant current regime), the authors used pulse anodization of aluminum with periodic pulses in alternating regimes of mild (MA) and hard anodizations (HA) for the synthesis of the AAO with modulated pore diameter. It was shown that the designed AAO structure consists of alternating high and low refractive index layers and behaves as a distributed Bragg mirror reflecting light in two different ranges of wavelength (Fig. 8.31). Such behavior is extremely

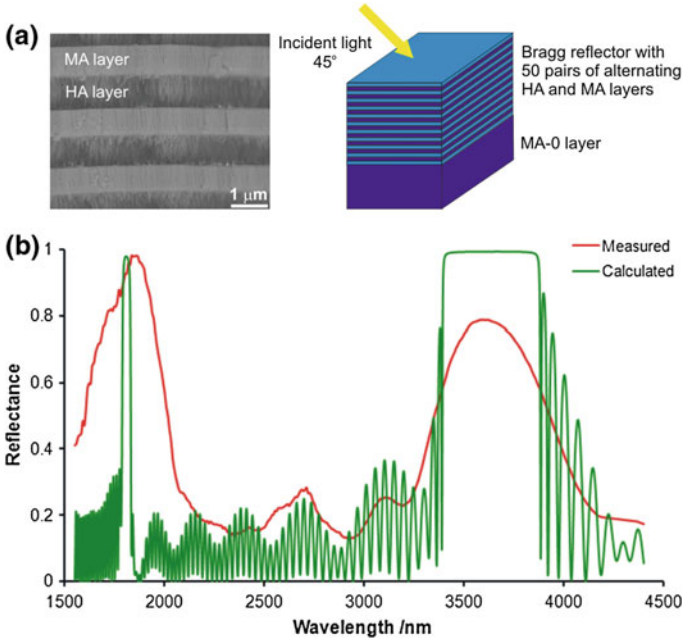

Fig. 8.31 SEM cross-sectional view and schematic diagram of the Bragg reflector with 50 pairs of alternating HA and MA layers (**a**) together with the measured and calculated reflectance spectra of the designed mirror (**b**). The alternating high (MA) and low (HA) index layers have thicknesses of 750 and 800 nm, respectively. The thickness of the initial MA layer (MA-0 layer) was 7500 nm. After [44]

important in optical communication lines where two separate spectral bands of high reflectivity in the infrared region are desired.

Guo et al. [188] studied influence of number of periods in the Bragg stack on the transmittance spectra. The AAO-based Bragg reflectors were formed by pulse anodization at the constant current regime. By periodical modulation of the current density they precisely controlled the porosity and thickness of each layer in the AAO structure. They showed that the reflected light intensity increases, and its position is blue shifted when in number of alternating layers in the Bragg stack increases.

8.6 Chemical Modification of AAO

The porous anodic alumina films are optically transparent, however, the optical properties of AAO can be easily modified by the presence of different guest molecules/materials, i.e. metallic and inorganic nanoparticles, metallic and polymer nanowires, xerogels and other compounds. It is also possible to deposit metallic or inorganic thin layers on the surface of AAO films in order to change their UV-Vis

and photoluminescence spectra. The inorganic species immobilized on the surface, incorporated or embedded into the oxide structure can also modify the optical properties of AAO. The AAO with organic substances adsorbed on the surface of pore walls can be used for optical sensing applications [128, 191–193].

The AAO membranes are used not only as templates for the synthesis nano-sized materials but also, in the presence of an electron accepting guest organic molecules, as a convenient light-energy collecting materials for both energy and electron transport from AAO to nanopore-embedded inorganic quantum dots and nanowires. The mechanism of the ultrafast excited state deactivation from the host AAO to the guest molecules and inorganic nanostructures can be associated with charge transfer, Förster energy transfer, and nano-surface energy transfer [194]. Optical properties of the AAO with different guest molecules and materials have been extensively studied in recent years, therefore, only the most important examples will be presented here.

8.6.1 Nanowires in AAO

8.6.1.1 Metal Nanowires in AAO

In recent years, many researches took an effort to thoroughly investigate the optical properties of AAO films with metallic nanowires (NWs) embedded inside the pores. In this regard many AAO-NWs composites based on deposited metals such as Ag [33, 195–202], Au [200, 202–207], Co [110, 208], Cu [209], Fe [210], Ni [107–109, 211, 212], and Sn [213] were investigated. In addition, the AAO composites with multilayered Au/Ag nanowires [202] and heterojunction nanowires such as Au nanowires with a thin top layer of Ag [199] or Ag nanowires with a thin AgI segment [214] were also fabricated.

It is widely recognized that as-grown anodic oxide films on aluminum are optically transparent. For practical applications, therefore, the process of anodization is followed by AC electrodeposition of metallic layers into the AAO nanopores (electrolytic coloring). Due to the fact, that metallic NWs deposited in the AAO exhibit distinctive reflection peaks in the UV-Vis, it is possible to investigate optical properties of such materials by UV-Vis spectroscopy. Structural colors originate from the constructive interference among reflecting light having different optical pathlengths, namely the light reflected from the air/AAO interface and the light reflected from the air/metal or AAO/Al interface (Fig. 8.32) [107, 109]. It is worth mentioning that different reflection spectra are observed when the light is incident on the bottom side of the AAO-NWs composite films [33]. In case when the light is incident on the bottom side of the composite film, the beam is considerably attenuated during propagation through the metallic (e.g., Ag) layer. When the reduced diffraction light of the porous alumina propagates through the Ag layer again, the diffraction is suppressed seriously. The deposited metal layer enhances the color saturation of the composite film. It is attributed to partial adsorption of the

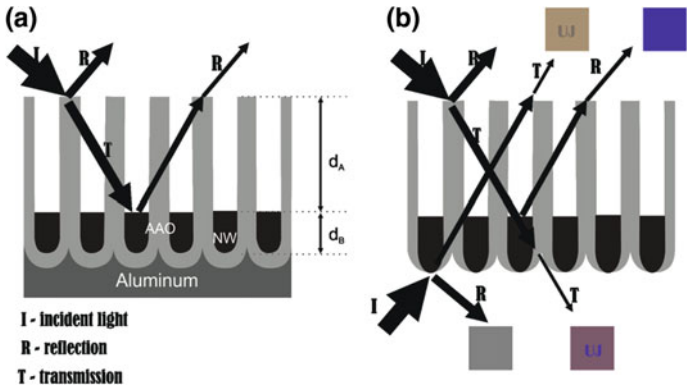

Fig. 8.32 Scheme of interference of reflected lights on AAO filled with NWs

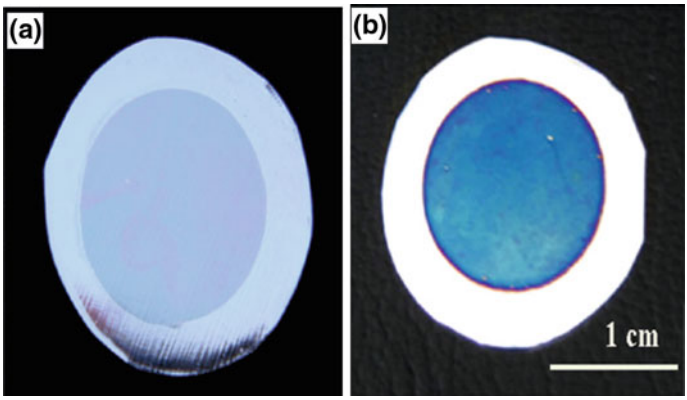

Fig. 8.33 Photographs (**a**) of the AAO film anodized for 11 min and (**b**) AAO film with deposited Ni NWs. Reprinted with permission from [109]

incident and reflected light from the AAO/Al interface by loose metallic nanograins (Fig. 8.33).

The optical properties of AAO with embedded NWs depend upon the thickness of the oxide layer (depth of pores), thickness of the deposited metallic layer (length of NWs) and the quality of deposit (size of metallic grains, compactness etc.). Therefore, the optical properties of AAO-NWs can be changed by altering the conditions of anodization (i.e. applied potential, anodization time) and deposition of NWs (i.e. current density of deposition). The colors of the AAO-NWs composite films vary with increasing the thickness of the sample [109] and depend on the observable angle [109, 124]. It is widely recognized that the wavelength of maximum reflectance decreases (blue shift is observed) with increasing incident angle. For the same sample, the reflection spectra collected at different incident angles exhibit peaks at different wavelengths. For instance, the color of the same ultra-thin

AAO-Ni NWs sample gradually changes from reddish-brown to green when the incident angle increases [109].

In order to better understand this effect, Bragg's law has to be considered

$$2d\sin\theta = n\lambda \tag{8.5}$$

where d, n, θ and λ are lattice spacing, an order of diffraction, diffraction angle and wavelength, respectively. For the constant lattice spacing, detected reflection wavelengths depend on the observable angle. Different order of diffraction is represented by different reflection peaks in the spectrum. Since the thickness of the AAO layer affects d value, the color of the metal plates could be controlled by anodizing time (Fig. 8.34). Zhang et al. observed a red-shift in the peak positions with increasing anodizing time and, consequently, film thickness of the samples [109, 110, 208, 210]. The length of deposited nanowires also affects the observed color of the fabricated AAO-NWs composites [107].

It is widely recognized that noble metal nanostructures (e.g., Ag and Au nanoparticles, nanorods, and nanowires) show characteristic absorption peaks, known as localized surface plasmon resonance (LSPR), being a result of the collective oscillation of the conduction electrons in nanostructures with the incident electromagnetic field [215–217]. There are two main consequences of existing the LSPR: (i) selective photon absorption and (ii) generation of locally enhanced or amplified electromagnetic fields at the nanoobject surface. The LSPR for noble metal nanostructures occurs in the visible and IR regions of the spectrum and can be measured by UV-Vis-IR absorption spectroscopy. The LSPR band of a noble metal nanostructure relies on its size, shape, composition and its surrounding medium

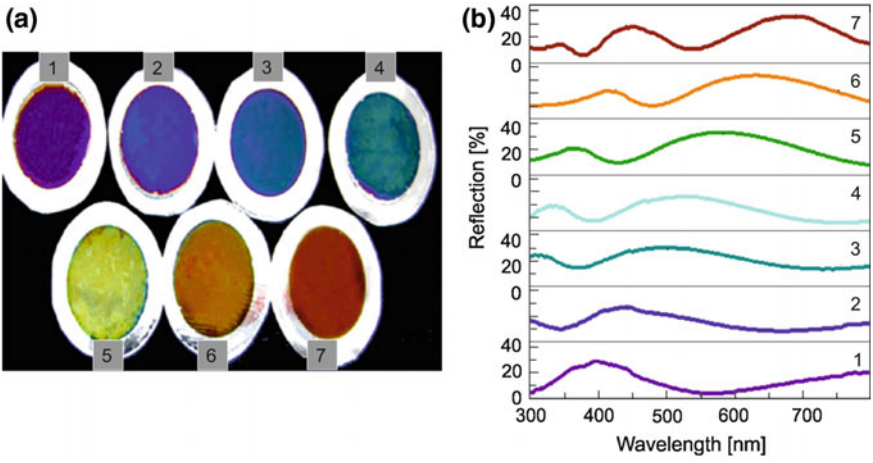

Fig. 8.34 Photographs of AAO films with deposited Ni NWs taken in natural light at nearly normal incidence (**a**). The AAO films were formed at different anodizing times: (*1*) 9 min , (*2*) 10 min , (*3*) 11 min , (*4*) 12 min , (*5*) 13 min , (*6*) 14 min , (*7*) 15 min (*7*). The corresponding UV-Vis reflection spectra of the AAO-NWs nanocomposite films (**b**). Adapted with permission from [109]

(refractive index of environment) [191, 216]. In particular, nanowires show two LSPR peaks corresponding to the transverse and the longitudinal resonance mode. The transverse resonance mode is related to the electron motion perpendicular to the nanowire long axes and can be excited with the light having an electric-field component perpendicular to it. On the other hand, the longitudinal resonance mode is related to the electron oscillations along the nanowire axes and requires p-polarized light to be excited with a component of the incident electric field along the nanowire [205]. For Au nanowires embedded into the AAO membrane, the transverse mode resonance occurs at fixed wavelength of about 520 nm, whereas the longitudinal mode wavelength shifts towards near infrared (from 700 to 900 nm) with an increase in the nanowire length (from 260 to 360 nm) [200, 204, 205]. A slight red shift in the longitudinal peak position was reported for the composite films containing Au nanowires with the diameter of 20 nm and length ranging from 75 to 330 nm (Fig. 8.35) [206]. The transverse plasmon bands at about 360–390 nm for the Ag-based [195, 199, 200] and at 560–580 nm for the Cu-based AAO-NWs [209, 218] composite were observed. The longitudinal peak for these AAO-NWs composite films is typically observed at broad wavelength range of 500–845 nm [199, 200, 218]. The diameter of embedded nanowires has the influence only on the longitudinal peak position. When the diameter of Ag nanowires increases in the range between 22 and 40 nm, and consequently aspect ratio of NWs decreases, a gradual blue-shift of the longitudinal peak from 734 to 509 nm is observed (Fig. 8.36a) [199, 207]. Similar behavior was also reported for Au NWs embedded in the AAO membrane [207]. On the other hand, for the Au-Ag alloy nanowires deposited in the AAO membranes, the position of the transverse peak was found to dependent linearly on the NW composition varying between 390 nm for pure Ag and 520 nm for pure Au (see Fig. 8.36b) [199]. The same position of transverse resonance peak (520 nm) for the AAO-Au NWs composite film was observed by Yan et al. in the photoluminescence spectrum [203]. Surprisingly, they observed a significant suppression or quench of the PL intensity of the AAO-Au

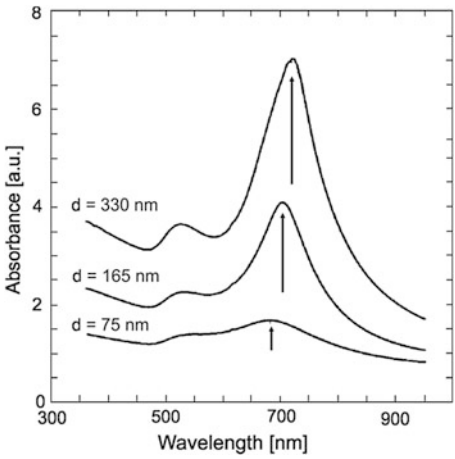

Fig. 8.35 Transmission data for P-polarized light at 60° angle of incidence and various Ni nanowire lengths in the AAO-NWs composites. Reprinted with permission from [206]

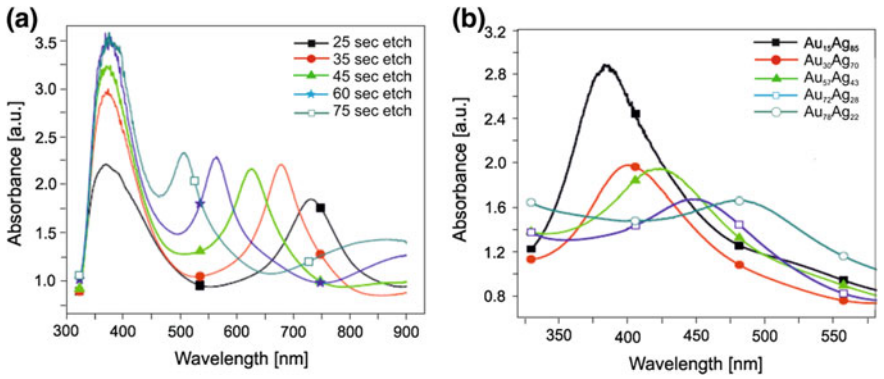

Fig. 8.36 Effect of changing nanorod diameter (aspect ratio) on the transmission spectra of 400 nm long silver NWs embedded in a 450 nm thick film of porous AAO with a 60 nm interpore distance. The angle of TM polarized incidence was 40° in all cases (**a**). Transverse resonance peaks for the 24 nm diameter and 300 nm long AAO-Ag NWs composites with different Au-Ag compositions (**b**). Reprinted with permission from [199]

NWs composite in comparison with the PL spectrum for the pure AAO film. This quenching was attributed to an efficient fluorescent resonance energy transfer (FRET) between the plasmonic absorption of the Au nanowire array and the PL band of the AAO membrane. This phenomenon depends on the donator acceptor separation which is small, due to the spatial proximity of the nanowires and the AAO.

Recently, it has been demonstrated that metal NWs embedded vertically in a dielectric medium, such as AAO, can change the propagation of light and can exhibit negative refraction in the visible wavelengths or infrared region [197, 200, 201]. As was mentioned previously, the AAO-NWs composite films have two surface plasmon resonances (LSPR): a longitudinal LSPR and transverse LSPR. It is widely recognized that the AAO-NWs composite should be excited with higher wavelengths (with TM polarized light) than the longitudinal resonance mode in order to observed negative refraction phenomenon [219]. This type of materials with such extraordinary optical properties do not exist in the nature and are known as negative index metamaterials. Typical applications for these materials include the development of next-generation optical devices such as flat lens and superlenses, waveguiding, as well as imaging, optical communication, and biosensing [197, 205, 219, 220].

As it was mentioned earlier, the ideally ordered nanopore array of AAO can be directly used as a 2D photonic crystal material in the near infrared (IR) and visible wavelength regions [178]. The theoretical studies showed that negative refraction can also be achieved in some 2D photonic crystals [201, 219, 221]. Moreover, by incorporating silver or gold into AAO template with various pore diameter, photonic crystal band gap or the TM polarization can be tuned from near-infrared to visible region for AAO with 100 and 200nm diameter, respectively [222]. The

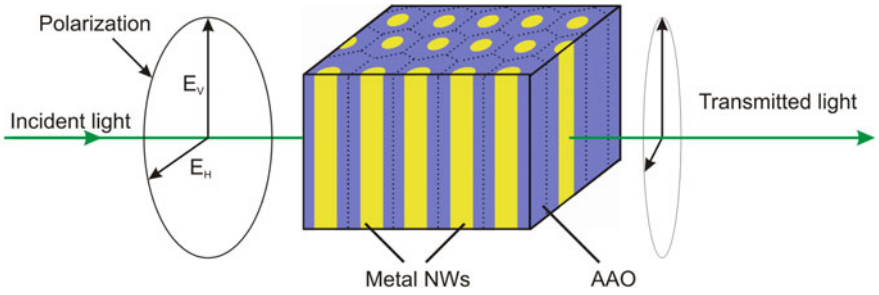

Fig. 8.37 Schematic illustration of a wire grid micropolarizer made of the AAO-NWs composite. The micropolarizer transmits the light polarized vertically (E_V) and attenuates the light polarized horizontally (E_H)

Table 8.2 Characteristics of various AAO-based micropolarizes

Type	Pore diameter (filled with metal) (nm)	Wavelength (μm)	Extinction ratio (dB)	Insertion loss (dB)	References
Ag/AAO	90	1.0–2.2	25–26	0.77	[226]
Co/AAO	20	1.3	22	n.a.	[227]
Cu/AAO	20	1.25–1.46	24.9–14.9	n.a.	[209]
	90	1.0–2.2	24–32	0.5	[228]
Ni/AAO	30	1.3	30	2–4	[229]
	70	1.0–2.5	25–30	1.07	[230]
Pb/AAO	40	1.0–2.2	17–18	0.4	[231]

n.a. Not available data

theoretical concept has been recently demonstrated in practice. When AAO template is filled with a metallic component, e.g. Ag [197], Au [223], new metal-dielectric photonic crystals with negative refraction index were fabricated.

It is widely recognized that anodic porous alumina exhibits anisotropic optical properties. In case when its channels are filled with a metallic material starts to behave as a wire-grid micrpolarizer (Fig. 8.37) [224, 225]. A number of studies have documented the fabrication of micropolarizers from AAO membranes filled with Ag [226], Co [227], Cu [209, 228], Ni [229, 230], and Pb [231]. The optical characteristics of fabricated micropolarizes is summered in Table 8.2.

8.6.1.2 Polymer Nanowires in AAO

Although various polymers are often deposited inside the pores of AAO membranes, the optical properties such composite materials are rather occasionally studied except the following polymer NWs embedded in AAO films: poly (2,5-dibutoxy-1,4-phenylenevinylene) (DBO-PPV) [232], poly(2,3-diphenyl)phenylene vinylene) (DP-PPV) [233], poly[2-methoxy-5-(20-ethyl-hexyloxy)-

p-phenylene vinylene] (MEH-PPV) [poly[2-methoxy-5-(20-ethyl-hexyloxy)-p-phenylene vinylene] (MEH-PPV) [233–237], poly[3-(2-methoxyphenyl)thiophene] (PMP-Th) [120, 238], poly(3-hexylthiophene) (P3HT) [239, 240], and poly (N-vinylcarbazole)/tris(8-hydroxyquinoline) aluminum composite (PVK-Alq_3) [241]. As can be seen, mainly conjugated polymers are deposited due to their high potential to be applied in light-emitting diodes, solar cells, and optoelectronic devices. In the nanoscale, the polymer chains exhibit intrinsically anisotropic properties, such as luminescence polarization and highly directional charge transport [242].

The preparation of the conjugated polymer nanostructures (e.g., nanotubes and nanowires) in AAO templates is not really problematic, and impregnation or wetting processes as well as chemical and electrochemical techniques are commonly used. The optical properties of the conjugated polymers embedded in AAOs are remarkably different from those in films, as a result of preferential axial orientation of the polymer chains within the nanowires/nanotubes, possible isolation of the polymer chains and chemical interaction between both components [120, 233–235, 239, 243]. As shown in photoluminescence studies, the optical properties can be altered by adjusting the diameter of the nanopores of AAO, and the type and concentration of the polymer solution used for polymerization [235–237]. Nguyen et al. demonstrated that the polarity of solvent has a strong influence on the chain conformation, which in turn, affects the PL yield [237]. It was found that polymer chains fill the nanopores in a form of polymer bunch and the number of the polymer chains in the bunch depends on both: the concentration of polymer solution and the pore diameter of AAO [234]. When the concentration of polymer solution increases bunches of chains in nanopores are more compact and contain larger number of polymer chains. As a result of enhanced interchain interactions, the number of the energy levels increases and a red shift in the PL spectrum is observed [234].

The most important factor which influences the optical properties of AAO membranes with embedded polymer nanowires is a size confinement effect. The isolation of polymer chains embedded in the nanopores of AAO membranes is directly responsible for the blue shifts in the PL spectra and great enhancements in photoluminescence intensity [120, 232, 233, 236, 238]. The effective conjugation length of polymers in the AAO nanopores is much shorter than in the film and, therefore, the optical energy gap is larger. Furthermore, the blue shift depends on the pore diameter of the AAO membrane (Fig. 8.38). It was found that the lower the pore diameter is, the more evident effect is observed [120, 234, 237]. A little blue-shift in PL for the samples with small pore size is related with a high portion of the ordered polymeric chains (regular, compact packing and alignment of chains) inside the nanopores. It was also suggested that the observed PL intensity enhancement is a result of (i) Förster energy transfer from oxygen vacancies in AAO, acting as donors, to polymer molecules, acting as acceptors [120, 238] or (ii) higher density of polymeric material embedded into the nanopores [240]. Therefore, a lack of oxygen vacancies in the AAO prepared in sulfuric acid is the main reason for a lower energy transfer efficiency and, consequently, lower intensity of the PL spectra [120, 238].

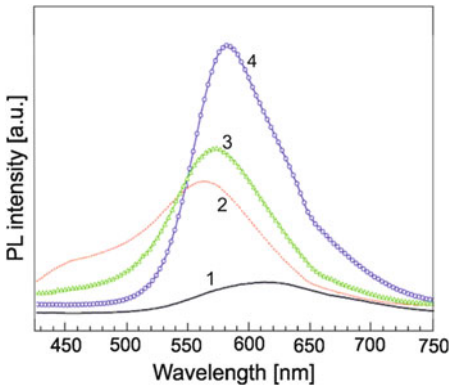

Fig. 8.38 Photoluminescence of the (*1*) PMP-Th film electropolymerized on Pt and AAO-PMP-Th composites with a AAO pore diameter of: (*2*) 60 nm , (*3*) 70 nm , and (*4*) 80 nm . Reprinted with permission from [238]

Chemical interactions between polymer and the AAO walls influence considerably the optical properties of the conjugated polymer nanostructures embedded into the AAO membranes. The Lewis acid/base and hydrogen-bonding-type interactions between conjugated polymers and AAO membranes significantly affect the optical properties of theses composites compared to bulk materials [233, 236, 241]. Kong et al. suggested that the aromatic rings and the ether groups in the MEH-PPV chains interact with the Lewis acid Al centers on the surfaces of the nanopore walls via electron donation, and with the Brønsted acid surface hydroxyl groups via a hydrogen-bonding-type interactions [233, 234, 236]. Consequently, the planar conformations of the polymer chains is destroyed and the short conjugation of the conjugated polymer in the nanopores appeared. As a result of this preferable alignment of the polymer chains, a blue shift is observed in the PL spectrum. The effect of chemical interactions between polymer chains and AAO surface is often accompanied by the size confinement effect [234].

From the photoluminescence studies it was revealed that for some nanocoposites (e.g., AAO-PMP-Th [120, 238], AAO-DBO-PPV [232]), the nano-size effect is only responsible for the blue shift of the PL peaks, while for other nanocomposites (e.g., AAO-MEH-PPV [234, 236], AAO-PVK-Alq_3 [241]) the interaction between the AAO and polymer chains or both mentioned effects influence the PL behavior.

8.6.2 Nanoparticles in AAO

Optical properties of nanoparticles (NPs) embedded into the AAO membranes were extensive studied. Many AAO-NPs composites based on deposited metals such as Ag [244–251], Au [252–261], and other materials e.g. PbS [262], TiO_2 [263], and

ZnO [264, 265] were investigated. In general, the optical properties of such systems depend on the type of nanoparticle material, particle size, surrounding material and particle interactions. The effective medium theory predicted, that even large amount of metal nanoparticles can be transparent, because the wavelength of light is much larger than their dimensions [252]. The anodic porous alumina membranes are especially useful as templates to produce small nanoparticles [266] and, due to the optical transparency of AAO, to investigate optical properties of nanoparticles [254].

The nanoparticles in the nanoporous AAO membranes can be deposited randomly or as layered structures as shown in Fig. 8.39 [250, 259]. As was demonstrated, the layered structure of deposited Ag NPs influences the LSPR peak in absorption spectra [250, 259, 260]. The absorption was dependent on the number of layers of Ag NPs. With an increase in the number of NP layers the intensity of the absorption peak increased and its position shifted from 450 to 400 nm (Fig. 8.39). The observed blue shift originates from the surface-plasmon coupling between the Ag NPs closely arranged in the AAO membrane. Sandrock et al. considered the plasmon resonance of the AAO-NPs composites with two layers of gold spheres, rods and rod-sphere pairs [259]. The influence of spacing between particles on the optical properties of the paired sphere composites was investigated. It was found that the plasmon resonance peak position does not change when the distance between NPs is larger than three particle diameters. However, when the interparticle spacing is smaller than the NP diameter, a red-shift and broadening of the peak can be observed. The smaller distance between sphere nanoparticles, the higher plasmon resonance [259, 260].

The size of NPs embedded into the AAO membrane is also important. When the Au particle diameter exceeds 200 nm, the AAO-NPs composite films are transparent in IR spectrum but opaque in near IR and visible range [252, 253]. The

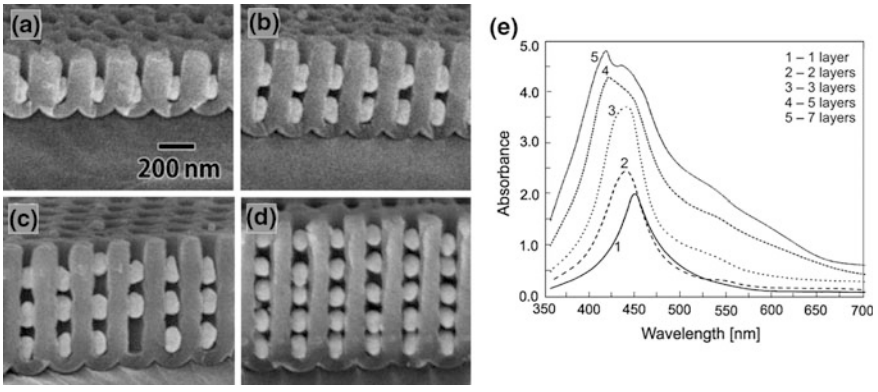

Fig. 8.39 SEM images of the layered structure of Ag NPs in the AAO membrane. One layer (**a**), two layers (**b**), three layers (**c**), and five layers of Ag nanoparticles (**d**) in the AAO membranes and their corresponding absorption spectra (**e**). Reprinted with permission from [250]

composites with the smaller particle diameter than 50 nm and aspect ratio of 1 are fully transparent in NIR and UV-Vis spectrum, except the strong absorption band of about 520 nm typical for LSPR of Au NPs [252]. Moreover, it is possible to design color of these composites by changing the shape of nanoparticles. With decreasing diameter of nearly spherical Au NPs (from 60 to 30 nm) a blue shift in the resonance peak was noticed [253]. For the rod-like Au nanoparticles (aspect ratio larger than 1) embedded in the AAO, in the intensity of the Au plasmon resonance increases and the peak shifts to lower wavelengths with increasing aspect ratio of NPs [252, 254, 255]. All those observation are consistent with effective medium theory formulated by Maxwell-Garnett theory [255, 258, 267, 268].

Moreover, the optical properties of Au nanoparticles embedded in the AAO membrane can be altered by heat treatment of the nanocomposite up to 400 °C, however, the effect is observable only for the NPs with irregular shape [255]. A low-temperature heating induces changes in the size and shape of Au nanoparticles and, consequently, affects the optical properties without interference from nanoparticle coalescence (Fig. 8.40). This is possible because each nanoparticle is confined to its own nanopore. The low aspect ratio (much lower than 3) Au nanoparticles have irregular structure (shape and size), however, after the heat treatment at low temperatures, they become dense and spherical. A blue shift in the plasmon band is observed with increasing annealing temperature (Fig. 8.40). On the other hand, no considerable changes in the optical absorption spectra with

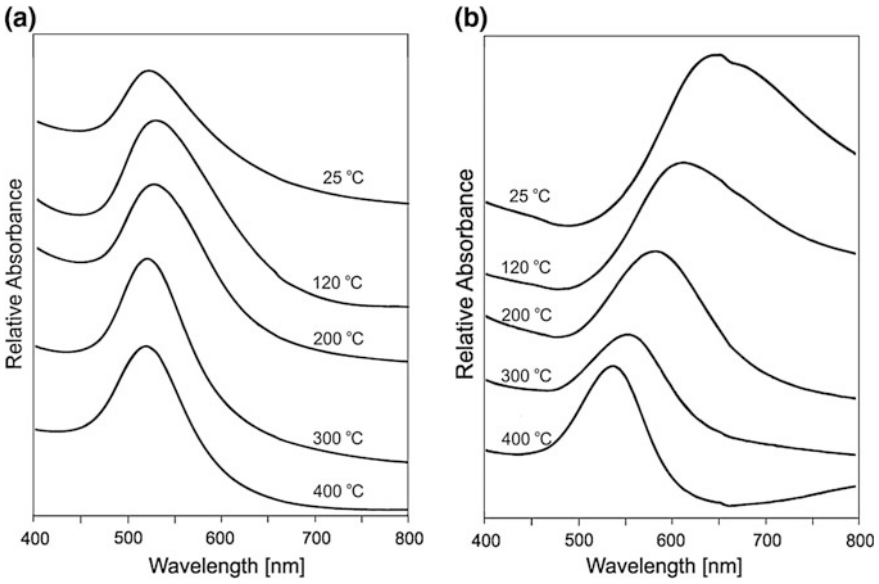

Fig. 8.40 Absorption spectra obtained before and after heating the AAO-Au NPs composites with Au NPs aspect ratio of about 3 (**a**) and 1 (**b**). The annealing temperatures were as indicated. Reprinted with permission from [255]

increasing annealing temperature were observed for the particles with the aspect ratio of about 3 [255]. Hu et al. studied the reflectivity of the AAO membranes containing Ag NPs and they observed the reduced reflectivity at the wavelength of ~465 nm caused by the strong plasmonic absorption [247]. The aggregation of NPs, accompanied by a considerable increase in their size (from 10 to 40 nm), was observed upon annealing. In contrast to the results reported by Hulteen et al. [255] for Au NPs, they [247] found that the increasing temperature of annealing shifts the plasmon absorption peak of Ag towards longer wavelengths. A similar red shift in the position of plasmon absorption peak (from 395 to 432 nm) with increasing diameter of Ag nanoparticles (from 46 to 90 nm) embedded in the AAO membranes was observed by Huang et al. [245].

As it was shown in Fig. 8.39, metallic nanoparticles can be deposited in the AAO membrane at the bottom of pores. Huang et al. studied absorption properties of the AAO-NPs composites at the bottom side of the AAO membranes [244]. The remaining aluminum layer was removed and Ag NPs were illuminated through the existing barrier layer of AAO (Fig. 8.41). The effect of the thinning of the barrier layer on absorption properties was studied for different thicknesses of the barrier layer ranging from about 15 to 0 nm. From the obtained spectra it was revealed that decreasing the barrier layer thickness shifts the LSPR peak location from 435 to 398 nm. The observed red-shift in the excitation spectra of the AAO-Ag NPs composites was attributed to higher refractive index of AAO as compared to refractive index of air or vacuum.

Various inorganic nanoparticles were loaded into the pores of AAO membranes and optical properties such composites were studied. For instance, an intense blue PL emission peaked around 450–485 nm was observed after ZnO nanoparticles

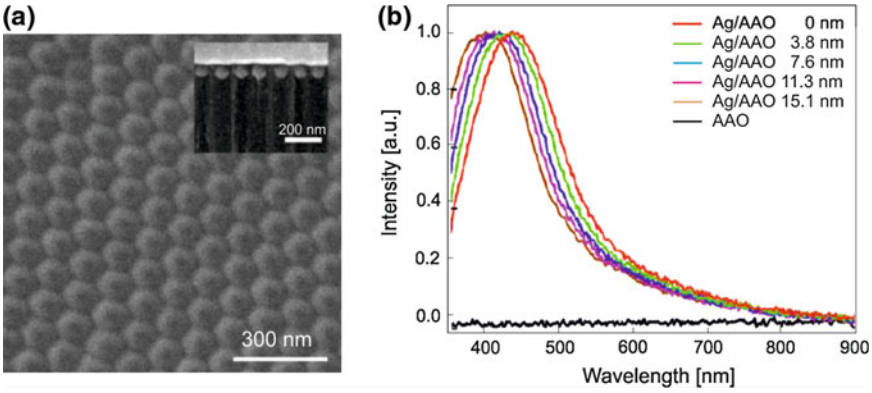

Fig. 8.41 SEM image of the bottom side of the AAO-Ag NPs film (**a**). *Inset* Cross-sectional SEM image of the Ag/AAO substrate where the back-end alumina layer has been chemically etched for 30 min to reduce the layer thickness to 3.8 nm. Silver nanoparticles were deposited inside the tube-like nanochannels. The extinction spectra of an AAO film without Ag and Ag/AAO films with different etching times for thinning the back-end alumina layer (**b**). Reprinted with permission from [244]

embedded into the AAO films [264, 265]. The PL intensity of the AAO-Zn NPs composite was 20 times higher than that of the nanostructured thin ZnO film. The luminescence enhancement was attributed to the increased number of singly ionized oxygen vacancies (F^+ centers) in the ZnO nanoparticles located in the pores of the AAO membrane [264, 265]. In general, blue shifts in absorption spectra were observed for the composites with embedded ZnO, PbS and TiO_2 nanoparticles [262, 263, 265]. This phenomenon was ascribed to the size confinement effect occurring in the AAO-NPs composites.

8.6.3 Xerogels in AAO

One of the simplest method used for the synthesis of luminescence materials is deposition of xerogels into the pores of the AAO membranes by a sol-gel technique. Generally, solutions are deposited inside the pores of AAO by spinning and during subsequent heat treatment xerogels (dry gels) are formed in nanopores. So far, the application of sol–gel techniques on AAO was used for the preparation of xerogels such as: Eu-doped Al_2O_3 [269, 270], Tb_2O_3-doped Al_2O_3 [271, 272], Y-doped Al_2O_3 [273], Er_2O_3-doped Fe_2O_3 [274], Er-doped In_2O_3 [275], Eu-doped In_2O_3 [269], Tb-doped SiO_2 [272, 276], Er_2O_3-doped TiO_2 [180, 274, 277–282], Eu_2O_3-doped TiO_2 [269, 278, 283–289], Tb-doped TiO_2 [180], Tb_2O_3-doped TiO_2 [277, 290, 291], and Tb-doped ZrO_2 [272]. All these nanocomposite materials exhibit enhanced photoluminescence compared to xerogels fabricated on planar substrates [269, 288–290]. It is widely recognized that PL of lanthanides from the AAO-xerogel composites increases with the thickness of AAO (Fig. 8.42a) [285, 290] and, for some excitation wavelength, increases with the number of xerogel layers deposited inside the AAO nanopores (Fig. 8.42b) [278, 282, 288, 290, 291], and even with the concentration of lanthanides in xerogels (Fig. 8.42c) [270, 271, 278, 290]. However, the PL spectra of the AAO-xelogel composites strongly depend on the annealing temperature e.g., [271, 273, 282, 290–292], etc.

8.6.4 Metallic and Other Layers Deposited on the AAO Surface

A controllable synthesis of nanoporous metals with a high degree of regularity in a form of metallic thin layers or nanomeshes has attracted recently much attention due to interest in fundamental optics and applications. The ordered metallic nanohole arrays demonstrate novel and unusual optical properties such as localized surface plasmon resonance (LSPR) due to surface corrugation at the subwavelength scale, which is significantly different from surface plasmon polaritons (SPPs) of planar surfaces [216, 217]. Since the LSPR is responsible for the electromagnetic-field enhancement that leads to surface-enhanced Raman scattering (SERS), this

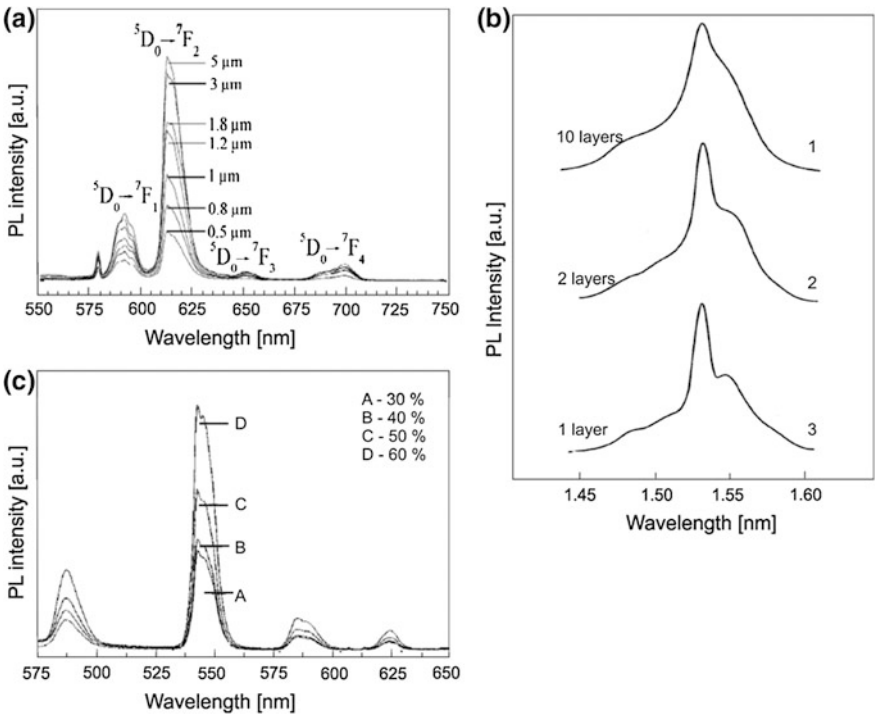

Fig. 8.42 Photoluminescence spectra of AAO-xerogels composites with one layer of the Eu-doped TiO_2 xerogel deposited at the AAOs with different thicknesses (**a**), different numbers of Er-doped TiO_2 xerogel layers deposited at the AAOs (**b**), and one layer of the Tb_2O_3-doped Al_2O_3 xerogels containing different Tb_2O_3 contents (**c**). Reprinted with permission from [285] (**a**), [282] (**b**), and [271] (**c**)

technique is commonly used for probing the thin metal films on the AAO membranes with adsorbed various molecules [293, 294]. These unique properties of metallic nanoporous arrays have generated potential applications in the field of antireflection materials, high-density capacitors and electrodes, photonic crystals, wave guides and lasing materials. A great variety of chemo- and biosensors based on absorbance, reflection, fluorescence, chemiluminescence, surface plasmon resonance and Raman scattering properties of the metal-coated AAO films were developed [128, 191, 193, 295–300].

Although the fabrication of nanoporous metal and metal oxide layers on AAO membranes has been widely explored over the last decades, the investigation of the optical properties is rather limited to noble metal layers. The studies on the optical properties of nanoporous metal layers deposited on the AAO membranes include such metals as: Ag [68, 105, 294, 301–303], Au [114, 193, 296–298, 303–306], Cr [105, 307], Fe [105], Ni [105], Pt [106, 308, 309], and Ti [105]. More recently, the optical properties of thin $Si_{1-x}Ge_x$ [310] and TiO_2 [307] layers deposited on the AAO membranes were also studied.

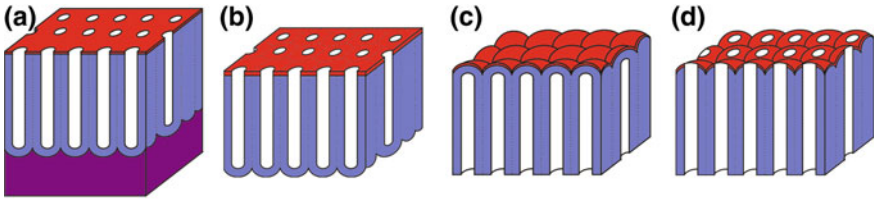

Fig. 8.43 Schematic structures of AAOs with the deposited thin layers on: the *top side* of the anodized sample (**a**), the *top side* of the membrane after Al removal (**b**), the barrier layer of the membrane (**c**), the barrier layer of the membrane with opened pores (**d**)

In general, nanoporous anodic alumina may be used in various variants as a substrate for the deposition of thin metallic layers (Fig. 8.43). However, the most frequently utilized is the mechanically stable AAO with the remaining aluminum layer-structure (a) (Fig. 8.43a).

UV-Vis absorption of the structures (b) – (d) (Fig. 8.43b–d) covered with sputtered Ag layers was studied in detail [294, 301, 302]. The observed distinct surface bands in the UV-Vis absorption spectra (e.g., different shape and position of the band) were attributed to differences in the shape and size of deposited Ag nanoparticles. In addition, the PL spectra recorded to the (b) – (d) composites showed a broad emission band centered at $\sim$500 nm, with the luminescence intensity increasing in the order (b) < (d) < (c) [301]. It is worth mentioning that for the pure AAO membrane intensity of the PL peak was the highest among all the spectra and the PL band was centered at 470 nm that is typical for the membranes obtained by anodization in oxalic acid. Yao et al. reported transmission spectra of the AAO samples coated with Au films (type (c) and (d)) [303]. It was stated that transmittance of the samples decreases in comparison with the un-coated AAO films because the Au layer creates a mirror-like surface and blocks most of the incident light. For the (d) structures with partially opened pores, a strongly enhanced transmission peak in the visible light range was observed and ascribed to LSPR of Au [303]. The highly ordered AAO films with higher porosities exhibit stronger the transmission enhancement effect. When the interpore distance in the AAO membranes decreases the effect weakens [303].

Similarly to NWs deposited inside the AAO membranes, the composite consisting of metallic or other inorganic layers deposited on the AAO membrane can be considered as a layered structure with different refractive indices (Fig. 8.44). Therefore, light interaction with such a structure, and especially interference enhancement can be described by the Bragg reflection principle (8.6)

$$2(n_d d_d \cos\theta_d + n_{AAO} d_{AAO} \cos\theta_{AAO}) = m\lambda \tag{8.6}$$

where n_d, d_d, d_{AAO}, θ_d and θ_{AAO} are effective reflective index of the deposited film, thickness of the deposited film, pore-depth in AAO (thickness of the AAO film), refractive angle in the deposited film and refractive angle in the AAO membrane,

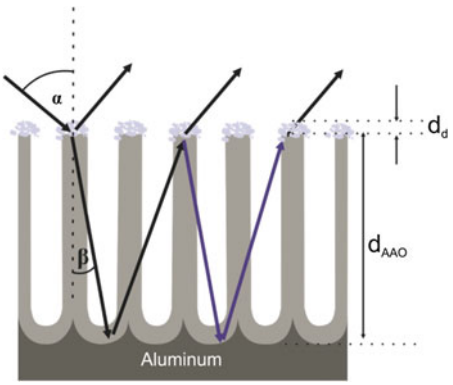

Fig. 8.44 Schematic of reflectance from a porous AAO membrane with deposited thin metallic layer

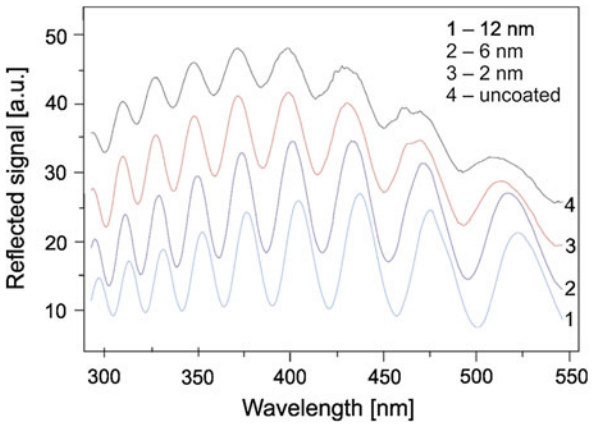

Fig. 8.45 Reflectance spectra of AAO films with different thicknesses of the deposited Pt layer. The pore diameter and thickness of the AAO film was 31 and 1600 nm, respectively. Reprinted with permission from [106]

respectively. All of the wavelengths which fits the equation will be strongly enhanced (at certain frequencies) and the others will be quenched, resulting in distinguish color of the sample [311]. Thus, the interference enhancement depends on the optical path difference, thickness of the AAO film, effective reflective index of the AAO structure (porosity), and incident angle.

The AAO film covered with thin metallic layer can be treated as a Fabry-Pérot interferometer containing nanometer size cavities [112]. Therefore, the reflectance signal varies upon the changes of the effective refractive index in cavities. As a result, oscillations in the reflectance spectrum are observed [106]. Fabry-Pérot interference of reflected light from the AAO membranes covered with thin metal layer forms the maximum peaks whose sharpness is determined by the effective thickness of the metal-coated AAO membranes (see Fig. 8.45) and by optical loss during propagation and reflection inside the sample [114, 191, 305–307]. Recently, a series of oscillations in the reflectance spectra was also demonstrated for the bilayered AAO structure (two layers with different pore diameters and consequently different porosities) covered with a thin Au layer [304].

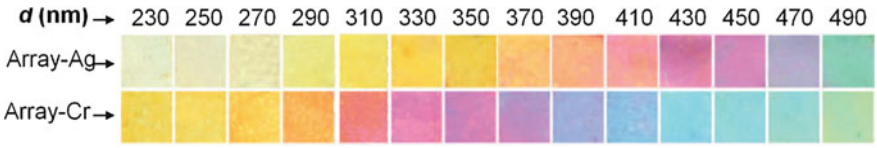

Fig. 8.46 Colors of AAO films with sputtering Ag and Cr layers. The thickness of the AAO film (pore depth, d) was ranged from 230 to 490 nm with 20-nm interval. The pore diameter and interpore distance of AAO was 40 and 100 nm, respectively. Reprinted with permission from [105]

One of the most effective method to change the color of the anodized AAO sample is to precisely control the thickness of the AAO film (pore depth, d_{AAO}). Wang et al. demonstrated that the best effect and the most distinct colors can be obtained by sputtering thin (c.a.7 nm) Ag and Cr layers on the surface of the AAO films. Due to the different refractive indices of Cr and Ag, the structures with the same pore depth exhibit different colors (Fig. 8.46) [105, 307]. As expected colors of AAO films coated with thin metal layers can be also tuned by the depth of pores in the AAO membrane. It was demonstrated that the colors of the AAO membranes anodized for longer period of time or using higher anodization potentials, and then covered with a metal layer, tend to become brighter due to increased thicknesses of the AAO layers [68, 308]. The structural color of the metal-coated AAO films can be alter by changing pore diameter of AAO [308]. The changing of incident angle is also a very effective procedure to tune color of the AAO membranes coated with thin films other than metals, e.g. TiO_2 [307].

8.6.5 Other Guest Molecules and Compounds in AAO

The presence of other ions, guest molecules, dyes and compounds inside the nanopores of the AAO membranes affects their optical properties. It is a direct result of interaction of the guest with the exposed aluminum atoms in the pores of the AAO films. The diversity in optical behavior of the modified AAO membranes is related mainly with a different nature of the immobilized/embedded/deposited guest and, therefore, different interactions with the alumina. The following examples are far from a complete list of possible chemical modifications of nanopores which influence the optical properties of AAO membranes, e.g., Cr^{3+} ions [84], Eu^{3+} ions [312], Tb^{3+} ions [312, 313], CdS [314], Ru(II)(4,4′-dicarboxyl-2,2′-bipyridyl)$_2$(SCN)$_2$) dye [315], $[Ru(dpp)_3]^{2+}$ (dpp = 4,7-diphenyl-1,10-phenanthroline) [316], siloxane with repeating Si_3OSiH and Si_3SiH moieties [266], Alizacin red S [317], 8-anilino-1-naphtalene-sulfonic acid [318], 7-diethyl amino-4-methylcumarin [318], diiodofluorescein [317], tetraiodofluorescein [317], 8-hydroxyquinoline [319, 320], Rhodamine B [321], Rhodamine 6G [87, 318, 322], Rhodamine110 (Rh110) [323], paraterphenyl and perylene [324], *N,N*′-diphenyl-*N, N*′-bis(3-methylpheny-l,1′-biphenyl-4,4′-diamine) (TPD) + 5 % rubrene (5,6,11,12-

tetraphenylnaphthacene) [325], tetrhydroxyflavanol [326], morin (3,5,7,2′,4′-pentahydroxyflavone) [327–329], morin-human serum albumen (HSA) [327], morin-human immunoglobulin (IgN) [329], morin-lysozyme (lys) [330], morin-trypsin (Try) [328].

Kurashima et al. [81] studied the saturable absorption effect of semiconducting single-wall carbon nanotubes for mode-locking devices of short pulse lasers. The optical absorption spectra of AAO membranes with different amount of carbon nanotubes were compared. The optical absorption spectra in a near-infrared showed that the absorption of the AAO membranes could be controlled by the content of the nanotubes in the pores.

As a general remark can be concluded that the porous alumina enhances considerably the photoluminescence intensity of the studied systems.

Acknowldgments Some of the research presented here was supported by the National Science Centre (Grant No. 2011/01/N/ST5/02510).

References

1. K.P. Han, J.L. Fang, Decorative-protective coatings on aluminum. Surf. Coat. Tech. **88**, 178–182 (1996)
2. L. Anicai, A. Meghea, C. Sirean, L. Dima, Analysis of electrochemically coloured aluminium anodic films by diffuse reflectance spectra. Mater. Sci. Forum **185–188**, 489–496 (1995)
3. F. Behzadi, M. Moradi, H.R. Karimi-Alavijeh, A. Gharavi, The effect of anodization voltage and surface morphology on the capacitance properties of Al-Al_2O_3-Al nanocapacitors. Vacuum **99**, 204–210 (2014)
4. G.D. Sulka, A. Brzózka, L. Zaraska, M. Jaskuła, Through-hole membranes of nanoporous alumina formed by anodizing in oxalic acid and their applications in fabrication of nanowire arrays. Electrochim. Acta **55**, 4368–4376 (2010)
5. T. Gao, J.C. Fan, G.W. Meng, Z.Q. Chu, L.D. Zhang, Thin Au film with highly ordered arrays of hemispherical dots. Thin Solid Films **401**, 102–105 (2001)
6. K. Nielsch, F.J. Castaño, S. Matthias, W. Lee, C.A. Ross, Synthesis of cobalt/polymer multilayer nanotubes. Adv. Eng. Mater. **7**, 217–221 (2005)
7. H. Masuda, H. Tanaka, N. Baba, Preparation of porous material by replacing microstructure of anodic alumina film with metal. Chem. Lett. **19**, 621–622 (1990)
8. Sulka, G.D.: *Highly ordered anodic porous alumina formation by self-organised anodising and template-assisted fabrication of nanostructured materials*, ed. by A. Eftekhari. Nanostructured Materials in Electrochemistry (Wiley-VCH, 2008), pp. 1–116
9. S.A. Bagshaw, T.J. Pinnavaia, Mesoporous alumina molecular sieves. Angew. Chem. Int. Ed. Engl. **35**, 1102–1105 (1996)
10. M.D. Henry, S. Walavalkar, A. Homyk, A. Scherer, Alumina etch masks for fabrication of high-aspect-ratio silicon micropillars and nanopillars. Nanotechnology **20**, 255305 (2009)
11. H. Moghadam, A. Samimi, Solar absorptivity of nano-porous anodic alumina (NPAA): effects of structural features. J. Porous Mater. **21**, 331–336 (2014)
12. W.L. Xu, H. Chen, M.J. Zheng, G.Q. Ding, W.Z. Shen, Optical transmission spectra of ordered porous alumina membranes with different thicknesses and porosities. Opt. Mater. **28**, 1160–1165 (2006)

13. G.D. Sulka, S. Stroobants, V. Moshchalkov, G. Borghs, J.-P. Celis, Synthesis of well-ordered nanopores by anodizing aluminum foils in sulfuric acid. J. Electrochem. Soc. **149**, D97–D103 (2002)
14. G.D. Sulka, M. Jaskuła, Defects analysis in self-organized nanopore arrays formed by anodization of aluminium at various temperatures. J. Nanosci. Nanootechnol. **6**, 3803–3811 (2006)
15. G.D. Sulka, K.G. Parkoła, Anodising potential influence on well-ordered nanostructures foremd by anodisation of aluminium in sulphuric acid. Thin Solid Films **515**, 338–345 (2006)
16. G.D. Sulka, K.G. Parkoła, Temperature infuence on well-ordered nanopore grown by anodization of auminium in sulphuric acid. Electrochim. Acta **52**, 1880–1888 (2007)
17. G.D. Sulka, W.J. Stępniowski, Structural features of self-organized nanopore arrays formed by anodization of aluminum in oxalic acid at relatively high temperatures. Electrochim. Acta **54**, 3683–3691 (2009)
18. L. Zaraska, G.D. Sulka, M. Jaskuła, The effect of n-alcohols on porous anodic alumina formed by self-organized two-step anodizing of aluminum in phosphoric acid. Surf. Coat. Technol. **204**, 1729–1737 (2010)
19. W. Lee, S.-J. Park, Porous anodic aluminum oxide: anodization and templated synthesis of functional nanostructures. Chem. Rev. **114**, 7487–7556 (2014)
20. W. Lee, J.-C. Kim, U. Gösele, Spontaneous current oscillations during hard anodization of aluminum under potentiostatic conditions. Adv. Funct. Mater. **20**, 21–27 (2010)
21. H. Han, S.J. Parh, J.S. Jang, H. Ryu, K.J. Kim, S. Baik, W. Lee, In situ determination of the pore opening point during wet-chemical etching of the barrier layer of porous anodic aluminum oxide: nonuniform impurity distribution in anodic oxide. ACS Appl. Mater. Interfaces **5**, 3441–3448 (2013)
22. G.E. Thompson, R.C. Furneaux, G.C. Wood, Electron microscopy of ion beam thinned porous anodic films formed on aluminium. Corros. Sci. **18**, 481–498 (1978)
23. G. Meng, F. Han, X. Zhao, B. Chen, D. Yang, J. Liu, Q. Xu, M. Kong, X. Zhu, Y.J. Jung, Y. Yang, Z. Chu, M. Ye, S. Kar, R. Vajtai, P.A. Ajayan, A general synthetic approach to interconnected nanowire/nanotube and nanotube/nanowire/nanotube heterojunctions with branched topology. Angew. Chem. Int. Ed. **48**, 7166–7170 (2009)
24. Y.T. Tian, G.W. Meng, T. Gao, S.H. Sun, T. Xie, X.S. Peng, C.H. Ye, L.D. Zhang, Alumina nanowire arrays standing on a porous anodic alumina membrane. Nanotechnology **15**, 189–191 (2004)
25. L. Zaraska, E. Kurowska, G.D. Sulka, M. Jaskuła, Porous alumina membranes with branched nanopores as templates for fabrication of y-shaped nanowire arrays. J. Solid State Electrochem. **16**, 3611–3619 (2012)
26. K.O. Jeong, Y.C. Choi, J. Kim, J.K. Han, S.A. Yang, S.D. Bu, Porous alumina templates with various shaped nanochannels. J. Korean Phys. Soc. **51**, S105–S110 (2007)
27. G. Meng, Y.J. Jung, A. Cao, R. Vajtai, P.M. Ajayan, Controlled fabrocation of hierarchically branched nanopores, nanotubes, and nanowires. Proc. Nat. Acad. Sci. **102**, 7074–7078 (2005)
28. W. Cheng, M. Steinhart, U. Gösele, R.B. Wehrspohn, Tree-like alumina nanopores generated in a non-steady-state anodization. J. Mater. Chem. **17**, 3493–3495 (2007)
29. A.Y.Y. Ho, H. Gao, Y.C. Lam, I. Rodríguez, Controlled fabrication of multitiered three-dimensional nanostructures in porous alumina. Adv. Funct. Mater. **18**, 2057–2063 (2008)
30. B. Wang, G.T. Fei, M. Wang, M.G. Kong, D. Zhang, Preparation of photonic crystals made of air pores in anodic alumina. Nanotechnology **18**, 1–4 (2007)
31. J. Ferré-Borrull, M.M. Rahman, J. Pallarès, L.F. Marsal, Tuning nanoporous anodic alumina distributed-Bragg reflectors with the number of anodization cycles and the anodization temperature. Nanoscale Res. Lett. **9**(416), 1–6 (2014)
32. Z.-Y. Ling, S.-S. Chen, X. Hu, X. Hu, Y. Li, Optical transmission spectra of anodic aluminum oxide membranes with a dual layer-by-layer structure. Chinese Phys. Lett. **26**, 1–3 (2009)

33. X. Hu, Y.J. Pu, Z.Y. Ling, Y. Li, Coloring of aluminum using photonic crystals of porous alumina with electrodeposited Ag. Opt. Mater. **32**, 382–386 (2009)
34. M.M. Rahman, L.F. Marsal, J. Pallares, J.F. Borrull, Tuning the photonic stop bands of nanoporous anodic alumina-based distributed Bragg reflectors by pore widening. ACS Appl. Mater. Interfaces **5**, 13375–13381 (2013)
35. Y. Su, G.T. Fei, Y. Zhang, P. Yan, H. Li, G.L. Shang, L.D. Zhang, Controllable preparation of the ordered pore arrays anodic alumina with high-quality photonic band gaps. Mater. Lett. **65**, 2693–2695 (2011)
36. C.K. Chung, R.X. Zhou, T.Y. Liu, W.T. Chang, Hybrid pulse anodization for the fabrication of porous anodic alumina films from commercial purity (99 %) aluminium at room temperature. Nanotechnology **20**(055301), 1–5 (2009)
37. W. Lee, R. Ji, U. Gösele, K. Nielsch, Fast fabrication of long-range ordered porous alumina membranes by hard anodization. Nat. Mater. **5**, 741–747 (2006)
38. W. Lee, K. Schwirn, M. Steinhart, E. Pippel, R. Scholz, U. Gösele, Structural engineering of nanoporous anodic aluminium oxide by pulse anodization of aluminium. Nat. Nanotechnol. **3**, 234–239 (2008)
39. W. Lee, R. Scholz, U. Gösele, A continuous process for structurally well-defined Al_2O_3 nanotubes based on pulse anodization of aluminum. Nano Lett. **8**, 2155–2160 (2008)
40. W. Lee, J.-C. Kim, Highly ordered porous alumina with tailor-made pore structures fabricated by pulse anodization. Nanotechnology **21**, 1–8 (2010)
41. K. Pitzschel, J.M. Montero Moreno, J. Escrig, O. Albrecht, K. Nielsch, J. Bachmann, Controlled introduction of diameter modulations in arrayed magnetic iron oxide nanotubes. ACS Nano **3**, 3463–3468 (2009)
42. K. Schwirn, W. Lee, R. Hillebrand, M. Steinhart, K. Nielsch, U. Gösele, Self-ordered anodic aluminum oxide formed by H_2SO_4 hard anodization. ACS Nano **2**, 302–310 (2008)
43. G.D. Sulka, A. Brzózka, L. Liu, Fabrication of diameter-modulated and ultrathin porous nanowires in anodic auminum oxide templates. Electrochim. Acta **56**, 4972–4979 (2011)
44. G.D. Sulka, K. Hnida, Distributed Bragg reflector based on porous anodic alumina fabricated by pulse anodization. Nanotechnology **23**, 1–8 (2012)
45. D. Losic, M. Lillo, D. Losic, Porous alumina with shaped pore geometries and complex pore architectures fabricated by cyclic anodization. Small **5**, 1392–1397 (2009)
46. D. Losic, D. Losic, Preparation of porous anodic alumina with periodically perforated pores. Langmuir **25**, 5426–5431 (2009)
47. M. Noormohammadi, M. Moradi, M.A. Kashi, A. Ramazani, Y. Mayamai, Structural engineering of nanoporous alumina by controlling the anodization voltage during the spontaneous current oscillation in hard anodization. Surf. Coat. Tech. **223**, 104–109 (2013)
48. M. Raoufi, H. Schonherr, Improved synthesis of anodized aluminum oxide with modulated pore diameters for the fabrication of polymeric nanotubes. RSC Adv. **3**, 13429–13436 (2013)
49. W.J. Zheng, G.T. Fei, B. Wang, Z. Jin, L.D. Zhang, Distributed Bragg reflector made of anodic alumina membrane. Mater. Lett. **63**, 706–709 (2009)
50. W.J. Zheng, G.T. Fei, B. Wang, L.D. Zhang, Modulation of transmission spectra of anodized alumina membrane distributed Bragg reflector by controlling anodization temperature. Nanoscale Res. Lett. **4**, 665–667 (2009)
51. A. Santos, L. Vojkuvka, M. Alba, V.S. Balderrama, J. Ferre-Borrull, J. Pallares, L.F. Marsal, Understanding and morphology control of pore modulations in nanoporous anodic alumina by discontinuous anodization. Phys. Status Solidi A **209**, 2045–2048 (2012)
52. C.K. Chung, M.W. Liao, O.K. Khor, Fabrication of porous anodic aluminum oxide by hybrid pulse anodization at relatively high potential. Microsyst. Technol. **20**, 1827–1832 (2014)
53. W. Lee, The anodization of aluminum for nanotechnology applications. JOM **62**, 57–63 (2010)
54. T. Nagaura, F. Takeuchi, S. Inoue, Fabrication and structural control of anodic alumina films with inverted cone porous structure using multi-step anodizing. Electrochim. Acta **53**, 2109–2114 (2008)

55. T. Nagaura, F. Takeuchi, Y. Yamauchi, K. Wada, S. Inoue, Fabrication of ordered Ni nanocones using a porous anodic alumina template. Electrochem. Comm. **10**, 681–685 (2008)
56. Y. Yamauchi, T. Nagamura, A. Ishikawa, T. Chikyow, S. Inoue, Evolution of standing mesochannels on porous anodic alumina substrates with designed conical holes. J. Am. Chem. Soc. **130**, 10165–10170 (2008)
57. A. Yamaguchi, K. Hotta, N. Teramae, Optical waveguide sensor based on a porous anodic alumina/aluminum multilayer film. Anal. Chem. **81**, 105–111 (2009)
58. W.S. Im, Y.S. Cho, G.S. Choi, F.C. Yu, D.J. Kim, Stepped carbon nanotubes synthesized in anodic aluminum oxide templates. Diam. Relat. Mater. **13**, 1214–1217 (2004)
59. R. Krishnan, C.V. Thompson, Monodomain high-aspect-ratio 2D and 3D ordered porous alumina structures with independently controlled pore spacing and diameter. Adv. Mater. **19**, 988–992 (2007)
60. Y.T. Tian, G.M. Meng, G.Z. Wang, F. Phillipp, S.H. Sun, L.D. Zhang, Step-shaped bismuth nanowires with metal-semiconductor junction characteristics. Nanotechnology **17**, 1041–1045 (2006)
61. Y.C. Sui, D.R. Acosta, J.A. Gonzalez-Leon, A. Bermudez, J. Feuchtwanger, B.Z. Cui, J.O. Flores, J.M. Saniger, Structure, thermal stability, and deformation of multibranched carbon nanotubes synthesized by CVD in the AAO template. J. Phys. Chem. B **105**, 1523–1527 (2001)
62. Y.C. Sui, J.A. Gonzales-Leon, A. Bermudez, J.M. Saniger, Synthesis of multi branched carbon nanotubes in porous anodic aluminum oxide template. Carbon **39**, 1709–1715 (2001)
63. X. Zhu, L. Liu, Y. Song, H. Jia, H. Yu, X. Xiao, X. Yang, Oxygen bubble mould effect: serrated nanopore formation and porous alumina growth. Monatsh. Chem. **139**, 999–1003 (2008)
64. M. Ghrib, R. Ouertani, M. Gaidi, N. Khedher, M.B. Salem, H. Ezzaouia, Effect of annealing on photoluminescence and optical properties of porous anodic alumina films formed in sulfuric acid for solar energy applications. Appl. Surf. Sci. **258**, 4995–5000 (2012)
65. S. Gong, A. Stolz, G. Myeong, E. Dogheche, A. Gokarna, S. Ryu, D. Decoster, Y. Cho, Effect of varying pore size of AAO films on refractive index and birefringence measured by prism coupling technique. Opt. Lett. **36**, 4272–4274 (2011)
66. S. Green, J.A. Badan, M. Gilles, A. Cortes, G. Riveros, D. Ramirez, H. Gomez, E. Quagliata, E.A. Dalchiele, R.E. Marotti, Optical properties of nanoporous Al_2O_3 obtained by aluminum anodization. Phys. Status Solidi A **4**, 618–621 (2007)
67. K. Kant, S.P. Low, A. Marshal, J.G. Shapter, D. Losic, Nanopore gradients on porous aluminum oxide generated by nonuniform anodization of aluminum. ACS Appl. Interfaces **2**, 3447–3454 (2010)
68. Y. Liu, H.H. Wang, J.E. Indacochea, M.L. Wang, A colorimetric sensor based on anodized aluminum oxide (AAO) substrate for the detection of nitroaromatics. Sensor. Actuat. B-Chem. **160**, 1149–1158 (2011)
69. A. Markovics, G. Nagy, B. Kovacs, Reflection-based sensor for gaseous ammonia. Sensor. Actuat. B-Chem. **139**, 252–257 (2009)
70. A. Markovics, B. Kovacs, Fabrication of optical chemical ammonia sensors using anodized alumina supports and sol-gel method. Talanta **109**, 101–106 (2013)
71. L.F. Marsal, L. Vojkouvka, J. Ferre-Borrull, T. Trifonov, J. Pallares, Optical characterization of self-ordered porous alumina membranes of various thicknesses. Phys. Status Solidi C **4**, 1918–1922 (2007)
72. J. Marthe, E. Meillot, G. Jeandel, F. Enguehard, J. Ilavsky, Enhancement of scattering and reflectance properties of plasma-sprayed alumina coatings by controlling the porosity. Surf. Coat. Tech. **220**, 80–84 (2013)
73. Q. Xu, H.-Y. Sun, Y.-H. Yang, L.-H. Liu, Z.-Y. Li, Optical properties and color generation mechanism of porous anodic alumina films. Appl. Surf. Sci. **258**, 1826–1830 (2011)
74. Q. Xu, Y. Yang, J. Gu, Z. Li, H. Sun, Influence of Al substrate on the optical properties of porous anodic alumina films. Mater. Lett. **74**, 137–139 (2012)

75. W. Zaghdoudi, M. Gaidi, R. Chtourou, Microstructural and optical properties of porous alumina elaborated on glass substrate. J. Mater. Eng. Perform. **23**, 869–874 (2013)
76. H. Efeoglu, T. Karacali, K. Meral, I.Y. Erdogan, Y. Onganer, Anodization of aluminium thin films on p++ Si and annihilation of strong luminescence from Al_2O_3. J. Lumin. **130**, 157–162 (2010)
77. D.H. Fan, G.Q. Ding, W.Z. Shen, M.J. Zheng, Anion impurities in porous alumina membranes: existence and functionality. Micropor. Mesopor. Mater. **100**, 154–159 (2007)
78. T. Gao, G.-W. Meng, L.-D. Zhang, Origin of the blue luminescence in porous anodic alumina films formed in oxalic acid solutions. Chinese Phys. Lett. **20**, 713–716 (2003)
79. T. Gao, G.-W. Meng, L.-D. Zhang, Blue luminescence in porous anodic alumina films: the role of the oxalic impurities. J. Phys.: Condens. Matter **15**, 2071–2079 (2003)
80. T. Gao, G.-W. Meng, L.-D. Zhang, Ultraviolet photoluminescence of porous anodic alumina films. Chinese Sci. Bull. **48**, 1090–1092 (2003)
81. Y. Kurashima, Y. Yokota, I. Miyamoto, H. Katura, Y. Sakakibara, Mode-locking nanoporous alumina membrane embedded with carbon nanotube saturable absorber. Appl. Phys. Lett. **94**(223102), 1–3 (2009)
82. Y.X. Gan, X. Zeng, L. Su, L. Yang, B.J. Gan, L. Zhang, Synthesis and enhanced light absorption of alumina matrix nanocomposites containing multilayer oxide nanorods and silver nanoparticles. Mater. Res. Bull. **46**, 1828–1836 (2011)
83. Y. Li, G.H. Li, G.W. Meng, L.D. Zhang, F. Phillipp, Photoluminescence and optical absorption caused by the f^+ centres in anodic alumina membranes. J. Phys.: Condens. Matter **13**, 2691–2699 (2001)
84. T. Li, S. Yang, L. Huang, J. Zhang, B. Gu, Y. Du, Strong photoluminescence from Cr^{3+} doped porous anodic alumina. J. Phys.: Condens. Matter **16**, 2463–2469 (2004)
85. N.I. Mukhurov, S.P. Zhvavyi, I.V. Gasenkova, S.N. Terekhov, P.P. Pershukevich, V.A. Orlovich, Photoluminescence of F-centers in films of anodic alumina. J. Appl. Spectrosc. **77**, 549–555 (2010)
86. C. Xu, Q. Xue, Y. Zhong, Y. Cui, L. Ba, B. Zhao, N. Gu, Photoluminescent blue-shift of organic molecules in nanometre pores. Nanotechnology **13**, 47–50 (2002)
87. Y. Yang, Q. Gao, Influence of sulfosalicylic acid in the electrolyte on the optical properties of porous anodic alumina membranes. Phys. Lett. A **333**, 328–333 (2004)
88. S. Garabagiu, G. Mihailescu, Thinning anodic aluminum oxide films and investigating their optical properties. Mater. Lett. **65**, 1648–1650 (2011)
89. G. Peitao, X. Zhilin, X. Yiyu, H. Caihua, Z. Lixin, Morphology and transmittance of porous alumina on glass substrate. Appl. Surf. Sci. **257**, 3307–3312 (2011)
90. C. Hong, T.T. Tang, C.-Y. Hung, R.-P. Pan, W. Fang, Liquid crystal alignment in nanoporous anodic aluminum oxide layer for LCD panel applications. Nanotechnology **21**, 1–10 (2010)
91. C.H. Jeon, D.H. Kim, Y.S. Lee, J.K. Han, Y.C. Choi, S.D. Bu, H.Y. Shin, S. Yoon, Strong pore-size dependence of the optical properties in porous alumina membranes. J. Korean Phys. Soc. **63**, 1789–1793 (2013)
92. L.-R. Zhao, J. Wang, Y. Li, Ch-W Wang, F. Zhou, W.-M. Liu, Anodic aluminum oxide films formed in mixed electrolytes of oxalic and sulfuric acid and their optical constants. Physica B **405**, 456–460 (2010)
93. Y. Katsuta, A. Yasumori, K. Wada, K. Kurashima, S. Suehara, S. Inoue, Three-dimensionally nanostructured alumina film on glass substrate: anodization of glass surface. J. Non-Cryst. Solids **354**, 451–455 (2008)
94. Y.-F. Liu, Y.-F. Tu, S.-Y. Huang, J.-P. Sang, X.-W. Zou, Effect of etch-treatment upon the intensity and peak position of photoluminescence spectra for anodic alumina films with ordered nanopore array. J. Mater. Sci. **44**, 3370–3375 (2009)
95. S. Jeon, D.-H. Kang, G.W. Lee, Difference of optical properties between porous alumina and sapphire using two-substrate method at elevated temperature. Curr. Appl. Phys. **13**, 1594–1599 (2013)

96. C.-H. Peng, C.-C. Hwang, C.-S. Hsiao, Structure and photoluminescence properties of strong blue-emitting alumina film developed from a liquid sol at low temperature. J. Alloy. Compd. **491**, 129–132 (2010)
97. S. Stojadinovic, I. Belca, M. Tadic, B. Kasalica, Z. Nedic, L. Zekovic, Galvanoluminescence properties of porous oxide films formed by anodization of aluminum in malonic acid. J. Electroanal. Chem. **619–620**, 125–130 (2008)
98. S. Stojadinovic, Z. Nedic, I. Belca, R. Vasilic, B. Kasalica, M. Petkovic, L. Zekovic, The effect of annealing on the photoluminescent and optical properties of porous anodic alumina films formed in sulfamic acid. Appl. Surf. Sci. **256**, 763–767 (2009)
99. S. Stojadinovic, R. Vasilic, Z. Nedic, B. Kasalica, I. Belca, L. Zekovic, Photoluminescen properties of barrier anodic oxide films on aluminum. Thin Solid Films **519**, 3516–3521 (2011)
100. I. Vrublevsky, A. Jagminas, S. Hemeltjen, W.A. Goedel, Effect of heat treatment on the structure of incorporated oxalate species and photoluminescent properties of porous alumina films formed in oxalic acid. J. Solid State Electrochem. **254**, 7326–7330 (2008)
101. I.A. Vrublevsky, K.V. Chernyakova, A. Ispas, A. Bund, N. Gaponik, A. Dubavik, Photoluminescence properties of heat-treated porous alumina films formed in oxalic acid. J. Lumin. **131**, 938–942 (2011)
102. J. Wang, C.-W. Wang, Y. Li, W.-M. Liu, Optical constans of anodic aluminum oxide films formed in oxalic acid solution. Thin Solid Films **516**, 7689–7694 (2008)
103. Z. Xia, Q. Xu, P. Guo, R. Wu, Laser-induced damage characteristic of porous alumina optical films. Opt. Commun. **284**, 4033–4037 (2011)
104. W.L. Xu, M.J. Zheng, S. Wu, W.Z. Shen, Effects of high-temperature annealing on structural and optical properties of highly ordered porous alumina membranes. Appl. Phys. Lett. **85**, 4364–4366 (2004)
105. X. Wang, H. Zhang, D. Zhang, Y. Ma, H.-J. Fecht, J.Z. Jiang, Color tuning by local sputtering metal nanolayer on microstructured porous alumina. Microsc. Res. Techniq. **75**, 698–701 (2012)
106. Y. Zhang, S.J. Son, H. Ju, Anodized aluminum oxide membranes of tunable porosity with platinum nanoscale-coating for photonic application. Curr. Appl. Phys. **12**, 1561–1565 (2012)
107. H.M. Chen, C.F. Hsin, R.-S. Liu, S.-F. Hu, C.-Y. Huang, Controlling optical properties of aluminum oxide using electrochemical deposition. J. Electrochem. Soc. **154**, K11–K14 (2007)
108. F. Davione, P.A. Galione, J.R. Ramos-Barrado, D. Leinen, F. Martin, E.A. Dalchiele, R.E. Marotti, Modeling of gradient index solar selective surfaces for solar thermal applications. Sol. Energy **91**, 316–326 (2013)
109. J.-J. Zhang, Z.-Y. Li, Z.J. Zhang, T.-S. Wu, H.-Y. Sun, Optical and magnetic properties of porous anodic alumina/Ni nanocomposite films. J. Appl. Phys. **113**(244305), 1–5 (2013)
110. J.-J. Zhang, Z.-Y. Li, H.-M. Zhang, H. Xue, H.-Y. Sun, Optical and magnetic properties of porous anodic alumina films embedded with Co nanowires. Chinese Phys. B **22**(087805), 1–4 (2013)
111. K. Huang, Y. Li, Z. Wu, C. Li, H. Lai, J. Kang, Asymmetric light reflectance effect in AAO on glass. Opt. Express **19**, 1301–1309 (2011)
112. T. Zhang, Z. Gong, R. Giorno, L. Que, A nanostructured Fabry-Pérot interferometer. Opt. Express **18**, 20282–20288 (2010)
113. F. Trivinho-Strixino, H.A. Guerreio, C.S. Gomes, E.C. Pereira, F.E.G. Guimaraes, Active waveguide effects from porous anodic alumina: an optical sensor proposition. Appl. Phys. Lett. **97**(011902), 1–3 (2010)
114. L.P. Hernandez-Eguia, J. Ferre-Borrull, G. Macias, J. Pallares, L.F. Marsal, Engineering optical properties of gold-coated nanoporous anodic alumina for biosensing. Nanoscale Res. Lett. **9**, 1–8 (2014)
115. G.S. Huang, X.L. Wu, G.G. Siu, P.K. Chu, On the origin of light emission from porous anodic alumina formed in sulfuric acid. Solid State Commun.**137**, 621–624 (2006)

116. K. Huang, L. Pu, Y. Shi, P. Han, R. Zhang, Y.D. Zheng, Photoluminescence oscillations in porous alumina films. Appl. Phys. Lett. **89**(201118), 1–2 (2006)
117. S. Gardelis, A.G. Nassiopoulou, V. Giannetta, M. Theodoropoulou, Photoluminescence-induced oscillations in porous anodic aluminum oxide films grown on Si: effect of the interface and porosity. J. Appl. Phys. **107**(113104), 1–5 (2010)
118. I. Vrublevsky, A. Jagminas, S. Hemeltjen, W. Goedel, Behavior of acid species during heat treatment and re-anodizing of porous alumina films formed in malonic acid. J. Solid State Electrochem. **13**, 1873–1880 (2009)
119. K.-W. Lee, T.-H. Yang, W.-L. Lu, M.-P. Houng, Fabricating 20 cm × 20 cm porous template using anodic aluminum oxide. Integr. Ferroelectr. **143**, 47–57 (2013)
120. X. Liu, F. Xu, Z. Li, W. Zhang, Photoluminescence of poly(thiophene) nanowires confined in porous anodic alumina membrane. Polymer **49**, 2197–2201 (2008)
121. W.J. Stępniowski, M. Norek, M. Michalska-Domańska, A. Bombalska, A. Nowak-Stępniowska, M. Kwaśny, Z. Bojar, Fabrication of anodic aluminium oxide with incorporated chromate ions. Appl. Surf. Sci. **259**, 324–330 (2012)
122. W.J. Stępniowski, M. Norek, M. Michalska-Domańska, A. Nowak-Stępniowska, A. Bombalska, M. Włodarski, Z. Bojar, Incorporation of copper chelate ions into anodic alumina walls. Mater. Lett. **106**, 242–245 (2013)
123. Y. Du, W.L. Cai, C.M. Mo, J. Chen, L.D. Zhang, X.G. Zhu, Preparation and photoluminescence of alumina membranes with ordered pore arrays. Appl. Phys. Lett. **74**, 2951–2953 (1999)
124. J.H. Chen, C.P. Huang, C.G. Chao, T.M. Chen, The investigation of photoluminescence centers in porous alumina membranes. Appl. Phys. A-Mater. **84**, 297–300 (2006)
125. J. Hohlbein, U. Rehn, R.B. Wehrspohn, In-situ optical characterization of porous alumina. Phys. Status Solidi A **201**, 803–807 (2004)
126. K.H. Lee, J.H. Crawford Jr, Luminescence of the F-center in sapphire. Phys. Rev. B **19**, 3217–3221 (1979)
127. S. Jheeta, D.C. Jain, R. Kumar, F. Singh, K.B. Garg, Photoluminescence study of swift heavy ion (SHI) induced defect centers in sapphire. J. Nucl. Mater. **353**, 190–192 (2006)
128. A. Santos, T. Kumeira, D. Losic, Nanoporous anodic alumina: a versatile platform for optical biosensors. Materials **7**, 4297–4320 (2014)
129. G.S. Huang, X.L. Wu, Y.F. Mei, X.F. Shao, Strong blue emission from anodic alumina membranes with ordered nanopores. J. Appl. Phys. **93**, 582–585 (2003)
130. M.E. Nasir, B. Hamilton, Measurement of the physical and electronic properties of ordered nanoporous alumina using XUV excitation spectroscopy. J. Phys. D Appl. Phys. **42**(195404), 1–7 (2009)
131. T.-E. Nee, C.-H. Fang, J.-C. Wang, P.-L. Fan, J.-A. Jiang, Characterization of the anomalous luminescence properties from self-ordered porous anodic alumina with oxalic acid electrolytes. Thin Solid Films. **518**, 1439–1442 (2009)
132. Y.-L. Shi, X.-G. Zhang, H.-L. Li, Enhanced photoluminescence of Eu(III)-anchored porous anodic alumina films. Spectrosc. Lett. **34**, 419–426 (2001)
133. J. Wang, C.-W. Wang, S.-Y. Li, F. Zhou, The effect of oxalic and sulfuric ions on the photoluminescence of anodic aluminium oxide formed in a mixture of sulfuric and oxalic acid. Appl. Phys. A-Mater. **94**, 939–942 (2009)
134. I. Vrublevsky, A. Jagminas, S. Hemeltjen, W.A. Goadel, Photoluminescent behavior of heat-treated porous alumina films formed in malonic acid. Appl. Surf. Sci. **256**, 2013–2017 (2010)
135. Y. Yamamoto, N. Baba, S. Tajima, Coloured materials and photoluminescence centres in anodic film on aluminium. Nature **289**, 572–574 (1981)
136. P.P. Pershukevich, D.V. Shabov, V.P. Osipov, J. Schreiber, V.A. Lapina, Luminescence properties of oxide coatings of aluminum alloys. J. Appl. Spectrosc. **78**, 524–533 (2011)
137. M. Kokonou, A.G. Nassiopoulou, A. Travlos, Structural and photoluminescence properties of thin alumina films on silicon, fabricated by electrochemistry. Mater. Sci. Eng. B-Adv. **101**, 65–70 (2003)

138. A. Rauf, M. Mehmood, M. Ahmed, M. Hasan, M. Aslam, Effects of ordering quality of the pores on the photoluminescence of porous anodic alumina prepared in oxalic acid. J. Lumin. **130**, 792–800 (2010)
139. Y.B. Li, M.J. Zheng, L. Ma, High-speed growth and photoluminescence of porous anodic alumina films with controllable interpore distances over a large range. Appl. Phys. Lett. **91** (073109), 1–3 (2007)
140. Y. Li, M. Zheng, M. Li, W. Shen, Fabrication of highly ordered nanoporous alumina films by stable high-field anodization. Nanotechnology **17**, 5101–5105 (2006)
141. L. Zaraska, G.D. Sulka, M. Jaskuła, Anodic alumina membranes with defined pore diameters and thicknesses obtained by adjusting the anodizing duration and pore opening/widening time. J. Solid State Electrochem. **15**, 2427–2436 (2011)
142. A. Santos, M. Alba, M.M. Rahman, P. Formentin, J. Ferre-Borrull, J. Pallares, L.F. Marsal, Structural tuning of photoluminescence in nanoporous anodic alumina by hard anodization in oxalic and malonic acids. Nanoscale Res. Lett. **7**, 1–11 (2012)
143. I.A. Vrublevsky, K.V. Chernyakova, A. Ispas, A. Bund, S. Zavadski, Optical properties of thin anodic alumina membranes formed in a solution of tartaric acid. Thin Solid Films **556**, 230–235 (2014)
144. G.H. Li, Y. Zhang, L.D. Zhang, Wavelength dependent photoluminescence of anodic alumina membranes. J. Phys.: Condens. Matter **15**, 8663–8671 (2003)
145. Z. Li, K. Huang, Blue luminescence in porous anodic alumina films. J. Phys.: Condens. Matter **19**, 1–7 (2007)
146. N.I. Mukhurov, S.P. Zhvavyi, S.N. Terekhov, A.Y. Panarin, I.F. Kotova, P.P. Perhukevich, I. A. Khodasevich, I.V. Gasenkova, V.A. Orlovich, Influence of electrolyte composition on photoluminescent properties of anodic aluminum oxide. J. Appl. Spectrosc. **75**, 214–218 (2008)
147. G.G. Khan, A.K. Singh, K. Mandal, Structure dependent photoluminescence of nanoporous amorphous anodic aluminium oxide membranes: role of F^+ center defects. J. Lumin. **134**, 772–777 (2013)
148. Y.F. Mei, G.G. Siu, J.P. Zou, X.L. Wu, Color centers vs electrolytes for Si-based porous anodic alumina. Phys. Lett. A **324**, 479–483 (2004)
149. Y. Li, Ch-W Wang, L.-R. Zhao, W.-M. Liu, Photoluminescence properties of porous anodic aluminium oxide membranes formed in mixture of sulfuric and oxalic acid. J. Phys. D Appl. Phys. **42**(045407), 1–5 (2009)
150. A. Nourmohammadi, S.J. Asadabadi, M.H. Yousefi, M. Ghasemzadeh, Photoluminescence emission of nanoporous anodic aluminum oxide films prepared in phosphoric acid. Nanoscale Res. Lett. **7**, 1–7 (2012)
151. Z. Li, K. Huang, Optical properties of alumina membranes prepared by anodic oxidation process. J. Lumin. **127**, 435–440 (2007)
152. S. Shingubara, Fabrication of nanomaterials using porous alumina templates. J. Nanopart. Res. **5**, 17–30 (2003)
153. X. Sun, F. Xu, Z. Li, W. Zhang, Photoluminescence properties of anodic alumina membranes with ordered nanopore arrays. J. Lumin. **121**, 588–594 (2006)
154. Z. Li, K. Huang, The effect of high-temperature annealing on optical properties of porous anodic alumina formed in oxalic acid. Luminescence **22**, 355–361 (2007)
155. Y. Han, L. Cao, F. Xu, T. Chen, Z. Zheng, K. Qian, W. Huang, Quantitative investigation in the influence of oxalic impurities on photoluminescence properties of porous AAOs. Mater. Chem. Phys. **129**, 1247–1251 (2011)
156. J.H. Wu, X.L. Wu, N. Tang, X.M. Bao, Strong ultraviolet and violet photoluminescence form Si-based anodic porous alumina films. Appl. Phys. A-Mater. **72**, 735–737 (2001)
157. A. Santos, G. Macias, J. Ferre-Borrull, J. Pallares, J.F. Marsal, Photoluminescent enzymatic sensor based on nanoporous anodic alumina. ASC Appl. Mater. Interfaces **4**, 3584–3588 (2012)
158. C.-L. Feng, Z. Zhong, M. Steinhart, A.-M. Caminade, J.-P. Majoral, W. Knoll, Graded-bangap quantum-dot-modified nanotubes: a sensitive biosensor for enhnanced detection of DNA hybridization. Adv. Mater. **19**, 1933–1936 (2007)

159. A. Santos, T. Kumeria, D. Losic, Optically optimized photoluminescent and interferometric biosensors base on nanoporous anodic alumina: a comparison. Anal. Chem. **85**, 7904–7911 (2013)
160. S.-J. Yuan, Q.-S. Li, Z.-F. Pan, Y.-F. Dong, Q.-T. Wang, H.-H. Ji, Photoluminescence spectra of organic dyes embedded in porous alumina. Chin. J. Semicond. **22**, 1406–1410 (2001)
161. X. Wu, S. Xiong, J. Guo, L. Wang, C. Hua, Y. Hou, P.K. Chu, Ultrathin amorphous alumina nanoparticles with quantum-confined oxygen-vacancy-induced blue photoluminescence as fluorescent biological labels. J. Phys. Chem. C **116**, 2356–2362 (2012)
162. Y. Cao, J.O. Schenk, M.A. Fiddy, Third order nonlinear effect near a degenerate band edge. Optic. Photo. Lett. **1**, 1–7 (2008)
163. M.E. Calvo, S. Colodrero, N. Hidalgo, G. Lozano, C. Lopez-Lopez, O. Sanchez-Sobrado, H. Miguez, Porous one dimensional photonic crystals: novel multifunctional materials for environmental and energy applications. Energ. Environ. Sci. **4**, 4800–4812 (2011)
164. M.J.A. De Dood, E. Snoeks, A. Moroz, A. Polman, Design and optimization of 2D photonic crystal waveguides based on silicon. Opt. Quant. Electron. **34**, 145–159 (2002)
165. J. Choi, Y. Luo, R.B. Wehrspohn, R. Hillebrand, J. Schilling, U. Gösele, Perfect two-dimensional porous alumina photoni crystals with duplex oxide layer. J. Appl. Phys. **94**, 4757–4762 (2003)
166. A. Sato, Y. Pennec, T. Yanagishita, H. Masuda, W. Knoll, B. Djafari-Rouhani, G. Fytas, Cavity-type hypersonic phononic crystals. New J. Chem. **14**(113032), 1–13 (2012)
167. J.D. Joannopoulos, S.G. Johnson, J.N. Winn, R.D. Meade, *Photonic Crystals* (Princeton University Press, Molding the Flow of Light, 2008)
168. T. Maka, D.N. Chigrin, S.G. Romanov, C.M. Sotomayor Torres, Three dimensional photonic crystals in the visible regime. Prog. Electromagn. Res. **41**, 307–335 (2003)
169. R.B. Wehrspohn, J. Schilling, Electrochemically prepared pore arrays for photonic-crystal applications. MRS Bull. **26**, 623–626 (2001)
170. H. Masuda, M. Ohya, H. Asoh, M. Nakao, M. Nohtomi, T. Tamamura, Photonic crystal using anodic porous alumina. J. Appl. Phys. **38**, L1403–L1405 (1999)
171. H. Masuda, M. Ohaya, K. Nishio, H. Asoh, M. Nakao, M. Nohtomi, A. Yakoo, T. Tamamura, Electrochemically prepared pore arrays for photonic-crystal applications. Jpn. J. Appl. Phys. **39**, L1039–L1041 (2000)
172. H. Masuda, M. Ohya, H. Asoh, K. Nishio, Photonic band gap in naturally occurring ordered anodic porous alumina. Jpn. J. Appl. Phys. **40**, L1217–L1219 (2001)
173. H. Masuda, M. Yamada, F. Matsumoto, S. Yokoyama, S. Mashiko, M. Nakao, K. Nishio, Lasing from two-dimensional photonic crystals using anodic porous alumina. Adv. Mater. **18**, 213–216 (2006)
174. J. Choi, K. Schilling, K. Nielsch, R. Hillebrand, M. Reiche, R.B. Wehrspohn, U. Gösele, Large-area porous alumina photonic crystals via imprint method. Mat. Res. Soc. Symp. Proc. **722**, 2.1–2.6 (2002)
175. H. Masuda, T. Kondo, K. Nishio, Functional optical devices using highly ordered hole array architectures of anodic porous alumina. Proc. SPIE **8204**, 820414 (2011)
176. I. Mikulskas, S. Juodkazis, R. Tomasiunas, J.G. Dumas, Aluminum oxide photonic crystals grown by a new hybrid method. Adv. Mater. **13**, 1574–1577 (2001)
177. V. Mizeikis, I. Mikulskas, R. Tomasionas, S. Juodkazis, S. Matsuto, H. Misawa, Optical characteristics of two-dimensional photonic crystals in anodic aluminum oxide films. Jpn. J. Appl. Phys. **43**, 3643–3647 (2004)
178. R.B. Wehrspohn, A.P. Li, K. Nielsch, F. Müller, W. Erfurth, U. Gösele, Highly ordered alumina films: pore growth and applications. Electrochem. Soc. 271–282 (2000)
179. M. Saito, M. Miyagi, Anisotropic optical loss and birefrigence of anodized alumina film. J. Opt. Soc. Am. A **6**, 1895–1900 (1989)
180. G.K. Maliarevich, I.S. Molchan, N.V. Gaponenko, A.V. Mudryi, S.V. Gaponenko, A.A. Lutich, G.E. Thompson, Optoelectronic applications of lantanide-doped sol-gel products and porous anodic alumina. J. Soc. Inf. Display **14**, 583–588 (2006)

181. A.A. Lutich, I.S. Molchan, N.V. Gaponenko, S.V. Gaponenko, Scattering, propagation and polarization changes of light in nanoporous anodic alumina. Proc. SPIE **6258**, 1–9 (2006)
182. A.A. Lutich, I.S. Molchan, N.V. Gaponenko, Briefringence in porous anodic aluminum oxide. Opt. Spectrosc. **97**, 817–821 (2004)
183. A.A. Lutich, M.B. Danailov, S. Volchek, V.A. Yakovtseva, V.A. Sokol, S.V. Gaponenko, Birefringence of nanoporous alumina: dependence on structure parameters. Appl. Phys. B-Lasers Opt. **84**, 327–331 (2006)
184. X. Hu, Z.-Y. Ling, S.-S. Chen, X.-X. He, Influence of light scattering on transmission spectra of photonic crystals of anodized alumina. Chinese Phys. Lett. **25**, 3284–3287 (2008)
185. G.L. Shang, G.T. Fei, Y. Zhang, P. Yan, S.H. Xu, L.D. Zhang, Preparation of narrow photonic bandgaps located in the near infrared region and their applications in ethanol gas sensing. J. Mater. Chem. C **1**, 5285–5291 (2013)
186. G.L. Shang, G.T. Fei, Y. Zhang, P. Yan, S.H. Xu, H.M. Ouyang, L.D. Zhang, Fano resonance in anodic aluminium oxide based photonic crystals. Sci. Rep. **4**, 1–6 (2014)
187. L. Pavesi, Porous silicon dielectric multilayers and microcavities. Riv. Nuovo Cimento **20**, 1–76 (1997)
188. D.-L. Guo, L.-X. Fan, F.-H. Wang, S.-Y. Huang, X.-W. Zou, Porous anodic aluminum oxide Bragg stacks as chemical sensors. J. Phys. Chem. C **112**, 17952–17956 (2006)
189. M. Francon, *Optical Interferometry* (Academic Press, New York ,1966), p. 178
190. J. Hawkes, I. Latimer, *Lasers: Theory and Practice* (Prentice-Hall , Lebanon, 1995), p. 222
191. T. Kumeria, A. Santos, D. Losic, Nanoporous anodic alumina platforms: engineered surface chemistry and structure for optical sensing applications. Sensors **14**, 1187–11918 (2014)
192. K. Malek, A. Brzózka, A. Rygula, G.D. Sulka, SERS imaging of silver coated nanostructured Al and Al_2O_3 substrates. The effect of nanostructure. J. Raman Spectrosc. **45**, 281–291 (2014)
193. S.-H. Yeom, O.-G. Kim, B.-H. Kang, K.-J. Kim, H. Yuan, D.-H. Kwon, H.-R. Kim, S.-W. Kang, Highly sensitive nano-porous lattice biosensor based on localized surface plasmon resonance and interference. Opt. Express **19**, 22882–22891 (2011)
194. A. Makhal, S. Sarkar, S.K. Pal, H. Yan, D. Wulferding, F. Cetin, P. Lemmens, Ultrafast excited state deactivation of doped porous anodic alumina membranes. Nanotechnology **23**, 1–8 (2012)
195. R.-L. Zong, J. Zhou, Q. Li, B. Du, B. Li, M. Fu, X.-W. Qi, L.-T. Li, Synthesis and optical properties of silver nanowire arrays embedded in anodic alumina membrane. J. Phys. Chem. B **108**, 16713–16716 (2004)
196. Z.-K. Zhou, X.-R. Su, X.-N. Peng, L. Zhou, Sublinear and superlinear photoluminescence from Nd doped anodic aluminum oxide templates loaded with Ag nanowires. Opt. Express **16**, 18028–18033 (2008)
197. J. Yao, Z. Liu, Y. Liu, Y. Wang, C. Sun, G. Bartal, A.M. Stacy, X. Zhang, Optical negative refraction in bulk metamaterials of nanowires. Science **321**, 930 (2008)
198. P.R. Evans, R. Kullock, W.R. Hendren, R. Atkinson, R.J. Pollard, L.M. Eng, Optical transmission properties and electric field distribution of interacting 2D silver nanorod arrays. Adv. Funct. Mater. **18**, 1075–1079 (2008)
199. P.R. Evans, W.R. Hendren, R. Atkinson, R.J. Pollard, Optical transmission measurements of silver, silver-gold alloy and silver-gold segmented nanorods in thin film alumina. Nanotechnology **19**, 1–8 (2008)
200. L. Menon, W.T. Lu, A.L. Friedman, S.P. Bennett, D. Heiman, S. Sridhar, Negative index metamaterials based on metal-dielectric nanocomposites for imaging applications. Appl. Phys. Lett. **93**(123117), 1–3 (2008)
201. X. Ao, S. He, Negative refraction of left-handed behaviour in porous alumina with infiltrated silver at an optical wavelength. Appl. Phys. Lett. **87**(101112), 1–3 (2005)
202. A. Yasui, M. Iwasaki, T. Kawahara, H. Tada, S. Ito, Color properties of gold-silver alternate nanowires electrochemically grown in the pores of aluminum anodic oxidation film. J. Colloid Interf. Sci. **293**, 443–448 (2006)

203. H. Yan, P. Lemmens, D. Wulferding, J. Shi, K.D. Becker, C. Lin, A. Lak, M. Schilling, Tailoring defect structure and optical absorption of porous anodic aluminium oxide membranes. Mater. Chem. Phys. **135**, 206–211 (2012)
204. M. Es-Souni, S. Habouti, Ordered nanomaterial thin films via supported anodized alumina templates. Front. Mater. **1**, 1–9 (2014)
205. A.V. Kabashin, P. Evans, S. Pastkovsky, W. Hendren, G.A. Wurtz, R. Atkinson, R. Pollard, V.A. Podolskiy, A.V. Zayats, Plasmonic nanorod metamaterials for biosensing. Nat. Mater. **8**, 867–871 (2009)
206. R. Atkinson, W.R. Hendren, G.A. Wurtz, W. Dickson, A.V. Zayats, P. Evans, R.J. Pollard, Anisotropic optical properties of arrays of gold nanorods embedded in alumina. Phys. Rev. B **73**(235402), 1–8 (2006)
207. P. Evans, W.R. Hendren, R. Atkinson, G.A. Wurtz, W. Dickson, A.V. Zayats, R.J. Pollard, Growth and properties of gold and nickel nanorods in thin film aumina. Nanotechnology **17**, 5746–5753 (2006)
208. Q. Xu, W.-J. Ye, S.-Z. Feng, H.-Y. Sun, Synthesis and properties of iridescent Co-containing anodic aluminum oxide films. Dyes Pigments **111**, 185–189 (2014)
209. H.J. Tang, F.Q. Wu, H.L. Wang, Y.H. Wei, Q.S. Li, Microstructure and optical properties of Cu/Al_2O_3 nanoarray composite structure. J. Appl. Phys. **100**(064316), 1–4 (2006)
210. J.-J. Zhang, X. Hou, L.-H. Liu, H.-Y. Sun, Optical and magnetic properties of PAA@Fe nanocomposite films. AIP Adv. **3**, 072116, 1–6 (2013)
211. E. Wäckelgård, A study of the optical properties of nickel-pigmented anodic alumina in the infrared region. J. Phys.: Condens. Matter **8**, 5125–5138 (1996)
212. L. Arurault, G. Zamora, V. Vilar, P. Winterton, R. Bes, Electrical behaviour, characteristics and properties of anodic aluminium oxide films coloured by nickel electrodeposition. J. Mater. Sci. **45**, 2611–2618 (2010)
213. R. Akolkar, Y.-M. Wang, H.-H. Kuo, Kinetics of the electrolytic coloring process on anodized aluminum. J. Appl. Electrochem. **37**, 291–296 (2007)
214. C. Liang, K. Terabe, T. Tsuruoka, M. Osada, T. Hasegawa, M. Aono, AgI/Ag heterojunction nanowires: facile electrochemical synthesis, photoluminescence, and enhanced ionic conductivity. Adv. Funct. Mater. **17**, 1466–1472 (2007)
215. E. Hutter, J.H. Fendler, Exploitation of localized plasmon resonance. Adv. Mater. **16**, 1685–1706 (2004)
216. S.K. Ghosh, T. Pal, Interparticle coupling effect on the surface plasmon resonance of gold nanoparticles: from theory to applications. Chem. Rev. **107**, 4749–4862 (2007)
217. W.L. Barnes, A. Dereux, T.W. Ebbesen, Surface plasmon subwavelength optics. Nature **424**, 824–830 (2003)
218. R.-L. Zong, J. Zhou, B. Li, M. Fu, S.-K. Shi, L.-T. Li, Optical properties of transparent copper nanorod and nanowire arrays embedded in anodic aumina oxide. J. Chem. Phys. **123** (094710), 1–5 (2005)
219. W.T. Lu, S. Sridhar, Superlens imaging theory for anisotropic nanostructured metamaterials with broadband all-angle negative refraction. Phys. Rev. B **77**(233101), 1–4 (2008)
220. X. Hu, C.T. Chan, Photonic crystals with silver nanowires as a near-infrared superlens. Appl. Phys. Lett. **85**, 1520–1522 (2004)
221. X. Zhang, Absolute negative, refraction and imaging of unpolarized electromagnetic waves by two-dimensional photonic crystals. Phys. Rev. B **70**(205102), 1–6 (2004)
222. O. Takayama, M. Cada, Two-dimensional metallo-dielectric photonic crystals embedded in anodic porous alumina for optical wavelengths. Appl. Phys. Lett. **85**, 1311–1313 (2004)
223. D. Pullini, P. Repetto, S. Bernard, L. Doskolovich, P. Perlo, Rigorous calculations and fabrication by self-assembly techniques of 2D subwavelength structures of gold for photonic applications. Appl. Optics **44**, 5127–5130 (2005)
224. M. Saito, M. Miyagi, Micropolarizer using anodized alumina with implanted metallic columns: theoretical analysis. Appl. Optics **28**, 3529–3533 (1989)

225. J. Zhang, Y. Yan, X. Co, L. Zhang, Microarrays of silver nanowires embedded in anodic alumina membrane templates: size dependence of polarization characteristics. Appl. Optics **45**, 297–304 (2006)
226. Y.T. Pang, G.W. Meng, Q. Fang, L.D. Zhang, Silver nanowire array infrared polarizers. Nanotechnology **14**, 20–24 (2003)
227. H.J. Tang, F.Q. Wu, S. Zhang, Optical properties of Co/Al_2O_3 nano-array composite structure. Appl. Phys. A-Mater. **85**, 29–32 (2006)
228. Y.T. Pang, G.W. Meng, Y. Zhang, Q. Fang, L.D. Zhang, Copper nanowire arrays for infrared polarizer. Appl. Phys. A-Mater. **76**, 533–536 (2003)
229. M. Saito, M. Kirihara, T. Taniguchi, M. Miyagi, Micropolarizer made of the anodized alumina film. Appl. Phys. Lett. **55**, 607–609 (1989)
230. Y.-T. Pang, G.-W. Meng, W.-J. Shan, Q. Fang, L.-D. Zhang, Micropolarizer of ordered Ni nanowire arrays embedded in porous anodic alumina membrane. Chinese Phys. Lett. **30**, 144–147 (2003)
231. Y.-T. Pang, G.-W. Meng, L.-D. Zhang, Y. Qin, X.-Y. Gao, A.-W. Zhao, Q. Fang, Arrays of ordered Pb nanowires and their optical properties for laminated polarizers. Adv. Funct. Mater. **12**, 719–722 (2002)
232. Y. Zhao, D. Yang, C. Zhou, Q. Yang, D. Que, Photoluminescence properties of the composite of porous alumina and poly(2,5-dibutoxy-1,4 phenylenevinylene). J. Lumin. **105**, 57–60 (2003)
233. D. Qi, K. Kwong, K. Rademacher, M.O. Wolf, J.F. Young, Optical emission of conjugated polymers adsorbed to nanoporous alumina. Nano Lett. **3**, 1265–1268 (2003)
234. F. Kong, X.L. Wu, G.S. Huang, Y.M. Yang, R.K. Yuan, C.Z. Yang, P.K. Chu, G.C. Siu, Optical emission from Nano-poly[2-methoxy-5-(2-ethyl-hexyloxy)-p-phenylene vinylene] arrays. J. Appl. Phys. **98**(074304), 1–4 (2005)
235. F. Kong, G.S. Huang, Y.M. Yang, C.Z. Yang, X.M. Bao, R.K. Yuan, Conformation and luminescence characteristics of nano-poly[2-metoxy-5-(20-ethyl-hexyloxy)-p-phenylene vinylene] in two-dimensional arrays. J. Polym. Sci. Part B: Polym. Phys. **44**, 3037–3041 (2006)
236. F. Kong, Y. Yang, X. Zhang, B. Lin, Z. Qi, T. Qiu, Effect of absorption to nanopore on optical properties of conjugated polymers in porous anode alumina. J. Appl. Phys. **109** (044309), 1–5 (2011)
237. T.P. Nguyen, S.H. Yang, P. Le Rendu, H. Khan, Optical properties of poly(2-methoxy-5-(2′-ethyl-hexyloxy)-phenylene vinylene) deposited on porous alumina substrates. Compos. Part A-Appl. Sci. Manuf. **36**, 515–519 (2005)
238. X. Liu, F. Xu, Z. Li, J. Zhu, W. Zhang, Synthesis and optical properties of Poly[3-(2-methoxyphenyl)thiophene] nanowires confined in porous anodic alumina membrane. Opt. Mater. **30**, 1861–1866 (2008)
239. K.M. Coakley, B.S. Srinivasan, J.M. Ziebarth, C. Goh, Y. Liu, M.D. McGehee, Enhanced hole mobility in regioregular polythiophene infiltrated in straight nanopores. Adv. Funct. Mater. **15**, 1927–1932 (2005)
240. J. Martin, M. Campoy-Quiles, A. Nogales, M. Garriga, M.I. Alonso, A.R. Goni, M. Martin-Gonzales, Poly(3-hexylthiophene) nanowires in porous alumina: internal structure under confinement. Soft Matter **10**, 3335–3346 (2014)
241. H.-W. Shin, E.-J. Shin, S.Y. Cho, S.-L. Oh, Y.-R. Kim, Enhanced energy transfer within pvk/alq3 polymer nanowires induced by the interface effect of nanochannels in porous alumina membrane. J. Phys. Chem. C **111**, 15391–15396 (2007)
242. T.Q. Nguyen, J. Wu, V. Doan, B.J. Schwartz, S.H. Tolbert, Control of energy transfer in oriented conjugated polymer-mesoporous silica composites. Science **288**, 652–656 (2000)
243. S. Moynihan, D. Iacopino, D. O'Carroll, P. Lovera, G. Redmond, Template synthesis of highly oriented polyfluorene nanotube arrays. Chem. Mater. **20**, 996–1003 (2008)
244. C.-H. Huang, H.-Y. Lin, S. Chen, C.-Y. Liu, H.-C. Chui, Y. Tzeng, Electrochemically fabricated self-aligned 2-D silver/alumina arrays as reliable SERS sensors. Opt. Express **19**, 11441–11450 (2011)

245. C.-H. Huang, H.-Y. Lin, Y. Tzeng, C.-H. Fan, C. Lu, C.-Y. Li, C.-W. Huang, N.-K. Chen, H.-C. Chui, Optical characteristics of pore size on porous anodic aluminium oxide films with embedded silver nanoparticles. Sensor. Actuat. A-Phys.**180**, 49–54 (2012)
246. N. Ji, W. Ruan, C. Wang, Z. Lu, B. Zhao, Fabrication of silver decorated anodic aluminum oxide substrate and its optical properties on surface-enhanced raman scattering and thin film interference. Langmuir **25**, 11869–11873 (2009)
247. Q. Hu, H.H. Lee, D.-Y. Jeong, Y.-S. Kim, K.-B. Kim, J. Xu, T.-S. Yoon, Reflectivity spectra and colors of porous anodic aluminum oxide containing silver nanoparticles by plasmonic absorption. J. Nanosci. Nanotechnol. **12**, 1979–1983 (2012)
248. G. Giallongo, C. Durante, R. Pilot, D. Garoli, R. Bozio, F. Romanto, A. Gennaro, G.A. Rizzi, G. Granozzi, Growth and optical properties of silver nanostructures obtained on connected anodic aluminum oxide templates. Nanotechnology **23**(325604), 1–10 (2012)
249. H.-H. Wang, C.-Y. Liu, S.-B. Wu, N.-W. Liu, C.-Y. Peng, T.H. Chan, C.-F. Hsu, J.-K. Wang, Y.L. Wang, Highly raman-enhancing substrates based on silver nanoparticle arrays with tunable sub-10 nm gaps. Adv. Mater. **18**, 491–495 (2006)
250. T. Kondo, K. Nishio, H. Masuda, Mutilayered three-dimensional structures of Ag nanoparticles in anodic porous alumina. Jpn. J. Appl. Phys. **49**(025002), 1–3 (2010)
251. S. Ye, Y. Hou, R. Zhu, S. Gu, J. Wang, Z. Zhang, S. Shi, J. Du, Synthesis and photoluminescence enhancement of silver nanoparticles decorated porous anodic alumina. J. Mater. Sci. Technol. **27**, 165–169 (2011)
252. C.A. Foss, L.H. Gabor, J.A. Stockert, C.R. Matrin, Optical properties of composite membranes containing arrays of nanoscopic gold cylinders. J. Phys. Chem. **96**, 7497–7499 (1992)
253. C.A. Foss, G.L. Hornyak, J.A. Stockert, C.R. Martin, Template-synthesized nanoscopic gold particles: optical spectra and the effects of particle size and shape. J. Phys. Chem. **98**, 2963–2971 (1994)
254. G.L. Hornyak, C.J. Patrissi, R. Martin, Fabrication, characterization, and optical properties of gold nanoparticle/porous alumina composites: the nonscattering Maxwell-Garnett limit. J. Phys. Chem. B **101**, 1548–1555 (1997)
255. J.C. Hulteen, C.J. Patrissi, D.L. Miner, E.R. Crosthwait, E.B. Oberhauser, C.R. Martin, Changes in the shape and optical properties of gold nanoparticles contained within alumina membranes due to low-temperature annealing. J. Phys. Chem. B **101**, 7727–7731 (1997)
256. C.K. Preston, M. Moskovits, Optical characterization of anodic aluminum oxide films containing electrochemically deposited metal particles. 1. Gold in phosporic acid anodic aluminum oxide films. J. Phys. Chem. **97**, 8495–8503 (1993)
257. T. Sawitowski, Y. Miquel, A. Heilmann, G. Schmid, Optical properties of quasi one-dimensional chains of gold nanoparticles. Adv. Funct. Mater. **11**, 435–440 (2001)
258. V.G. Stoleru, E. Towe, Plasmon resonant Au nanospheres and nanorods in anodic alumina matrix. Microelectron. Eng. **81**, 358–365 (2005)
259. M.L. Sandrock, C.A. Foss, Synthesis and linear optical properties of nanoscopic gold particle pair structures. J. Phys. Chem. **103**, 11398–11406 (1999)
260. M.L. Sandrock, M. El-Kouedi, M. Gluodenis, C.A. Foss, Optical properties of nanoparticle pair structures. Mat. Res. Soc. Symp. Proc. **635**, C2.1.1–C2.1.10 (2001)
261. S.M. Marinakos, L.C. Brousseau, A. Jones, D.L. Feldheim, Template synthesis of one-dimensional Au, Au-poly(pyrrole), and poly(pyrrole) nanoparticle arrays. Chem. Mater. **10**, 1214–1219 (1998)
262. J.-H. Chen, C.-G. Chao, J.-C. Ou, T.-F. Liu, Growth and characteristics of lead sulfide nanocrystals produced by the porous alumina membrane. Surf. Sci. **601**, 5142–5147 (2007)
263. Y. Ishikawa, Y. Matsumoto, Electrodeposition of TiO_2 photocatalyst into porous alumite prepared in phosphoric acid. Solid State Ionics **151**, 213–218 (2002)
264. G. Shi, C.M. Mo, W.L. Cai, L.D. Zhang, Photoluminescence of ZnO nanoparticles in alumina membrane with ordered pore arrays. Solid State Commun. **115**, 253–256 (2000)

265. T. Gao, G. Meng, Y. Tian, Y. Sun, X. Liu, L. Zhang, Photoluminescence of ZnO nanoparticles loaded into porous anodic alumina hosts. J. Phys.: Condens. Matter **14**, 12651–12656 (2002)
266. G. Schmid, Materials in nanoporous alumina. J. Mater. Chem. **12**, 1231–1238 (2002)
267. J.C. Maxwell Garnett, Colours in metal glasses and in metallic films. Philos. Trans. R. Soc. London A **203**, 385–420 (1904)
268. J.C. Maxwell Garnett, Colours in metal glasses, in metallic films, and in metallic solutions. II. Philos. Trans. R. Soc. London A **205**, 237–288 (1906)
269. R. Kudrawiec, A. Podhorecki, N. Mirowska, J. Misiewicz, I. Molchan, N.V. Gaponenko, A. A. Lutich, S.V. Gaponenko, Photoluminescence investigation of Europium-doped alumina, titania and indium sol–gel-derived films in porous anodic alumina. Mater. Sci. Eng. B-Adv. **105**, 53–56 (2003)
270. I.S. Molchan, N.V. Gaponenko, R. Kudrawiec, J. Misiewicz, L. Bryja, G.E. Thompson, P. Skeldon, Visible luminescence from europium-doped alumina sol-derived films confined in porous anodic alumina. J. Alloy. Compd. **341**, 251–254 (2002)
271. N.V. Gaponenko, I.S. Molchan, O.V. Sergeev, G.E. Thompson, A. Pales, P. Skeldon, R. Kudrawiec, L. Bryja, J. Misiewicz, J.C. Pivin, B. Hamilton, E.A. Stepanova, Enhancment of green terbium-related photoluminescence from higly doped microporous alumina xerogels in mesoporous anodic alumina. J. Electrochem. Soc. **149**, H49–H52 (2002)
272. J.C. Pivin, N.V. Gaponenko, I. Molchan, R. Kudrawiec, J. Misiewicz, L. Bryja, G.E. Thompson, P. Skeldon, Comparsion of terbium photoluminescence from ion implanted and sol–gel-derived films. J. Alloy. Compd. **341**, 272–274 (2002)
273. A. Podhorodecki, M. Banski, J. Misiewicz, J. Serafińczuk, N.V. Gaponenko, Influence of annealing on excitation of terbium uminescence in $YAlO_3$ films deposited onto porous anodic alumina. J. Electrochem. Soc. **157**, H628–H632 (2010)
274. N.V. Gaponenko, D.M. Unuchak, A.V. Mudryi, G.K. Malyarevich, O.B. Gusev, M.V. Stepikhova, L.V. Krasilnikova, A.P. Stupak, S.M. Kleshcheva, M.I. Samoilovich, M.Y. Tsvetkov, Modification of erbium photoluminescence excitation spectra for the emission wavelength 1.54 μm in mesoscopic structures. J. Lumin. **121**, 217–221 (2006)
275. A. Podhorodecki, R. Kudrawiec, J. Misiewicz, N.V. Gaponenko, D.A. Tsyrkunov, 1.54 μm photoluminescence from Er-doped sol-gel derived In_2O_3 films embedded in porous anodic alumina. Opt. Mater. **28**, 685–687 (2006)
276. N.V. Gaponenko, O.V. Sergeev, V.E. Borisenko, J.C. Pivin, P. Skeldon, G.E. Thompson, B. Hamolton, J. Misiewicz, L. Bryja, R. Kudrawiec, A.P. Stupak, E.A. Stepanova, Terbium photoluminescence in polysiloxane films. Mater. Sci. Eng. B-Adv. **81**, 191–193 (2001)
277. S.A. Klimin, E.P. Chukalina, M.N. Popova, E. Antic-Fidancev, P. Aschehoug, N.V. Gaponenko, L.S. Molchan, D.A. Tsyrkunov, Absorption and emission spectra of erbium-doped titania xerogels confined on porous anodic alumina. Phys. Lett. A **323**, 159–163 (2004)
278. N.V. Gaponenko, I.S. Molchan, D.A. Tsyrkunov, G.K. Maliarevich, M. Aegerter, J. Puetz, N. Al.-Dahoudi, J. Misiewicz, R. Kudrawiec, V. Lambertini, N. Li Pira, P. Repetto, Optical and structural properties of sol gel derived materials embedded in porous anodic alumina. Microelectron. Eng. **81**, 255–261 (2005)
279. M.T. Tsvetkov, S.M. Kleshcheva, M.I. Samoilovich, N.V. Gaponenko, A.N. Shushunov, Erbium photoluminescence in opal matrix and porous anodic alumina nanocomposites. Microelectron. Eng. **81**, 273–280 (2005)
280. N.V. Gaponenko, G.K. Malyarevich, D.A. Tsyrkunou, E.A. Stepanova, A.V. Mudrui, O.B. Gusev, E.I. Terukov, M.V. Stepikhova, L.V. Krasilnikova, Y.N. Drozdov, Optical properties of erbium-doped xerogels embedded in porous anodic alumina. Opt. Mater. **28**, 688–692 (2006)
281. M.I. Samoilovich, M.Y. Tsvetkov, S.M. Kleshcheva, A.V. Guryanov, Y.I. Chigirinskii, N.V. Gaponenko, L.I. Ivleva, A.F. Belyanin, Erbium luminescence in 3D- and 2D-mesoporous matrices. Proc. SPIE **5450**, 508–516 (2004)

282. N.V. Gaponenko, O.V. Sergeev, E.A. Stepanova, V.M. Parkun, A.V. Mudryi, H. Gnaser, J. Misiewicz, R. Heiderhoff, L.J. Balk, G.E. Thompson, Optical and structural characterization of erbium-doped TiO_2 xerogels films processed on porous anodic alumina. J. Electrochem. Soc. **148**, H13–H16 (2001)
283. N.V. Gaponenko, I.S. Molchan, A.A. Lutich, S.V. Gaponenko, Enhanced luminescence of europium in porous anodic alumina films. Solid State Phenom. **97–98**, 251–258 (2004)
284. I.S. Molchan, N.V. Gaponenko, R. Kudrawiec, J. Misiewicz, G.E. Thompson, Influence of porous anodic alumina matrix upon europium luminescence from sol–gel-derived films. Mater. Sci. Eng. B-Adv. **105**, 37–40 (2003)
285. R. Kudrawiec, J. Misiewicz, L. Bryja, I.S. Molchan, N.V. Gaponenko, Photoluminescence investigation of porous anodic alumina with spin–on europium-containing titania sol-gel films. J. Alloy. Compd. **341**, 211–213 (2002)
286. S. Molchan, E.A. Stepanova, G.E. Thompson, P. Skelton, N.V. Gaponenko, Europium photolumiescence in titania xerogel on porous anodic aluminum. Proc. SPIE **4511**, 58–60 (2001)
287. N.V. Gaponenko, I.S. Molchan, G.E. Thompson, P. Skeldon, A. Pakes, R. Kudrawiec, L. Bryja, J. Misiewicz, Photoluminescence of Eu-doped titania xerogel spin-on deposited on porous anodic alumina. Sensor. Actuat. A-Phys. **99**, 71–73 (2002)
288. I.S. Molchan, N.V. Gaponenko, R. Kudrawiec, J. Misiewicz, G.E. Thompson, P. Sheldon, Luminescence from sol-gel-derived europium-doped films confined in mesoporous anodic alumina. J. Electrochem. Soc. **151**, H16–H20 (2004)
289. A. Peng, E. Xie, C. Jia, R. Jiang, H. Lin, Photoluminescence properties of TiO_2:Eu^{3+} thin films deposited on different substrates. Mater. Lett. **59**, 3866–3869 (2005)
290. N.V. Gaponenko, J.A. Davidson, B. Hamilton, P. Skeldon, G.E. Thompson, X. Zhou, J.C. Pivin, Strongly enhanced Tb luminescence from titania xerogels solids mesoscopocally confined in porous anodic alumina. Appl. Phys. Lett. **76**, 1006–1008 (2000)
291. N.V. Gaponenko, Sol-gel-derived films in meso-porous matrices: porous silicon, anodic alumina and artificial opals. Synth. Met. **124**, 125–130 (2001)
292. A. Podhorodecki, N.V. Gaponenko, M. Banski, M.V. Rudenko, L.S. Khoroshko, A. Sieradzki, J. Misiewicz, Green emission from barium-strontium titanate matrix introduced into nano-porous anodic alumina. Opt. Mater. **34**, 1570–1574 (2012)
293. T. Qiu, W. Zhang, X. Lang, Y. Zhou, T. Cui, P.K. Chu, Controlled assembly of highly raman-enhancing silver nanocap arrays templated by porous anodic alumina membranes. Small **5**, 2333–2337 (2009)
294. R.J. Walsh, G. Chumanov, Silver coated porous alumina as a new substrate for surface-enhanced raman scattering. Appl. Spectrosc. **55**, 1695–1700 (2001)
295. A.M. Md Jani, D. Losic, N.H. Voelcker, Nanoporous anodic aluminium oxide: advances in surface engineering and emerging applications. Prog. Mater. Sci. **58**, 636–704 (2013)
296. K. Hotta, A. Yamaguchi, N. Teramae, Properties of a metal clad waveguide sensor based on a nanoporous-metal-oxide/metal multilayer film. Anal. Chem. **82**, 6066–6073 (2010)
297. K. Hotta, A. Yamaguchi, N. Teramae, Nanoporous waveguide sensor with optimized nanoarchitectures for highly sensitive label-free biosensing. ACS Nano **6**, 1541–1547 (2012)
298. D. Kim, K. Kerman, M. Salto, R.R. Salthulurl, T. Endo, S. Yamamura, Y.-Y. Kwon, E. Tamlya, Label-free DNA biosensor based on localized surface plasmon resonance coupled with interferometry. Anal. Chem. **79**, 1855–1864 (2007)
299. A. Santos, T. Kumeria, D. Losic, Nanoporous anodic aluminum oxide for chemical sensing and biosensors. Trends Anal. Chem. **44**, 25–38 (2013)
300. A. Santos, V.S. Balderrama, M. Alba, P. Formentin, J. Ferre-Borrull, J. Pallares, L.F. Marsal, Nanoporous anodic alumina barcodes: toward smart optical biosensing. Adv. Mater. **24**, 1050–1054 (2012)
301. S.N. Terekhov, P. Mojzes, S.M. Kachan, N.I. Mukhurov, S.P. Zhvavyi, A.Y. Panarin, I.A. Khodasevich, V.A. Orlovich, A. Thorel, F. Grillon, P.Y. Turpin, A comparative study of surface-enhanced raman scattering from silver-coated anodic aluminum oxide and porous silicon. J. Raman Spectrosc. **42**, 12–20 (2011)

302. J. Wang, L. Huang, H. Tong, L. Zhai, L. Yuan, L. Zhao, W. Zhang, D. Shan, A. Hao, X. Feng, Perforated nanocap array: facile fabrication process and efficient surface enhanced raman scattering with fluorescence suppression. Chinese Phys. B **22**, 047301-1-047301-5 (2013)
303. Z. Yao, M. Zheng, L. Ma, W. Shen, The fabrication of ordered nanoporous metal films based on high field anodic alumina and their selected transmission enhancement. Nanotechnology **19**(465705), 1–7 (2008)
304. G. Macias, L.P. Hernandes Eguia, J. Ferre Borrull, J. Pallares, L.F. Marsal, Gold-coated ordered nanoporous, anodic alumina bilayers for future label–free interferometric biosensors. Appl. Mater. Interfaces **5**, 8093–8098 (2013)
305. T. Kumeria, L. Parkinson, D. Losic, A nanoporous interferometric micro-sensor for biomedical detection of volatile sulphur compounds. Nanoscale Res. Lett. **6**, 1–7 (2011)
306. T. Kumeria, M.D. Kurkuri, K.R. Diener, L. Parkinson, D. Losic, Label-free reflectometric interference microchip biosensor based on nanoporous alumina for detection of circulating tumour cells. Biosens. Bioelectron. **35**, 167–173 (2012)
307. X. Wang, D. Zhang, H. Zhang, Y. Ma, J.Z. Jiang, Tuning color by pore depth of metal-coated porous alumina. Nanotechnology **22**(305306), 1–6 (2011)
308. J. Li, Z. Zhu, Y. Hu, J. Zheng, J. Chu, W. Huang, Numerical and experimental study of the structural color by widening the pore size of nanoporous anodic alumina. J. Nanomater. **819432**, 1–10 (2014)
309. Y. Wada, T. Yanagishita, H. Masuda, Ordered porous alumina geometries and surface metals for surface-assisted laser desorption/ionization of biomolecules: possible mechanistic implications of metal surface melting. Anal. Chem. **79**, 9122–9127 (2007)
310. H. Hu, D. He, The properties of $Si_{1-x}Ge_x$ nanodot arrays prepared by plasma-enhanced CVD on porous alumina templates. Chem. Vapor. Depos. **12**, 751–754 (2006)
311. S. Kinoshita, S. Yoshioka, Structural colors in nature: the role of regularity and irregularity in the structure. Chem. Phys. Chem. **6**, 1442–1459 (2005)
312. N.V. Gaponenko, Y.V. Hluzd, G.K. Maliarevich, I.S. Molchan, G.E. Thompson, S. Dabboussi, H. Elhouichet, S.Y. Prislopski, A.A. Lutich, Room-temperature photoluminescence from porous anodic alumina films with embedded terbium and europium species. Mater. Lett. **63**, 621–624 (2009)
313. S. Dabboussi, H. Elhouichet, C. Bouzidi, G.K. Maliarevich, N.V. Gaponenko, M. Oueslati, Excitation and emission processes of Tb^{3+} in porous anodic alumina. Appl. Surf. Sci. **255**, 4255–4258 (2009)
314. S.P. Mondal, A. Dhar, S.K. Ray, Optical properties of CdS nanowires prepared by DC electrochemical deposition in porous alumina template. Mater. Sci. Semicond. Process. **10**, 185–193 (2007)
315. Y.L. Shi, J. Wang, H.L. Li, Photoluminescence effect of ru dye on alumina membranes with ordered pore arrays. Appl. Phys. A-Mater. **75**, 423–426 (2002)
316. J.W. Gregory, K. Asai, M. Kameda, T. Liu, J.P. Sullivan, A review of pressure-sensitive paint for high-speed and unsteady aerodynamics. Proceed. Inst. Mech. Eng. Part G: J. Aerospace Eng. **222**, 249–290 (2008)
317. Y.-Q. Cheng, Y.-Z. Yang, C.-R. Niu, D.-Y. Miao, X.-G. Chen, Z.-D. Hu, Photoluminescence characteristics of several fluorescent molecules on nanometer porous alumina film. Acta Chim. Sinica **62**, 183–187 (2004)
318. Y. Yang, H.-Y. Li, H.-L. Chen, X.-M. Bao, Luminescence study of fluorescent dye impregnated into si-based nanoporous alumina. Chem. J. Chinese Univ. **23**, 768–771 (2002)
319. C. Xu, C. Xu, Q. Xue, L. Ba, B. Zhao, N. Gu, Y. Cui, Spectral behavior of 8-hydroxyquinoline aluminum in nanometer-sized holes of porous alumina. Chinese Sci. Bull. **46**, 1839–1841 (2001)
320. Y.-F. Dong, Q.-S. Li, Photoluminescent sectra of 8-hydroxyquinoline aluminum embedded in porous alumina. Acta Phys.Sinica **51**, 1645–1648 (2002)
321. A. Moadhen, H. Elhouichet, L. Nosova, M. Ouslati, Rhodamine B absorbed by anodic porous alumina: stokes and anti-stokes luminescence study. J. Lumin. **126**, 789–794 (2007)

322. I. Miura, Y. Okada, S. Kudoh, M. Nakata, Organic electroluminescence in porous alumina. Jpn. J. Appl. Phys. **43**, 7552–7553 (2004)
323. H. Elhouichet, N. Harima, H. Koyama, N.V. Gaponenko, Energy transfer in porous anodic alumina/rhodamine 110 nanocomposites. J. Lumin. **132**, 2232–2234 (2012)
324. A. Kukhto, E. Kolesnik, A. Mozalev, M. Taoubi, Luminescent properties of organic compounds in nanodimensional aluminium oxide structures. Proc. SPIE **3573**, 513–515 (1998)
325. H.J. Peng, Y.L. Ho, X.J. Yu, H.S. Kwok, Enhanced coupling of light from organic light emitting diodes using nanoporous films. J. Appl. Phys. **96**, 1649–1654 (2004)
326. S. Wang, H. Luo, Y. Wang, G. Gong, The effect of nanometer size of porous anodic aluminum oxide on adsorption and fluorescence of tetrahydroxyflavanol. Spectrochim. Acta B **59**, 1139–1144 (2003)
327. R.-P. Jia, Y. Shen, H.-Q. Luo, X.-G. Chen, Z.-D. Hu, D.-S. Xue, Photoluminescence spectra of human serum albumen and morin embedded in porous alumina membranes with ordered pore arrays. J. Phys.: Condens. Mater. **15**, 8271–8279 (2003)
328. R.P. Jia, Y. Shen, H.Q. Luo, X.G. Chen, Z.D. Hu, D.S. Xue, Enhanced photoluminescence properties of morin and trypsin absorbed on porous alumina films with ordered pores array. Solid State Commun. **130**, 367–372 (2004)
329. R.P. Jia, Y. Shen, H.Q. Luo, X.G. Chen, Z.D. Hu, D.S. Xue, Photoluminescence behaviors of morin-human immunoglobulin on porous anodized aluminum oxide films. Thin Solid Films **471**, 264–269 (2005)
330. R.P. Jia, Y. Shen, H.Q. Luo, X.G. Chen, Z.D. Hu, D.S. Xue, Enhanced photoluminescence properties of morin and trypsin absorbed on porous alumina films with ordered pores array. Solid State Commun. **233**, 343–351 (2004)